AN INVESTIGATION OF THE ROLE OF FRAMEWORK GEOLOGY ON MODERN BARRIER ISLAND TRANSGRESSION

A Dissertation

by

BRADLEY ALLEN WEYMER

Submitted to the Office of Graduate and Professional Studies of
Texas A&M University
in partial fulfillment of the requirements for the degree of

DOCTOR OF PHILOSOPHY

Chair of Committee,	John R. Giardino
Co-Chair of Committee,	Chris Houser
Committee Members,	Mark E. Everett
	Timothy Dellapenna
Head of Department,	Michael Pope

August 2016

Major Subject: Geology

ABSTRACT

The framework geology controls on modern barrier island transgression and the relationship of these controls to subsurface structure, hydrology, and island geomorphology are not well understood. Recent evidence suggests that alongshore variations in pre-Holocene geology of barrier islands modify nearshore hydrodynamic processes and sediment transport, ultimately affecting how barrier islands will respond to storms and relative sea-level rise. Explorations of Holocene barrier island geology are usually based on cores to supplement bathymetric, onshore/offshore seismic and/or ground-penetrating radar (GPR) surveys. Alternative near-surface geophysical methods including electromagnetic induction (EMI) sensors are increasingly being used for coastal research because they are non-invasive, provide continuous subsurface information across a variety of sub-environments, are capable of characterizing large areas in a short time, and are considerably more cost effective than the abovementioned techniques. This dissertation demonstrates the utility of using EMI methods for mapping large-scale (10^1 – 10^2 km) barrier island framework geology at Padre Island National Seashore (PAIS), Texas, USA. Instrument calibrations and tidal experiments suggest that although hydrology influences EMI signals along the beach, the effect of changing hydrology is not statistically significant over large spatial scales. For the first time, this study shows the importance of statistically modeling EMI spatial data and digital elevation model (DEM) extracted morphometrics to examine the statistical relationships (or lack thereof) between framework geology and geomorphology. A family of fractional autoregressive

integrated moving average ARIMA (*p*,*d*,*q*) models demonstrate each spatial data series is most accurately modeled by a single parameter, *d*, indicating a strong tendency towards long-range dependence (LRD) that suggests self-similarity. Dune height and EMI σ_a have nearly identical *d*-values (~ 0.35), which suggests a statistically significant connection between framework geology and dune height at a global scale (100 km). Variations in *d* at both regional (~30 km) and local (10 km) scales differ by varying degrees, providing further evidence that framework geology controls are more important at the largest spatial scales. By integrating EMI and DEM morphometrics with multivariate analysis and ARIMA modeling, this study offers a robust and novel way for accurately quantifying the entire geological complexity of a barrier island using only three parameters (*p*,*d*,*q*). Moreover, this study shows that EMI sensors are complementary to and offer significant advantages over traditional methods in support of an improved understanding of large-scale barrier island transgression.

DEDICATION

To my family and friends, all my love. This manuscript is dedicated to Ruifang Xie, Rick, and Beth Weymer.

ACKNOWLEDGEMENTS

This research would not have been possible without the support of my advisors, Drs. Chris Houser and Rick Giardino. You both have been amazing mentors during my time at Texas A&M University. Thank you for inspiring me and helping me realize my potential. I am grateful to my committee members Drs. Mark Everett and Tim Dellapenna. I especially thank Mark for introducing me to the fascinating world of geophysics. I would like to express my sincere gratitude to my supervisors Dr. Brad Clement, Dr. John V. Firth, Phil Rumford, and Brad Julson at the International Ocean Discovery Program (IODP) for providing funding assistance as a graduate research assistant. I will forever be indebted to their support in giving me an opportunity to pursue my dreams as a scientist, and to be a part of an incredible research organization.

Many thanks to Phil Wernette for working closely with me on this project over the years. Additionally, I am grateful to Patrick Barrineau, Aniela Chamorro, Carol Chamorro, Tim de Smet, Andy Evans, Alex van Plantinga, Michael Schwind, Sarah Trimble, and Brianna Hammond Williams. I acknowledge James Lindsay, Wade Stablein, Travis Clapp and Kristina Jenkin at the Padre Island National Seashore (PAIS) Science and Resource Management Division for their continued interest and stimulating conversations. Lastly, I am thankful for my family and friends for their love and support.

The data in this dissertation was collected under the National Park Service permit: #PAIS-2013-SCI-0005. This research is supported in part by Grants-in-Aid of Graduate Student Research Award by Texas Sea Grant College Program.

NOMENCLATURE

AEM	Airborne electromagnetic
AR	Autoregressive
ARMA	Autoregressive moving average
ARIMA	Autoregressive integrated moving average
CSEM	Controlled source electromagnetic
DEM	Digital elevation model
DOI	Depth of investigation
EM	Electromagnetic
EMI	Electromagnetic induction
ERT	Electrical resistivity tomography
FARIMA	Fractional autoregressive integrated moving average
FEM	Finite element method
fBm	Fractional Brownian motion
fGn	Fractional Gaussian noise
GPR	Ground-penetrating radar
GPS	Global positioning system
GSSI	Geophysical Survey Systems Incorporated
I	Imaginary (in-phase)
LiDAR	Light detection and ranging
LIN	Low induction number

LRD	Long-range dependence
MA	Moving average
MHW	Mean high water
MLW	Mean low water
MLLW	Mean lower low water
MTL	Mean tide level
NOAA	National Oceanographic Atmospheric Administration
PAIS	Padre Island National Seashore
P-MODE	In-line orientation
PSD	Power spectral density
Q	Quadrature (out of phase)
R	Statistical programming language
RMSE	Root-mean-square error
R/S	Rescaled-range
RX	Receiver
S/N	Signal-to-noise ratio
TDEM	Time-domain electromagnetic
TEM	Transient electromagnetic
T-MODE	Broadside orientation
TX	Transmitter
VD	Vertical dipole
WT	Water table

β	Slope of PSD
d	Degree of differencing
D	Fractal dimension
δ	Skin depth
h	Instrument height (above the ground)
H	Hurst parameter
kHz	Kilohertz
kyr	Kilo year
H_0	Primary magnetic field
H_S	Secondary magnetic field
MHz	Megahertz
mS/m	Milliseimens per meter
μ	Magnetic permeability
Myr	Million years
p	Order of autoregressive model
q	Order of moving average model
s	Coil separation (between TX-RX)
σ	Electrical conductivity
σ_a	Apparent conductivity
σ^2	Variance

TABLE OF CONTENTS

Page

ABSTRACT……. ii

DEDICATION iv

ACKNOWLEDGEMENTS v

NOMENCLATURE..... vi

TABLE OF CONTENTS ix

LIST OF FIGURES..... xii

LIST OF TABLES xiv

CHAPTER I INTRODUCTION AND PROBLEM STATEMENT..... 1

- Objectives..... 5
- Background 6
  - Barrier island response to sea level and storms..... 6
  - Traditional methods for investigating barrier island geology 9
  - Electromagnetic induction approach to assessing framework geology.. 12
  - Multivariate analysis, LRD, and FARIMA statistical modeling..... 13
  - EMI profiling as a new technique for investigating barrier island framework geology 15

CHAPTER II REVIEW OF ELECTROMAGNETIC INDUCTION FOR MAPPING BARRIER ISLAND FRAMEWORK GEOLOGY..... 17

- Introduction…… 17
- Geomorphological mapping using electromagnetic sensors..... 24
- Traditional methods of research into barrier island geologic inheritance..... 28
- The theory of the EMI geophysical method in coastal environments..... 33
  - The electromagnetic geophysical method..... 33
  - EMI response and computation of apparent conductivity..... 36
  - Portable EMI sensors 38
  - Past examples of coastal EMI surveys 42
  - Demonstration of EMI in support of this review 45
  - Conceptual model of groundwater effects on EMI signals..... 51

Summary and future research 54

CHAPTER III DIFFERENTIATING TIDAL AND GROUNDWATER DYNAMICS FROM BARRIER ISLAND FRAMEWORK GEOLOGY: TESTING THE UTILITY OF MULTI-FREQUENCY EMI PROFILERS 57

Introduction 57
Portable multi-frequency EMI systems 58
Application of EMI methods in coastal studies 65
Research objectives 67
Description of the study area 67
Methods 72
Calibration tests 73
Instrument orientation testing 77
Repeatability tests 80
Results 83
Tidal cycle experiments 83
Shore-normal EMI surveys 87
Alongshore EMI surveys 90
Discussion 95
Conclusions 98

CHAPTER IV LONG-RANGE DEPENDENCE IN COASTAL-BARRIER ELECTROMAGNETIC INDUCTION SPATIAL DATA SERIES 100

Introduction 100
Study area 103
Field methods and EMI spatial data series 104
Tests for long-range dependence 110
FARIMA statistical modeling and interpretation 113
Conclusions 119

CHAPTER V FRAMEWORK GEOLOGY CONTROLS ON LARGE-SCALE BARRIER ISLAND TRANSGRESSION 120

Introduction 120
Study area 124
Methods 126
Field EMI survey 126
Geomorphometry 128
Statistical methods 130
Results 134
Spatial data series 134
Tests for LRD 137

Arima (p,d,q) model results and multivariate analysis..... 139
Discussion 146
Conclusions 150

CHAPTER VI CONCLUSIONS 152

Future steps 158

REFERENCES..... 160

LIST OF FIGURES

Page

Figure 1-1. Conceptual model showing the traditional and contemporary geologic and geophysical methods used for investigating barrier island framework geology across the coastal zone 10

Figure 2-1. Schematic diagram depicting hypothetical geologic features along a barrier island at a variety of length-scales..... 26

Figure 2-2. Example of a handheld GSSI Profiler EMP-400™ being used in the backshore environment at Padre Island National Seashore, Texas 40

Figure 2-3. Location map of previously inferred Pleistocene streams identified by Fisk (1959) 47

Figure 2-4. Example of an EMI grid survey across the beach-dune environment..... 50

Figure 2-5. Conceptual model of groundwater dynamics in a barrier island and their effect on the EMI signal..... 52

Figure 3-1. Overview of the EMI handheld profiler configuration and conceptual model of the relationships between varying hydrology, lithology, and apparent conductivity σ_a..... 61

Figure 3-2. Location map of central PAIS and adjacent Laguna Madre wind-tidal flats in southern Texas, USA..... 69

Figure 3-3. (a) Survey design for instrument calibration and tidal experiments at the intersection of the AS and NS 75

Figure 3-4. Comparison of σ_a measurements taken with different profiler orientations: P-mode and T-mode 79

Figure 3-5. Off-site repeatability tests performed on campus at Texas A&M University in College Station, Texas..... 82

Figure 3-6. (a) Tidal cycle and step-function 3 kHz EMI response over a 12-hr sampling interval at the tie-point between the AS and NS..... 84

Figure 3-7. Shore-normal (a) and alongshore (b) 3 kHz repeat surveys measured over the course of a 12-hour tidal cycle 86

Figure 3-8. Shore-normal surveys and classification of each sub-environment for the northern (a), central (b), and southern (c) sites collected between August 7, 8 and 9, 2013, respectively 88

Figure 3-9. Alongshore EMI comparison with previously interpreted paleo-channels by Fisk (1959) and the approximate tidal states during data acquisition 91

Figure 3-10. Comparison of 3 kHz repeat alongshore surveys within the AS collected on November 28th, 2013, February 2nd, 2014 and October 11th, 2014 92

Figure 4-1. 100 km alongshore EMI survey. (a): DEM of study area and previously identified paleo-channel region by Fisk (1959) 107

Figure 4-2. 10 km alongshore EMI survey within the previously interpreted paleo-channel region (highlighted in green) by Fisk (1959) 109

Figure 4-3. Autocorrelations of measured σ_a values for the 100 km (a) and 10 km EMI surveys (d) 112

Figure 4-4. Family of ARIMA models for the 100 km EMI survey 116

Figure 4-5. Family of ARIMA models for the 10 km EMI survey 118

Figure 5-1. Location map of the study area in Padre Island National Seashore (PAIS), Texas, USA 125

Figure 5-2. Flow chart illustrating the methods for collecting, processing and analyzing the EMI and LiDAR data presented in this study 132

Figure 5-3. EMI survey and DEM metrics extracted from the aerial LiDAR data 136

Figure 5-4. R/S analysis for determining the degree of LRD (Hurst coefficient *H*) for each island metric and the EMI signal 138

Figure 5-5. Example of the best fit ARIMA (0,*d*,0) models for each signal: a) beach width, b) beach volume, c) dune height, d) dune volume, e) island width, f) island volume, and g) EMI σ_a 142

LIST OF TABLES

Page

Table 2-1. A summary of the coastal sub-system, methods and scientific applications for each of the publications investigating geologic controls on modern barrier island evolution discussed in this review 20

Table 2-2. The advantages and limitations of various geological, geophysical, bathymetric and remote sensing methods used for barrier island geologic framework research 22

Table 3-1. Theoretical skin depths (δ) in meters over the frequency bandwidth of the GSSI Profiler EMP-400™ for a range of apparent conductivities encountered across the coastal environment 64

Table 3-2. Tie points and relative difference of measured σ_a values between the alongshore and shore-normal surveys collected in August, 2013 81

Table 3-3. Daily tidal variations during each EMI survey. Survey times are listed relative to the high and low tides 94

Table 5-1. Comparison of residuals (RMSE) for each ARIMA model iteration used in this study 139

Table 5-2. Summary table showing the computed "global" *d* parameters that most appropriately model each ARIMA (0,*d*,0) iteration 140

Table 5-3. Summary table showing the computed "regional" *d* parameters that most appropriately model each ARIMA (0,*d*,0) iteration 144

Table 5-4. Summary table showing the difference between each metric with respect to EMI listed as absolute magnitudes for comparison 144

Table 5-5. Summary table showing the computed "local" *d* parameters that most appropriately model each ARIMA (0,*d*,0) iteration 145

Table 5-6. Summary table showing the difference between each metric with respect to EMI listed as absolute magnitudes for comparison 146

CHAPTER I

INTRODUCTION AND PROBLEM STATEMENT

Many coastlines in the United States are comprised of barrier islands, which Hayes (2005, pg. 117) defines as: ‘‘*An elongated, shore-parallel accumulation of unconsolidated materials (primarily sand), which is separated from the mainland by bays, lagoons, or wetland complexes*.” These low-elevation coastal landforms consist at least 10% of the world’s coastline (Cromwell, 1971; Stutz and Pilkey, 2001, 2011). The total length and area of U.S. barrier islands, which span 18 states along the U.S. Atlantic and Gulf Coasts are ~ 3,700 km and 6,800 km^2, respectively (Zhang and Leatherman, 2011). Barrier islands are the first line of defense from storms and sea level rise that would otherwise directly impact environmentally and economically important areas of the coast (McBride et al., 1992). Along the Atlantic and Gulf Coasts of the United States, barrier islands are the predominant geomorphic features and are particularly susceptible to storm-surge flooding and erosion in response to climate change and rising sea-level (Zhang and Leatherman, 2011). Globally, more than 60% (> 3.8 billion people) of the world’s population lives within 100 km of the coast (Vitousek et al., 1997). There is more than 1.4 million people living on barrier islands, according to 2000 census data and the population densities of barrier islands are three times those of coastal states on average, with an increased population by 14% from 1990 to 2000 (Zhang and Leatherman, 2011). Despite the inherent risks of living on barrier islands, the U.S. is experiencing continued population growth along its coast.

With the threat of increased sea level rise, extreme storms and coastal flooding, there are considerable challenges for coastal scientists, engineers, policy makers, and the public for developing sustainable management strategies that support resilient coastal communities. Part of the problem in understanding the susceptibility of barrier response to sea level rise and storms is that few studies have investigated the large-scale evolution of the entire island, which has been suggested to be influenced by pre-existing geologic features to varying degrees (e.g., Belknap and Kraft, 1985; Riggs et al., 1995; Lazarus and Murray, 2011; Lentz and Hapke, 2011). Most work has been modeling studies at this scale and there is a need for field data to guide the models. For example, shoreline evolution has been shown to be controlled (in part) by geologic features that can vary over a wide range of spatial and/or temporal scales (e.g., McNinch, 2004; Hapke et al., 2010; Houser, 2012). Our ability to understand and predict this variability is still limited, leading to misinterpretation of coastal change information (Stive et al., 2002), which impedes informed decision making. This urgency, both to humans and to terrestrial and aquatic ecosystems, makes it imperative that we understand the multi-scale processes and interactions between geology and surface morphology in these dynamic and vulnerable coastal environments (see Talley et al., 2003).

Previous studies suggest the underlying geology otherwise termed *framework geology* (in this study) of barrier islands can play a significant role in the evolution of coastal environments (Kraft et al., 1982; Belknap and Kraft, 1985; Evans et al., 1985; Riggs et al., 1995; Short, 2010). For example, pre-existing structures such as paleo-channels, offshore ridge and swale bathymetry, and relict transgressive features have been suggested to

influence geologic variations along the coast (see McNinch, 2004; Hapke et al., 2010; Lentz and Hapke, 2011; Houser, 2012). At the **coastal plain scale** (~ 10^2 km), framework geology influences the structure of the coastal plain, that may include glacial, fluvial, tidal, and/or inlet paleo-valleys and channels (Belknap and Kraft, 1985; Demarest and Leatherman, 1985; Colman et al., 1990), and paleo-deltaic systems offshore or beneath the modern coastal plain (Coleman and Gagliano, 1964; Frazier, 1967; Otvos and Giardino, 2004; Twichell et al., 2013; Miselis et al., 2014). At the **shelf scale** (~ 10^1 km), framework geology consists of feedbacks between geologic features and relict sediments within the littoral system (e.g., Riggs et al., 1995; Schwab et al., 2000; Rodriguez et al., 2001; Honeycutt and Krantz, 2003) and is an important control on dune formation (Houser et al., 2008) and shelf features, including sand ridges (e.g., Browder and McNinch, 2006; Schwab et al., 2013). At the **shoreface scale** (< 1 km), framework geology involves meso-to-micro-scale sedimentological changes (e.g., Murray and Thieler, 2004; Schupp et al., 2006), variations in thickness of shoreface sediments (Miselis and McNinch, 2006), and spatial variations in sediment transport across the island (Houser and Mathew, 2011; Lentz and Hapke, 2011; Houser, 2012). However, most of what is known regarding barrier island framework geology is based on studies at relatively small spatial-scales (e.g., McNinch, 2004; Hapke et al., 2010; Lentz and Hapke, 2011).

Little is known about the large-scale (10^1 – 10^2 km) geologic structure of barrier islands and the important length-scales of subsurface features that may influence alongshore variations in surface morphology, which in turn affects island response to storms and sea-level rise (i.e., transgression). Riggs et al. (1995) state that: *"It is essential to understand*

this geologic framework before attempting to model the large-scale behavior of these types of coastal systems….we must understand the detailed geologic framework underlying the shoreface and the inner shelf, as well as the physical dynamics operating within and upon regional segments of the shoreface system." Therefore, detailed assessments of framework geology are critical for coastal management and risk evaluation for both natural and anthropogenically-modified barrier islands (Hapke et al., 2010; Lentz and Hapke, 2011; Lentz et al., 2013).

Part of the difficulty in examining the relationships between framework geology and island morphology is that we cannot directly observe the large-scale framework geology below the surface using traditional labor intensive, low-resolution techniques such as coring. Thus, coastal scientists have increasingly turned to geophysical techniques including seismic imaging (e.g., Emery, 1969; Simms et al., 2006), ground-penetrating radar (e.g., Leatherman, 1987; Jol et al., 1996; Heteren et al., 1998; Neal and Roberts, 2000; Buynevich and Fitzgerald, 2003), and more recently, electromagnetic induction (e.g., Seijmonsbergen et al., 2004; Vrbancich, 2009) to characterize the underlying geology along the coast. EMI sensors are an attractive alternative to conventional methods used for barrier island research because they are non-invasive, provide continuous subsurface information across a variety of sub-environments, are capable of characterizing large areas in a short time, and are considerably more cost-effective than the abovementioned traditional geologic and/or geophysical techniques (Weymer et al., 2015b). However, EMI has been underutilized for several reasons

including: lack of awareness of the method by non-geophysicists, and data reliability (see George and Woodgate, 2002).

The purpose of this dissertation is to demonstrate the utility of EMI in coastal geologic surveying and integrating EMI with aerial LiDAR data to quantify the important process-form relationships between framework geology and surface morphology with respect to island response to storms and sea-level rise. Previous studies at the **coastal plain scale**, **shelf scale**, and **shoreface scale** suggest that framework geology plays an important role in the large-scale evolution of modern coastlines, but the spatial correlation between subsurface structures (e.g., paleo-channels) and surface features (e.g., beach width, and dune height) is not known, or has only been demonstrated locally. Most geologic studies mentioned above have been conducted at relatively small or coarse spatial scales. This study is unique in its attempt to use EMI for higher resolution mapping over a much larger scale.

Objectives

The primary objective of this research project is to obtain field data of sufficient quality and quantity to allow a detailed evaluation of using EMI apparent conductivity data σ_a as a proxy for determining the geologic controls that may influence island transgression and evolution of the world's longest undeveloped barrier island; Padre Island National Seashore (PAIS), Texas, USA. There are three working hypotheses driving the study design:

1. Electromagnetic induction (EMI) is a viable method for investigating subsurface barrier island framework geology

2. Subsurface features are related to/mirrored in the surface morphology along the shoreline and foredune ridge
3. Framework geology controls the current shoreline and dune morphology to varying degrees along the island

In order to test these hypotheses, three research objectives must be met:

1. Use EMI to measure variations in subsurface geology and hydrology along the shoreline of PAIS
2. Analyze the long-range-dependent structure (or lack thereof) of alongshore EMI measurements and DEM-extracted morphometrics
3. Determine, statistically, the spatial connections (or lack thereof) between EMI and DEM morphometrics along the island

The fieldwork and analytical work that motivates these hypotheses and objectives is presented in the following chapters.

Background

Barrier island response to sea level rise and storms

Over geologic timescales, change in sea-level is the dominant factor controlling barrier island evolution and migration. It is well documented that the framework geology also plays a significant role in determining how barrier island systems evolve (Kraft, 1971; Kraft and John, 1979; Kraft et al., 1982; Belknap and Kraft, 1985; Riggs et al., 1995; Dillenburg et al., 2000; Harris et al., 2005; Short, 2010). The overall configuration

of coastal barriers is primarily controlled by geologic features, which in turn influence wave refraction and attenuation, beach location, shape, type, morphodynamics and circulation. These processes govern sediment transport across the dunes and barrier system (Short, 2010). Consequently, geologic features also control contemporary response of the barrier island to extreme storms, and in turn the rate of island transgression to variations in sediment supply or an increase in mean sea-level (Houser, 2012).

Barrier island transgression is accomplished primarily by relative sea-level rise and extreme storms that are capable of breaching the dunes and depositing sediment to the back-barrier in the form of blowouts, washover fans and terraces (Morton and Sallenger, 2003; Stone et al., 2004; Houser, 2012). Houser (2012) suggests that the threshold storm surge required for foredunes to be overtopped or breached decreases as sea-level rises, and subsequently the probability of island overwash and island transgression increases. Dune scarping can also induce blowouts that are part of the transgression and can potentially create washover channels during extreme storms (Houser, 2012). Breaching and overwash is focused in areas where dune height is low (i.e., overwash regime), creating the potential for rapid transgression and even overstepping (Sallenger, 2000). The two-dimensional storm impact model proposed by Sallenger (2000) does not account for alongshore variability in dune height. Along relatively short sections of the same beach there can be significant differences in foredune height which may lead to different transgression histories alongshore (Weymer et al., 2015a). In areas where the dune heights are low, lateral dune erosion through the

expansion of washover conduits can develop, whereas, in areas where the dunes are high only the base of the dune is scarped and sediment is transported seaward.

Morphodynamics of barrier islands are governed by changes in littoral sediment supply and sea level, as well as to the dynamic processes associated with storms (Hayes, 1979; Houser et al., 2008; Davidson-Arnott, 2010; Houser, 2012). When a welded bar becomes subaerially exposed, it acts as a sediment source available for aeolian transport, thus enabling the foredune ridge to develop and migrate over time (Sherman and Lyons, 1994; Aagaard et al., 2004). The precise location of overwash during storms and dune erosion depends on the correspondence of alongshore variations in the incident forcing and on existing gaps and low lying areas along the dune line (Dolan and Hayden, 1981; Suter et al., 1982; Orford and Carter, 1984). As gaps in the dune line are breached and the berm crest is exceeded, sediment is transported landward as overwash and deposited as washover fans and, possibly, terraces if dune breaching is more extensive alongshore (Morton et al., 2000; Sallenger, 2000; Donnelly et al., 2006; Matias et al., 2008; Matias et al., 2009). It is by this process that barrier islands (in the absence of human modification) keep pace with sea level rise and transgress as sediment is redistributed landwards by successive storm events.

From the aforementioned discussion, the rate of island transgression depends on the washover as controlled by extreme storm events, related to the height and extent of the foredunes (see Sallenger, 2000; Masetti et al., 2008). The height of a dune when a storm makes landfall depends on the time since the previous storm, the level of erosion sustained in that storm and the rate of post-storm dune recovery (Houser and Hamilton,

2009). The rate of recovery, therefore, depends on the regional sediment budget (Psuty, 1992), and the ability of sediment to be transported from the beach and backshore to the dune (Short and Hesp, 1982; Sherman and Bauer, 1993). The preserved sedimentary structures can provide a relative chronology of how the beach-dune system responds to and recovers from extreme storms and the implications for island response to relative sea-level rise (i.e., transgression) (Houser et al., 2015).

Traditional methods for investigating barrier island geology

Studies investigating the framework geology controls on barrier island transgression have primarily focused on a specific sub-environment within the barrier island system (e.g., inner-shelf, nearshore, beach, backbarrier, bay). In the analysis of large-scale coastal evolution, the data collection techniques available force an arbitrary compartmentalization of each sub-environment within the barrier island system. Inner-shelf and nearshore studies mainly use bathymetric and seismic surveys respectively because these methods are best suited for shallow water and offshore environments (e.g., Riggs, 1979; Evans et al., 1985; Riggs et al., 1995; Foyle and Oertel, 1997; Schwab et al., 2000; Rodriguez et al., 2001; McNinch, 2004; Browder and McNinch, 2006). Conversely, beach and barrier studies have tended to use coring and/or remote sensing techniques (e.g., Otvos, 1970; Riggs et al., 1995; Fitzgerald and Van Heteren, 1999; Morton, 2002; Jackson et al., 2005; Mallinson et al., 2010; Cooper et al., 2012). It is important to note that the various methods listed above are used for different aims.

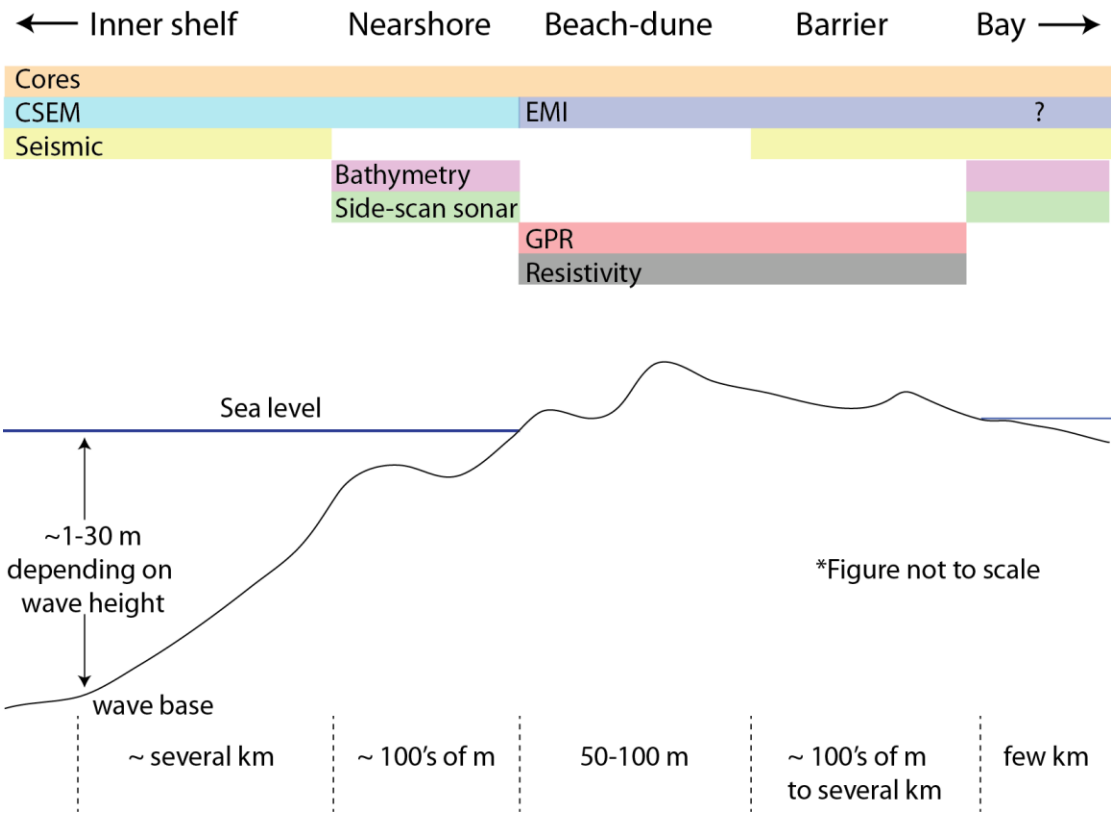

Figure 1-1. Conceptual model showing the traditional and contemporary geologic and geophysical methods used for investigating barrier island framework geology across the coastal zone.

Despite the utility of these methods, coring provides only point-source information and in many cases limited penetration depth, whereas seismic methods are not well suited for land-based surveys in unconsolidated, sandy sediments (Leatherman, 1987; Smith and Sjogren, 2006; Schrott and Sass, 2008). Thus, coastal researchers have turned to other geophysical techniques such as electrical resistivity tomography (ERT) and ground-penetrating radar (GPR). Since the 1980's, GPR techniques have continued to provide high-resolution imagery of subsurface stratigraphy, thereby improving interpretations of geologic

controls on barrier island evolution (e.g., Leatherman, 1987; Van Heteren et al., 1994; Jol et al., 1996; Bristow et al., 2000; Neal and Roberts, 2000; Buynevich and Fitzgerald, 2003; Mallinson et al., 2010). Because each method is best suited for a particular sub-environment, only a few studies have integrated multiple methods to explore the role of geologic inheritance on large-scale barrier island evolution and few have covered the entire island (see Fisk, 1959; Evans et al., 1985; Williams et al., 1991; McBride et al., 1995; Harris et al., 2005; Kulp et al., 2005; Mallinson et al., 2010).

There are alternative techniques available that have yet to be fully explored in coastal environments. For example, electromagnetic (EM) methods have potential for coastal environmental and engineering applications including; time-domain airborne transient electromagnetic (TEM) surveys (e.g., Vrbancich, 2009, 2012; Christensen and Halkjær, 2014), marine controlled-source electromagnetic (CSEM) surveys (e.g., Cheesman et al., 1993; Evans et al., 1999; 2000; Barker et al., 2012), and frequency-domain electromagnetic induction (EMI) surveys (e.g., Ruppel et al., 2000; Paine et al., 2004; Seijmonsbergen et al., 2004). EM sensors are designed to map subsurface geo-electric properties and, as such, they can help distinguish spatial variations in subsurface lithological and hydrological properties (including water content, porosity, clay content, etc). Despite the many benefits of using these different methods in combination, there are a number of limitations that need to be better understood before the EMI technique can be used with confidence in coastal applications for mapping barrier island geology.

Electromagnetic induction approach to assessing framework geology

Portable handheld EMI profilers are designed to measure variations in subsurface electrical conductivity σ as it is related to changes in geology and hydrology. EMI responses typically are irregular and represent a spatial averaging of σ (i.e, apparent conductivity σ_a), which in turn integrates the effects of all its controlling physical properties (e.g., porosity, water content, salinity, etc.). Thus, is it reasonable to expect that EMI sensors are capable of detecting changes in σ_a as it is related to variations in lithology along the island, such as contrasts between sand and clay. It has been shown by Seijmonsbergen et al. (2004), Vrbancich (2009), and others that EMI methods can accurately and efficiently characterize the underlying geology along coastlines. For example, Seijmonsbergen et al. (2004) used the EM34 (albeit not a portable multi-frequency EMI profiler) at 20 m station spacing and 20 m coil separation to acquire a 14.5 km transect along a segment of the Dutch coast, Netherlands. Using this configuration, the depth of exploration (DOI) is ~15 m. Results from the study suggest that subsurface σ_a can be used as a proxy to distinguish the spatial distribution of Holocene coastal deposits and previously identified pre-Holocene paleo-channels near a former outlet of the Rhine River. Nonetheless, few studies have used EMI methods in coastal environments (Paine et al., 2004; Seijmonsbergen et al., 2004; Vrbancich, 2009; Nenna et al., 2013; Christensen and Halkjær, 2014; Delefortrie et al., 2014b), with the majority of these focusing on mapping saltwater intrusion. Most of these studies employ Geonics™ EM31, 34, 38 and similar frequency-domain sensors; Geonics™ EM47, 63 and similar time-domain electromagnetic (TDEM) sensors in addition to various

airborne electromagnetic (AEM) systems. Previous coastal EMI studies have explored subsurface σ as it is related to framework geology (Seijmonsbergen et al., 2004; Vrbancich, 2009), classification of coastal wetlands (Paine et al., 2004), and investigation of coastal groundwater dynamics and pollution (Goldman et al., 1991; Fitterman and Deszcz-Pan, 1998; Nenna et al., 2013; Christensen and Halkjær, 2014).

While the above studies demonstrate the value of EMI sensors for coastal research, most have not examined in detail the effects of changing hydrology as it is related to framework geology over different spatial-temporal scales. Although EMI sensors have shown promise for coastal applications (Paine et al., 2004; Seijmonsbergen et al., 2004; Delefortrie et al., 2014b), a number of issues primarily related to variations in subsurface hydrology are needed to fully assess the benefits and limitations of this new technique. Because barrier island hydrology is dependent on the framework geology, the alongshore variation in groundwater can either exaggerate or partially mask geologic features. For example, in the swash zone, non-linear effects of waves, currents and tides combine to produce a landward-increasing superelevation of the mean freshwater water table (Nielsen, 1990), creating differences between fresh and saltwater than may influence EMI response parameters (i.e., σ_a). Seasonal variations in precipitation (i.e., wet vs. dry conditions) have also been suggested to influence σ_a alongshore (Paine et al., 2004).

Multivariate analysis, LRD, and FARIMA statistical modeling

EMI and DEM morphometric signals can be viewed as a spatial data series and are not dissimilar from other geophysical time-series. For example, fluctuations in river

levels (Hurst et al., 1965), and El Niño phenomenon (Cimino et al., 1999) represent a time-series of which its statistical properties can be analyzed using fundamental tools for modeling non-stationarity, long-range dependence (LRD), self-similarity, and fractal dimensions (see Adelman, 1965; Beran, 1994; Taqqu et al., 1995; Eke et al., 2000; Everett and Weiss, 2002; Doukhan et al., 2003). LRD occurs when the autocorrelations within a series tend to zero like a power function, and so slowly that their sums diverge (Doukhan et al., 2003). It is often observed in nature and is closely related to self-similarity (i.e., fractal dimensions). The intensity of LRD is related to the scaling exponent, or Hurst parameter H of a self-similar process, where $1/2 < H \leq 1$ indicates an increasing tendency towards such an effect (Taqqu, 2003).

Some of the most commonly used statistical methods for analyzing LRD are called fractional autoregressive integrated moving average (FARIMA) models (see Hosking, 1981). FARIMA is a generalization of the ARIMA (p,d,q) process where the degree of differencing d is permitted to take on fractional values to better model LRD (see Hosking, 1981). These models are intrinsically dependent on H and are discussed in detail by Taqqu et al. (1995). An ARIMA model of a time or spatial data series is defined by three terms (p,d,q), where the goal is to determine the integer values (e.g., 0, 1, 2, etc.) of p and q, and either the integer or the fractional values of d that most accurately model the patterns contained within the original data series. Different combinations of (p,d,q) provide important information on how the various length-scales within the framework geology relate to each other. As mentioned above, d is the differencing term that models LRD and it is normally inspected before p and q to

identify whether the process is stationary (i.e., constant mean and σ^2). If the series is nonstationary, it is differenced to remove either linear (d = 1) or quadratic (d = 2) trends, thereby making the mean of the series stationary and invertible (Cimino et al., 1999). This allows determination of the p and q parameters, which indicate the order of the autoregressive (AR) and moving-average (MA) components, respectively. Lazarus et al. (2011) have pointed out that geologic framework features, even if loosely spatially correlated with zones of shoreline change, could affect higher magnitudes of change over large spatial scales. They further suggest that shoreline change at small spatial scales (< 1 km) does not represent a peak in the shoreline change signal, and that change at larger spatial scales dominates the signal. This emphasizes the need for further studies to investigate long-term, large-scale shoreline change with respect to framework geology.

EMI profiling as a new technique for investigating barrier island framework geology

This study is designed to test the utility of EMI profiling as a new technique for mapping large-scale barrier island framework geology, and identifies some of the important applications, benefits, and limitations related to barrier island research. Examples of previous geologic framework studies highlighting traditional techniques used and their limitations relative to EMI are reviewed in Chapter II. The theory of the EMI method, background of portable EMI sensors, and the use of EM techniques in previous coastal research are also discussed. A detailed account of field methods, instrument calibration, and the effect of changing hydrology on EMI signals with respect

to tidal fluctuations and seasonal effects is presented in Chapter III. In Chapters IV and V, signal processing techniques, statistical tests for LRD, and FARIMA models are used to explore the spatial connections of the long-range dependent structure between framework geology and island morphometrics (e.g., beach width, dune volume, and island volume). These chapters provide important insight into the geologic controls on modern barrier island transgression. Lastly, Chapter VI summarizes the key findings from this study and the benefits of EMI sensors for geologic framework research. Recommendations for future studies regarding this new method are proposed and offer potential for an improved understanding of EMI methods for coastal research. The results from this study will benefit coastal geomorphologists, geographers, geologists, engineers and planners concerned with examining the influence of geologic framework on modern barrier response to storms and rising sea-level.

CHAPTER II

REVIEW OF ELECTROMAGNETIC INDUCTION FOR MAPPING BARRIER ISLAND FRAMEWORK GEOLOGY*

Introduction

Along sandy coastlines, stratigraphically-controlled bathymetric features modify hydrodynamic processes on the inner shelf and nearshore, in turn affecting beach morphodynamics along the adjacent shoreline (Riggs et al., 1995). This geologic framework has been suggested to play a considerable role in determining how barrier island systems evolve during storms and in response to local sea-level rise (Hoyt, 1967; Kraft, 1971; Kraft and John, 1979; Kraft et al., 1982; Belknap and Kraft, 1985; Riggs et al., 1995; Dillenburg et al., 2000; Honeycutt and Krantz, 2003; Harris et al., 2005; Lentz and Hapke, 2011). Processes in the nearshore environment including waves, currents and sediment transport exert important controls on nearshore and beach morphology (McNinch, 2004). However, antecedent geology has also been suggested to exert a first-order control on nearshore morphology (e.g., sandbars), which can modify surf zone dynamics and influence beach morphology (McNinch, 2004; Schupp et al., 2006).

The geology of a barrier island represents a time-integrated net depositional record of past coastal forcing, the sequence of which can be reconstructed using

_____

*Reprinted with permission from "Using electromagnetic induction to explore the geologic framework of barrier islands" by B.A. Weymer, M.E. Everett, T.S., de Smet, C. Houser, 2015. *Sedimentary Geology*, 321, 11-24. Copyright [2015] by Elsevier.

traditional geologic principles (Riggs et al., 1995; Woodroffe, 2002). For example, most barrier island systems along the passive continental margins of the U.S. east and Gulf coasts are underlain by Pleistocene (or older) morphostratigraphic features such as incised river valleys (Schupp et al., 2006), inlet channels (FitzGerald et al., 2012) and relict transgressive features (Houser, 2012). These inherited features, in part, affect the exchange of sediment amongst the nearshore, beach and dune, and therefore determine how the island responds to individual storms (Riggs et al., 1995; Schupp et al., 2006; Houser et al., 2008). For example, evidence from Santa Rosa Island, Florida, suggests that ridge and swale bathymetric features along the shoreface are transgressive features that reinforce alongshore variations in dune height and storm response (Houser, 2012). In this respect, the position and distribution of subsurface structures have significant implications for beach and dune morphology, which is a primary control on net barrier island response to rising sea level (Riggs and O'Connor, 1974; Riggs, 1979; Reinson, 1992; Jackson et al., 2005; Houser, 2012). Specifically, alongshore variations in beach-dune morphology not only control storm impacts (i.e., the ratio between wave runup height and dune height), but also determine which areas across the island are most likely to experience overwash and/or blowouts, ultimately governing large-scale barrier transgression (Sallenger, 2000; Morton, 2002; Houser et al., 2008; Houser, 2013; Masselink and van Heteren, 2014). Therefore, an assessment of antecedent geology (i.e., geologic framework) is critical for coastal management and risk assessment for anthropogenically-modified barrier islands (Hapke et al., 2010; Lentz and Hapke, 2011; Lentz et al., 2013).

Studies investigating the geologic framework controls on barrier island evolution

have primarily focused on a specific sub-environment within the barrier island system (Table 2-1). The cross-shore sequence of morpho-sedimentary sub-units was defined as a *coastal tract* by Cowell et al. (2003) and represents the continuum of mutually dependent morphological units. In the offshore direction, the barrier system consists of inner-shelf, nearshore, beach, barrier and lagoon backbarrier sub-environments (Cowell et al., 2003; Van Heteren, 2014). Conversely, the sub-environments in the alongshore direction include the barrier island system, tidal inlets and subtidal deltas. In the analysis of large-scale coastal evolution, the data collection techniques available force an arbitrary compartmentalization of each sub-environment within the barrier island system. Inner-shelf (e.g., Riggs, 1979; Foyle and Oertel, 1997; Schwab et al., 2000; Rodriguez et al., 2001) and nearshore (e.g., Evans et al., 1985; Riggs et al., 1995; McNinch, 2004; Browder and McNinch, 2006) studies mainly use bathymetric and seismic surveys, respectively, because these methods are best suited for shallow water and offshore environments. Conversely, beach and barrier studies (e.g., Otvos, 1970; Riggs et al., 1995; Fitzgerald and Van Heteren, 1999; Morton, 2002; Jackson et al., 2005; Mallinson et al., 2010; Cooper et al., 2012) have tended to use coring and/or remote sensing techniques. It is important to note that the various methods listed above are used for different aims. For example, seismic imaging provides information about structure but cannot be used for dating sediments and/or events. A more detailed discussion of the traditional methods for barrier island research, their benefits and limitations is given in section 3.

Table 2-1. A summary of the coastal sub-system, methods and scientific applications for each of the publications investigating geologic controls on modern barrier island evolution discussed in this review (Weymer et al., 2015).

Coastal Sub-system Investigated	Methods Used	Applications	Relevant Studies
Inner shelf	Seismic surveys, CSEM, sidescan-sonar, cores, sediment samples	Influence of antecedent geology on barrier island development and evolution	(Swift, 1975; Field and Duane, 1976; Foyle and Oertel, 1997; Evans et al., 2000; Schwab et al., 2000)
Inner shelf/nearshore transition	High-resolution bathymetry, sidescan-sonar, subbottom profiles, vibracores, shoreline change analysis, radiocarbon dataing, computer modelling	Influence of antecedent topography and geologic framework on barrier evolution, shoreline change, sediment budget, shoreface equilibrium	(Thieler et al., 1995; Dillenburg et al., 2000; Rodriguez et al., 2001; Hapke et al., 2010)
Nearshore	Seismic, sidescan-sonar, swath/chirp bathymetry, acoustic backscatter, vibracores, historical shoreline positions	Geologic controls on nearshore morphodynamics, preservation potential, shoreline change, implications for coastal management	(Belknap and Kraft, 1985; Honeycutt and Krantz, 2003; McNinch, 2004; Browder and McNinch, 2006; Schupp et al., 2006)
Nearshore/beach transition	Bathymetric surveys, shoreline position surveys, numerical modelling	Importance of geological framework related to the ability of the Bruun rule for hindcasting/forecasting rates of coastal shoreline erosion	(List et al., 1997)
Beach	LiDAR, RTK (GPS), aerial photography, observation, beach profiles	Geologic controls on morphodynamic beach state	(Jackson et al., 2005; Lentz and Hapke, 2011; Lentz et al., 2013)
Beach/barrier transition	GPR, vibracoring, drill cores, observation, aerial photography	Role of geologic framework in determining barrier formation, morphology and shoreface dynamics, storm impacts, barrier classification	(Otvos, 1970; Riggs et al., 1995; Fitzgerald and Van Heteren, 1999; FitzGerald et al., 2001; Morton, 2002; Mallinson et al., 2010; Cooper et al., 2012)
Barrier	Seismic surveys, GPR, EM surveys	Controls on freshwater lens morphology in small barrier islands	(Schneider and Kruse, 2003)
Barrier/lagoon transition	Cores, geophysical logs, radiocarbon dating	Geologic controls on transgressive and regressive barrier sequences	(Kraft and John, 1979)
Lagoon	Cores, probe samples, drill holes, radiocarbon dating	Geologic controls on barrier island transgression	(Kraft, 1971)
Entire barrier system	Seismic surveys, drive sampler and rotary core borings, vibracores, trenching, radiocarbon dating, digital shoreline plots	Geologic controls on the formation and evolution of barrier island systems, erosion and sediment availability, coastal restoration/management	(Fisk, 1959; Evans et al., 1985; Williams et al., 1991; Harris et al., 2005; Kulp et al., 2005; Mallinson et al., 2010)

Despite the utility of these methods, coring provides only point-source information and in many cases limited penetration depth, whereas the seismic method is not well suited for land-based surveys in unconsolidated, sandy sediments (Leatherman, 1987; Smith and Sjogren, 2006; Schrott and Sass, 2008). Thus, coastal researchers began to turn to other geophysical techniques such as electrical resistivity tomography (ERT) and ground-penetrating radar (GPR). Used since the 1980's, GPR techniques provide high-resolution imagery of subsurface stratigraphy, thereby improving interpretations of geologic controls on barrier island evolution (e.g., Leatherman, 1987; Van Heteren et al., 1994; Jol et al., 1996; Bristow et al., 2000; Neal and Roberts, 2000; Buynevich and Fitzgerald, 2003; Mallinson et al., 2010). Over the past decade, ERT has become an increasingly used method for time-lapse monitoring of saltwater intrusion dynamics (e.g., Bauer et al., 2006; Adepelumi et al., 2009; Martinez et al., 2009; Zarocca et al., 2011) and migration of contaminant plumes in coastal aquifers (e.g., Cassiani et al., 2006). Collectively, some of the strengths and weaknesses of each method used for barrier island studies are summarized in Table 2-2. Because each method is best suited for a particular sub-environment, only a few studies have integrated multiple methods to explore the role of geologic inheritance on large-scale barrier island evolution (see Fisk, 1959; Evans et al., 1985; Williams et al., 1991; McBride et al., 1995; Harris et al., 2005; Kulp et al., 2005; Mallinson et al., 2010).

Table 2-2. The advantages and limitations of various geological, geophysical, bathymetric and remote sensing methods used for barrier island geologic framework research (Weymer et al., 2015).

	Method	Advantages	Limitations
Geological	Coring (all types)	Relatively cheap, true geologic information	Invasive, provides only point-source information
Geophysical (terrestrial)	Terrestrial seismic	No signal attenuation by salinity	Slow method, not effective in unconsolidated beach/barrier sediments
	GPR	High resolution, can image subsurface structure directly	Significantly affected by saltwater, relatively expensive
	ERT	Capable of imaging complex subsurface structures, used for mapping fresh and saltwater dynamics, portable	Time consuming, expensive, measurements sensitive to electrode contact and different survey configurations
	EMI	Can probe multiple depths simultaneously, not affected by salinity, inexpensive, can cover large areas rapidly	Requires modeling and inversion to interpret data, can only distinguish a few layers
Geophysical (marine)	Marine seismic	Fast data acquisition, capable of both high resolution and deep subsurface investigations	Expensive, limited to either offshore/lagoon environments
	CSEM	Capable of detecting features missed by seismic, can cover large survey areas	Expensive, time consuming, difficult to operate in shallow water
Bathymetric	Single beam sonar	Widely used and capable of being deployed by all types of vessels	Does not have the best coverage and resolution
	Multibeam sonar	Better horizontal and depth resolution than single beam sonar systems, ideal for large-scale surveys	Data quality sensitive to ship maneuverability, complex setup, expensive
	Sidescan-sonar	Provides high-resolution images of the seafloor	Not capable of providing subsurface information
	Chirp-sonar	Wide spectrum of sonar signals used providing high-resolution images of the seafloor	More expensive than other types of sonar systems
Remote Sensing/GIS	Terrestrial LiDAR	Very high-resolution, useful to compare surficial landscapes with subsurface structures	Expensive, does not provide subsurface information
	Aerial LiDAR	Can cover large areas, high-resolution 3D data	No subsurface information, expensive to collect

All geophysical techniques are ultimately constrained by subsurface hydrology including saltwater intrusion and groundwater table position. The relationship between subsurface geologic structures and hydrologic processes in barrier islands is not well known

(Horn, 2002). Most coastal hydrology studies have focused either on nearshore/swash zone hydrodynamics (e.g., Lanyon et al., 1982; Nielsen, 1990; Hegge and Masselink, 1991; Gourlay, 1992; Turner, 1993; Oh and Dean, 1994; Horn, 2002) or hydrologic processes in backbarrier/lagoon environments (e.g., Amdurer and Land, 1982; Kocurek et al., 1992; Nielsen, 1999; Stevens et al., 2009). With the notable exceptions conducted by Nielsen and Kang (1996), Reide Corbett et al. (2000), and Ruppel et al. (2000), there is a paucity of information regarding groundwater dynamics throughout barrier island systems. Most coastal groundwater studies have relied on monitoring wells, piezometers and pressure transducers to monitor groundwater dynamics, such as the beach watertable response to low-frequency and wave tidal forcing (Horn, 2002).

There are alternative data collection techniques available that have yet to be fully explored in coastal environments. For example, a variety of electromagnetic (EM) methods have potential for coastal environmental and engineering applications including; time-domain airborne transient electromagnetic (TEM) surveys (e.g., Vrbancich, 2009, 2012; Christensen and Halkjær, 2014), marine controlled-source electromagnetic (CSEM) surveys (e.g., Cheesman et al., 1993; Evans et al., 1999; 2000; Barker et al., 2012), and frequency-domain electromagnetic induction (EMI) surveys (e.g., Ruppel et al., 2000; Paine et al., 2004; Seijmonsbergen et al., 2004). EM sensors are designed to map subsurface geoelectric properties and, as such, they can help distinguish spatial variations in subsurface lithological and hydrological properties (including water content, porosity, clay content, etc). Whilst aerial TEM surveys are capable of characterizing large areas over land and water, they are not considered in this review (see Viezzoli et al., 2008; Auken et al., 2009; Vrbancich, 2009,

2012). Terrestrial EMI surveys are useful in coastal habitat classification, mapping subsurface lithology and monitoring groundwater dynamics (e.g., Paine et al., 2004). Despite the many benefits of using these different methods in combination, there are a number of limitations that need to be better understood before the EMI technique can be used with confidence in barrier island research.

This paper reviews the theory and applications of the EMI geophysical method and identifies some of the important applications and problems related to barrier island geologic framework and groundwater research. First, a conceptual background on the spatial relationships between geomorphological features and EMI response parameters, or "signals" is discussed (Section 2.2). Examples of previous geologic inheritance research emphasizing the techniques used and their limitations relative to EMI is presented (Section 2.3). A basic overview of EM theory and EMI techniques with respect to coastal environments is then given (Section 2.4). Lastly, the paper summarizes the benefits of EMI sensors for geologic inheritance research and proposes recommendations for future studies to address key limitations.

Geomorphological mapping using electromagnetic sensors

Geologic features within barrier island systems occur naturally over a range of spatial scales (Figure 2-1). Large-scale geologic features including Pleistocene-Holocene fluvial/deltaic paleo-channels and incised river valleys that are remnant features from the last major glaciation (~20 kyr) and are found in most barrier island systems along the Atlantic and Gulf Coasts of the United States (e.g., Otvos, 1970; Kraft, 1971; Belknap

and Kraft, 1985; Morton et al., 1996; Foyle and Oertel, 1997; Browder and McNinch, 2006; Mallinson et al., 2010). During the late Holocene transgression (~6 kyr), these features were commonly overtopped and subsequently buried (Figure 2-1A). Washover channels and blowouts develop within sections of the beach that have lower dune heights. These features occur over shorter length-scales ranging from tens to hundreds of meters (Figure 2-1B). Smaller geomorphic features such as embryo or protodunes, welded bars and beach cusps develop over even shorter length-scales, less than tens of meters (Figure 2-1C). It is argued that buried antecedent geology influences the various length-scales of modern geomorphic features alongshore (Houser, 2012).

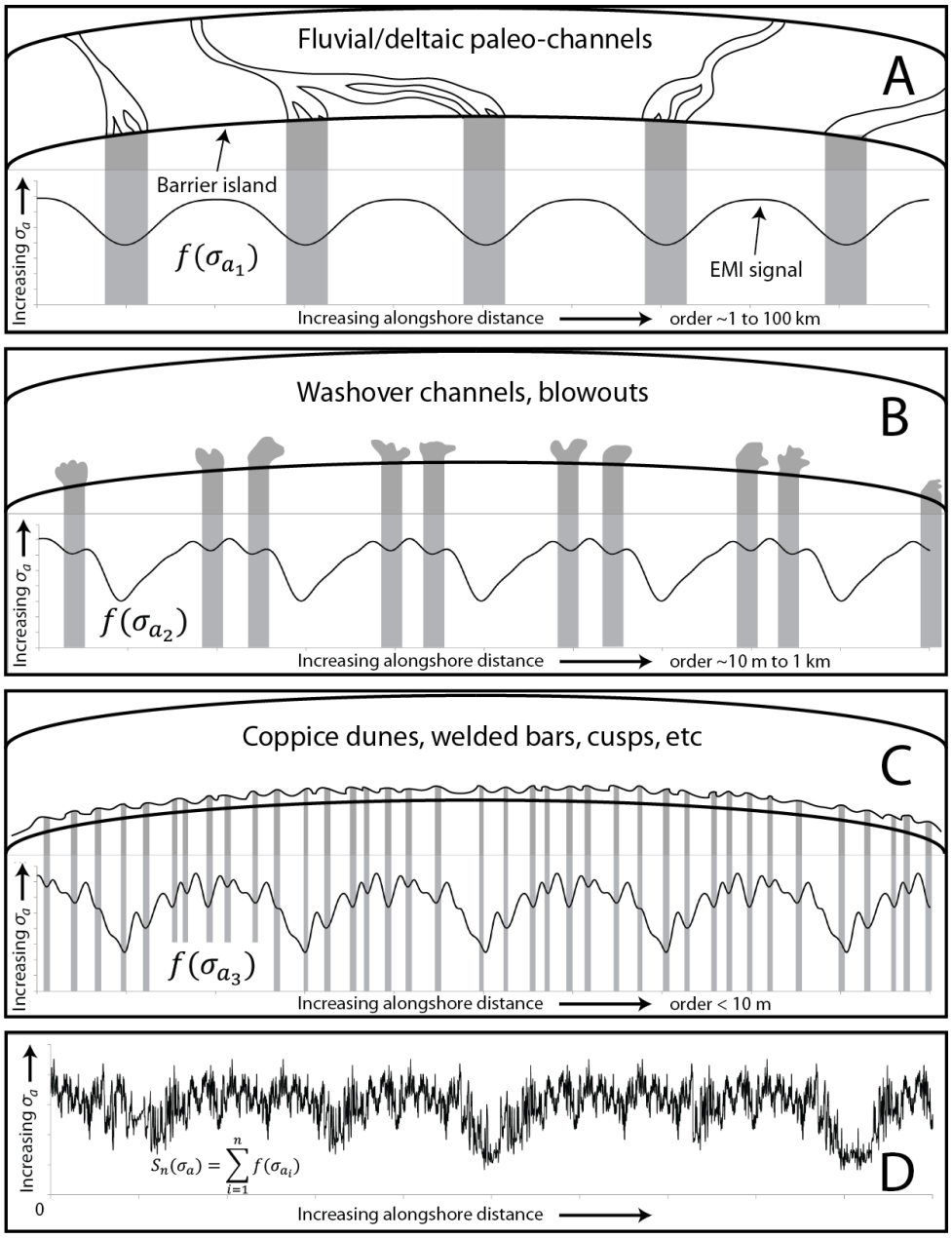

Figure 2-1. Schematic diagram depicting hypothetical geologic features along a barrier island at a variety of length-scales. Below each feature is a hypothetical EMI signal, representing different wavelengths between geologic structures. The long wavelengths indicate large-scale geologic framework, such as paleo-channels (A). Meso-scale features (e.g., washover channels) occur at moderate wavelengths (B). Small-scale features (e.g., welded bars) occur at increasingly smaller wavelengths (C). Each higher-frequency signal is superimposed on the lower-frequency signals, where the sum of all signals results in the complex, potentially non-stationary time series (D) (Weymer et al., 2015).

Variations in geologic features and hydrology are directly related to changes in subsurface geo-electric properties measured by an EMI sensor. A hypothetical EMI response parameter, for example, apparent conductivity (σ_a), is shown as a spatial data series in the bottom panel of Figure 2-1, in which the lowest-wavenumber signals are associated with geologic features that occur over the longest length-scales (e.g., Figure 2-1A). As the length-scale of the geologic features increases, so does the dominant wavenumber of the EMI signal (Figures 2-1B-C). The composite EMI spatial data series is shown in Figure 2-1D, where the overall signature is tsuperposition of many different-scale sedimentary processses. The total apparent conductivity $f(\sigma_a)$, for example, can be regarded as multiple-scale EMI responses piggy-backing on top of each other, i.e.

$$S_n(\sigma_a) = \sum_{i=1}^{n} f(\sigma_{a_i}) \tag{2.1}$$

where, *S* and *f* are functions, and *n* is the number of important length scales. There is mutual inductive coupling "to first order" between the various geological structures of different length-scales, such that Equation (1) is only a first-order approximation to the actual EMI signal. By further investigating the various important length-scales with LiDAR, vibracores and other data types, it is sometimes possible to relate the length-scales of variations observed in the EMI profiles to buried and exposed geological structures. Accordingly, an EMI spatial data series can be treated as if it is a time-series, and analyzed using fundamental tools for properties such as non-stationarity, long-range dependence, or long swings, etc. (see Adelman, 1965; Beran, 1994; Taqqu et al., 1995; Eke et al., 2000; Everett and Weiss, 2002; Doukhan et al., 2003).

Because an EMI data series is essentially a function of subsurface geoelectric properties, the groundwater dynamics within the barrier need to be taken into account when interpreting the data. The apparent electrical conductivity σ_a measured by an EMI sensor is directly related to the overall distribution of saline and freshwater (Christensen and Halkjær, 2014). Within barrier islands, the hydrologic regime is further controlled by wave action, currents, tides, precipitation, atmospheric pressure, weather/climate and framework geology (Nielsen, 1999; Horn, 2002). Similar to the length-scale-dependent structure of spatially-varying geologic features described above (refer to Figure 2-1), water table fluctuations may also vary at a range of temporal scales from seconds (waves), to hours (tides) to days/months (precipitation events and seasonal effects). Freshwater-saturated sediments and seawater are significantly more conductive than dry sand, therefore the location of the water table and the freshwater-seawater interface profoundly affect EMI response parameters, and is further discussed in section 2.4.6.

Traditional methods of research into barrier island geologic inheritance

Various geological, geophysical, bathymetric and remote sensing methods have been used to investigate the geologic controls on barrier island development and evolution (Table 2-2). The techniques chosen for a particular study are often determined by the sub-environment under investigation, as well as the aims and scale of the study. Most barrier coastlines are influenced by inherited geologic features (e.g., incised river channels) that occur beneath and seaward of the shoreface (Riggs et al., 1995). The studies reviewed in the following section are categorized into four general sub-

environments within the barrier island system 1) inner-shelf, 2) nearshore, 3) beach, and 4) backbarrier/lagoon. Examples of the main methods used in each sub-environment are presented and their advantages and limitations relative to EMI are discussed. Examples of EMI methods for coastal applications are further discussed in Section 2.4.4.

(1) Studies on the inner-shelf have almost exclusively used various seismic methods and/or coring techniques to investigate the influence of antecedent geology on the origin and evolution of barrier islands (e.g., Field and Duane, 1976; Foyle and Oertel, 1997; Schwab et al., 2000; Rodriguez et al., 2001). The first marine seismic surveys for this purpose were conducted in the 1980's and remain the standard method for mapping stratigraphy beneath the seafloor. Marine seismic surveys are often validated by coring and/or borehole logging (down-hole logging), but can also be augmented by electromagnetic surveying (Cheesman et al., 1993; Evans et al., 1999; Evans et al., 2000). Since the late 1990's geophysicists have increasingly turned to marine controlled-source electromagnetic (CSEM) methods for mapping fluid resistivities and providing bulk porosity estimates in areas previously characterized by seismic methods (Cheesman et al., 1993). It is important to note that marine CSEM methods use grounded (galvanic) sources and are different from the inductive techniques that are described in more detail in section 2.4.1. In some instances seismic and/or borehole data are affected by highly resistive bodies (i.e., low conductivity) that present significant seismic imaging challenges because of velocity and density contrasts (Barker et al., 2012).

The principle for using CSEM methods is based on the distribution and amount of seawater within seafloor sediments as well as the bulk resistivity structure of the

sediments. The electrical resistivity of sediment is directly related to porosity, which is also related to other physical properties including grain-size and texture (Evans et al., 1999). Thus, variations in lithology as related to porosity can be estimated and interpreted from measurements of electrical resistivity/conductivity by a marine EM system (Cheesman et al., 1993; Evans et al., 2000). For example, Evans et al. (2000) conducted an EM survey off the New Jersey coast (USA) to map the porosity structure of the continental margin. Two areas were surveyed in water depths of ~70 m that have been shown to contain buried paleo-channels previously interpreted from seismic surveys. A towed frequency-domain EM system measured apparent resistivities at ~ 2, 7 and 20 m depths below the seafloor, providing structural information of the underlying sediments (Evans et al., 2000). Apparent resistivity measurements were converted into porosity values allowing for detailed interpretations of the conditions under which the paleo-channels formed. Two distinct EM responses were measured across the seismically-imaged paleo-channels; one where higher (%) porosity matched the location of the channels, while the other failed to respond to the seismically observed channel (Evans et al., 2000). The EM response that captured the paleo-channels was located in an area where the channels incised the regional seismic reflector, whereas, the "failed response" was in an area where the paleo-channels did not incise the regional seismic reflector. Nevertheless, Evans et al. (2000) suggest that when combined with seismic and/or coring, EM surveys are a powerful tool to better understand offshore geologic structure.

(2) Nearshore studies on framework geology have utilized cores, seismic surveys,

sidescan-sonar, chirp bathymetry and acoustic backscatter profiling sensors (e.g., Belknap and Kraft, 1985; Honeycutt and Krantz, 2003; McNinch, 2004; Browder and McNinch, 2006; Schupp et al., 2006). High-resolution bathymetric and sidescan-sonar surveys are particularly useful for investigating nearshore bathymetric features (e.g., ridges and troughs). These types of surveys are useful for imaging the surface of the seafloor but are not capable of providing subsurface information. As noted above, marine seismic methods provide high-resolution subsurface information but shallow nearshore water depths (< 30 m) present significant logistical challenges for collecting seismic data. Alternatively, marine CSEM methods can be conducted in relatively shallow water depths ~30 m (Evans et al., 1999). Although portable EMI sensors are typically used in land-based applications, it is possible that they could also be used in the nearshore if properly calibrated and secured on a vessel that can navigate shallow water depths. In theory, portable EMI sensors could potentially measure a continuous subsurface profile across the nearshore and into the beach environment.

(3) Geologic framework studies regarding beach environments have been conducted by direct observation and beach profiling or by a combination of geologic, geophysical and remote sensing methods including cores, GPR, LiDAR and aerial photography (e.g., Riggs et al., 1995; Jackson et al., 2005; Mallinson et al., 2010; Lentz and Hapke, 2011; Lentz et al., 2013). Jol et al. (1996) suggest that although vibracoring provides inexpensive point-source information, this method provides limited depth penetration in unconsolidated sediments along coastal barriers. GPR may be able to accurately infer stratigraphic trends at cm-scale resolution along a continuous transect for hundreds of

meters to several kilometers, however. Therefore, they proposed that GPR is the most promising method available for coastal subsurface investigations. Presently, GPR remains one of the most powerful tools for investigating subsurface structures, however brackish/saline groundwater attenuates the GPR signal, often rendering the data uninterpretable (i.e., signal to noise ratio is too low). EMI signals can probe to greater depths because they operate at frequencies that are several orders of magnitude less than GPR (i.e., kHz instead of MHz). It is important to note that the physics are different between GPR and EMI, where the former propagates as a radar wave and the latter is a diffusive process. Nonetheless, EMI techniques can provide additional subsurface information over much larger areas in conductive environments compared to coring and/or GPR. Inductive methods are sensitive to conductive zones while galvanic methods are more sensitive to resistive zones. Herein, for the scope of this paper, we focus on EM methods with inductive sources.

(4) Relatively few studies on barrier evolution have been conducted across the barrier and into bay/lagoon environments (e.g., Kraft, 1971; Kraft and John, 1979; Schneider and Kruse, 2003; Garrison et al., 2010). Most of the methods used for these studies include various types of coring, seismic and GPR. The width of barrier islands ranges from less than 1 km up to several km, in the latter case presenting significant logistical challenges for collecting data across highly variable topography and dense vegetation cover. Shallow seismic techniques do not provide the resolution needed for detailed stratigraphic interpretation. Leatherman (1987) suggested that seismic surveying alone is unlikely to produce meaningful results on barrier islands and stratigraphic

correlations are difficult based on borehole data. However, seismic surveys may be useful for subsurface investigations within the bays/lagoons. Coring is invasive and in some protected areas is not permissible across the barrier/tidal flats. GPR is a viable alternative; however, as mentioned earlier the radar signal is attenuated in saline environments such as tidal flats and problems with muddy sediments. In comparison, EMI surveys conducted by Paine et al. (2004) successfully mapped subsurface features across the entire barrier island system including wind-tidal flats in Mustang Island, Texas (USA). From the above examples it is evident that EMI sensors can be used across the entire barrier island system, thus providing complementary and in some instances unique geophysical data in support of conventional geological methods.

The theory of the EMI geophysical method in coastal environments

The electromagnetic geophysical method

There are two classes of controlled sources used in the electromagnetic geophysical method. Depending on the application, either a *grounded* type or an *inductive* type may be used. In the grounded (or galvanic) type, direct electrical contact with the ground is made using electric dipoles as in the resistivity method. Conversely, in the inductive type, direct electrical contact with the ground is avoided by using for example an insulated wire-loop source (Everett, 2013). For the scope of this paper, only the inductive loop sources will be considered, mainly because galvanic sources are not "portable" and/or "easy-to-use." In the electromagnetic induction method the geologic medium under investigation, which could include a conductive target and its host, is

assumed to be electrically neutral. Any representative volume of the subsurface contains large, but equal numbers of positive and negative charge carriers. Some of the charge carriers are mobile while others are bound in place. Only the mobile charges play a role in shaping the low-frequency (quasi-static) EMI response (see Larsson, 2007). Everett (2013) explains that a voltage develops along any arbitrary closed path within a conducting body that is exposed to a time-varying magnetic field $\vec{B}(t)$. The notation used here for the primary and secondary magnetic fields is $\vec{B}_p$ and $\vec{B}_s$, respectively. In the CSEM method, the time variation of the primary $\vec{B}$ field is controlled by the geophysicist. The mobile charge carriers migrate with an average drift velocity v_d in response to the applied changing magnetic flux $\frac{\partial \vec{B}_p}{\partial t}$. The electrical conductivity σ is related to the density and mobility of the charge carriers by:

$$\sigma = nqm \tag{2.2}$$

where *n* is the number density of mobile charges, *q* is the mobile charge carrier, and *m* is the charge-carrier mobility (Gueguen and Palciauskas, 1994; Kittel, 2004). The drift of mobile charges constitutes the induced current that acts as a secondary source of electromagnetic field, in turn generating the response measured by an EMI sensor.

EMI signal penetration is limited by the conversion of the transmitted electromagnetic energy into kinetic energy of the mobilized subsurface charge carriers (Huang, 2005; Everett, 2013). Correspondingly, the depth probed by an EMI system depends on the rate of signal loss, or attenuation, in the subsurface. The higher the electrical conductivity σ, the greater the attenuation, thus reducing the depth of

investigation. The exponentially-decaying attenuation of signal with depth is known as the *skin effect*. The signal loses 1/e ~ 0.368 of its incident amplitude after penetrating one *skin depth* δ:

$$\delta = \sqrt{\frac{2}{\mu\sigma\omega}} = \frac{\sqrt{2i}}{\gamma} \tag{2.3}$$

where σ is the conductivity of the medium, μ is the magnetic permeability, $\omega = 2\pi f$ is the angular frequency and $\gamma = \sqrt{i\omega\mu_0\sigma}$ (McNeill, 1980). It is important to note that the term *depth of investigation* is not synonymous with *skin depth*. The depth of investigation is an empirical quantity and is affected by the heterogeneous geoelectrical properties of the medium as well as factors such as sensor sensitivity, accuracy, frequency, transmitter (TX) strength (dipole moment), coil configuration and offset, ambient noise, and data processing and interpretation methods (Huang, 2005). Under ideal conditions the depth of investigation is greater than the skin depth. However, in geologically complex and/or environmentally noisy areas, the depth of investigation can be less than the skin depth (Huang, 2005). In highly conductive barrier island systems, the depth of investigation is primarily affected by saltwater and/or changes in subsurface sand vs. clay content. Areas that have more saltwater (i.e., beach, tidal flat environments) reduce the depth of investigation, whereas areas that are drier, have thicker deposits of beach sand, or have reduced salinity (i.e., dunes, washover channels, valley-fill sequences) have a greater depth of investigation.

EMI response and computation of apparent conductivity

Finite-source excitation of a plane-layered Earth is a fundamental problem in near-surface applied geophysics (Everett, 2013). The electromagnetic response of a horizontal loop source of finite radius is controlled by the separation between the transmitting (TX) and receiving (RX) coils. Conversely, a loop of infinitesimal radius is called a "point dipole." With a large offset, $s \gg a$, the response of a loop-source of finite radius a can be approximated as the response of a dipole point. For clarification, δ is the skin depth, a property of the medium, whereas s is the TX-RX offset, a property of the apparatus. The depth of investigation depends on both the TX-RX coil offset and the frequency, which increases either by increasing the TX-RX coil offset or by decreasing the frequency.

The EM response of a uniform half-space for vertical magnetic dipole excitation is given by Frischknecht (1967), Ward (1967), Ward and Hohmann (1988) and others. The term *uniform half-space* used in this paper means the Earth has a uniform physical property value over the entire footprint of the geophysical sensor under consideration. For EMI sensors, if the TX/RX coils are both at height h above a uniform half-space, the secondary magnetic field H_s normalized by the primary field H_0 at RX is:

$$\left(\frac{H_s}{H_0}\right)_v = s^3 \int_0^\infty R(\lambda)\lambda^2 \exp(-2\lambda h) J_0(\lambda s) d\lambda \qquad (2.4)$$

where v denotes the response for a vertical dipole, s is the coil separation and J_0 is the Bessel function of the zeroth order. The reflection coefficient $R(\lambda)$ term can be written as:

$$R(\lambda) = \frac{\lambda - u_1}{\lambda + u_1} \quad (2.5)$$

where u_1 for a homogenous half-space is:

$$u_1 = \sqrt{\lambda^2 + iw\sigma\mu_0} \quad (2.6)$$

Most barrier islands are predominantly non-magnetic (i.e., mainly quartz sands), therefore $\mu = \mu_0$, the permeability of free space. Under certain conditions the expressions (Equation 4) can be simplified, if $s \ll \delta$ is used, this is known as the *low induction number* (LIN) approximation (McNeill, 1980, 1996). The LIN approximation is related to the skin depth δ (Equation 3) where the ratio of the coil spacing s to the skin depth δ (i.e., s/δ) is defined as the induction number B:

$$\gamma s = \sqrt{2i}B \quad (2.7)$$

If the coil separation is much less than the skin depth ($s \ll \delta$), Equation 4 reduces to the simplified expression:

$$\sigma_a = \frac{4}{\omega\mu_0 s^2}\frac{H_s}{H_0} \quad (2.8)$$

where $\frac{H_s}{H_0}$ are the imaginary parts while ω and s^2 depend on the frequency and coil offset, respectively (McNeill, 1980). A more detailed discussion of the LIN approximation is explained in the next section. The complex quantity H_s/H_0 when multiplied by 10^6 is expressed in parts per million (ppm) and consists of a real (in-phase; I) and an imaginary (quadrature; Q) component. EMI sensors typically record these variables, along with apparent conductivity σ_a. Apparent conductivity σ_a is related to the complex quantity $\frac{H_s}{H_0}$ by Equation 2.8. Since the ground is always heterogeneous, σ_a is actually a frequency-

dependent, spatial average of the underlying conductivity distribution between the TX and RX coils within the sensor footprint (Everett and Weiss, 2002).

Apparent conductivity is defined as the conductivity of a homogeneous half-space that would produce the same response as the one measured over the real Earth with the same sensor (Huang and Won, 2000). Apparent conductivity has units [S/m], whereas the normalized in-phase (I) and quadrature (Q) responses [ppm] are dimensionless. Apparent conductivity may be derived from either the in-phase or quadrature responses (Won et al., 1996), moreover it can be defined in a variety of ways (Huang and Won, 2000). All definitions of σ_a reduce to the actual conductivity σ when the Earth is a uniform half-space, but yield different results when the Earth is heterogeneous. The output of commercial sensors is generally the LIN σ_a and conversion to the quadrature component is simply performed by division by a constant for a given coil configuration. For the context of this paper, only the conventional definition of σ_a based on Equation 8 developed by (McNeill, 1980) will be considered, because this is the definition that is used in Geonics™ and GSSI™ terrain conductivity sensors, which are commonly available commercial field instruments.

Portable EMI sensors

Unlike traditional EMI sensors which are bulky and operate at a single frequency, newer, portable profilers record multiple frequencies simultaneously. Portable sensors are popular because they are relatively inexpensive and can cover large distances over a short amount of time. Portable EMI sensors normally consist of a fixed TX/RX geometry

(Figure 2-2). There is a variety of lightweight sensors available on the market including GSSI™, Geophex™, Dualem™, PROMIS™, GF Instruments™ and Stratagem™ systems. For example, the GSSI Profiler EMP-400™ sensor shown in the figure operates at three discrete frequencies simultaneously, selectable from the range 1-16 kHz in 1 kHz increments (Geophysical Survey Systems, 2007). The advantage of using multiple frequencies is based on the skin effect, as low-frequency signals probe deeper within the subsurface, whereas high-frequency signals are more sensitive to shallower structures. Depth sounding is achieved either by changing the separation between the TX/RX coils, which can be time-consuming, and moreover, it is difficult to maintain a precise coil separation. Additionally, depth sounding is also done by using several frequencies or by having multiple receivers at various coil spacings in a fixed housing (e.g., DUALEM 421S). Scanning through a range of frequencies is equivalent to depth sounding. It is important to note that there is a complicated relationship between changing frequency vs. changing the TX-RX offset, and detailed sensitivity studies should be conducted (refer to Guillemoteau et al., 2015). For shallow surveys, the frequency sounding method offers high spatial resolution, fast survey speed, simple logistics, and good data precision (Won et al., 1996).

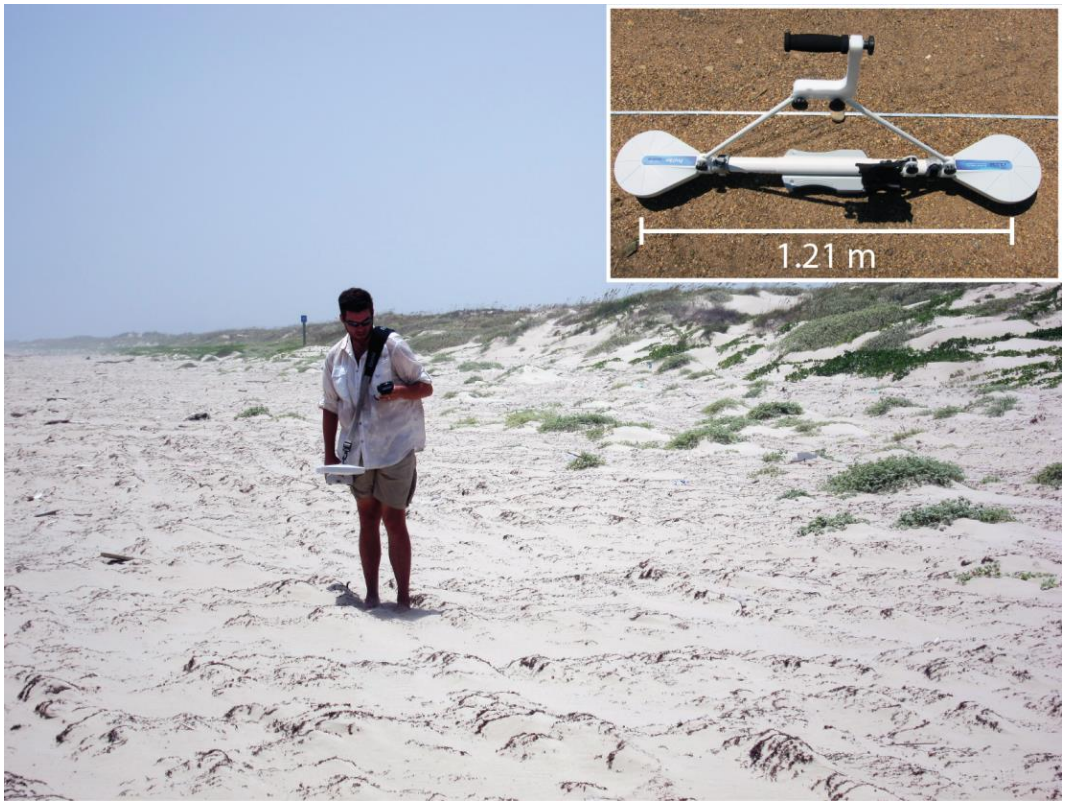

Figure 2-2. Example of a handheld GSSI Profiler EMP-400™ being used in the backshore environment at Padre Island National Seashore, Texas. The instrument is oriented in the vertical dipole (VD) orientation, in-line mode (*P-mode*). Person is facing in the direction of the profile. The fixed coil-separation between the transmitter (TX) and receiver (RX) is 1.21 m. Operating frequencies range from 1-16 kHz, where three frequencies can be recorded simultaneously during data acquisition. Image taken August 6, 2013 (Weymer et al., 2015).

Because EMI sensors are capable of probing multiple depths by varying the operating frequency, it is possible to map the underlying geoelectric depth structure. A common approach to differentiate changes in σ_a with depth is the use of EM inversion techniques (Santos et al., 2010), however, analysis of parameter uncertainty is equally important as an estimate of parameter values, but is unfortunately often overlooked

(Minsley, 2011). The notion that multi-frequency sensors are capable of depth sounding has been controversial in the EM geophysics community. McNeill (1996) argues that the use of multiple frequencies in a fixed-offset low induction number (LIN) instrument does not offer a significant advantage over a single-frequency system. McNeill (1996) suggests that in order to obtain useful geoelectric information about a layered Earth, a multi-frequency EMI sensor with a short intercoil spacing (e.g., 1.21 m) would require a frequency range into the MHz range, whereas most conventional sensors operate in the tens of kHz range. However, in an extraordinarily conductive environment the apparent conductivity may be sensitive to different aspects of the layering at different frequencies (McNeill, 1996).

Barrier islands are highly conductive environments and, as noted by McNeill (1980), as the terrain conductivity increases the instrument output σ_a is no longer proportional to the terrain conductivity. The LIN approximation breaks down and is especially critical for coastal EMI surveys (see Guillemoteau et al., 2015). In other words, in conductive environments where $\sigma_a > 50$ mS/m, there is a departure of measured σ_a from "true" conductivity σ, reducing the depth of investigation and increasing measurement error. A growing number of studies have investigated the effects of high conductivity on EMI signals and have proposed correction factors that can be applied to resolve this dilemma (e.g., McNeill, 1980; Sudduth et al., 2001; Beamish, 2011; Delefortrie et al., 2014b). For example, Beamish (2011) examined the effects of high conductivity in a beach environment on the departure of the LIN condition using a handheld multi-frequency EMI sensor. Beamish (2011) demonstrates theoretically and experimentally that the magnitudes and form of the spatial EMI measurements may be increasingly distorted in a nonlinear fashion

across data sets displaying variable conductivity. Therefore, he developed a simple correction procedure and look-up table (nomogram) where the user can convert measured σ_a values into LIN-equivalent corrected σ_a for a specific coil configuration. It is argued that, since EMI sensors now have a wide, non-geophysical user base, investigators should take into account the LIN breakdown, especially if working in conductive (i.e., coastal) environments (Beamish, 2011).

Other important issues that can affect the quality and interpretation of EMI data include random and systematic errors. Random errors from instrument and cultural noise can typically be reduced by applying a spatial low-pass filter to the data. However, systematic errors can have numerous sources including instrument calibration errors, drift, and improper data leveling (Minsley et al., 2012). These systematic errors are more difficult to account for and can negatively impact inversion of the data and ultimately data interpretation. Calibration methods have been developed to correct for errors in instrument gain, phase, and bias (Deszcz-Pan et al., 1998). For example, correction factors which minimize differences between measured and calculated values can be obtained by a least-squares method, thus reducing inversion misfit error. Nonetheless, it is critical to ensure the instrument is properly calibrated in the field prior to each survey to account for environmental conditions and the presence of the operator.

Past examples of coastal EMI surveys

The majority of EMI applications in the coastal environment has focused on saltwater intrusion (e.g., Fitterman and Stewart, 1986; Fitterman and Deszcz-Pan, 1998;

Duque et al., 2008; Wiederhold et al., 2010; Kirkegaard et al., 2011; Delefortrie et al., 2014b). Of these studies, most have utilized aerial TEM systems. To date, only a handful of coastal/barrier island studies known to the authors have used terrestrial EMI techniques to investigate subsurface geology and/or groundwater in relation to the surficial landscape (Paine et al., 2004; Seijmonsbergen et al., 2004; Weymer et al., *accepted*). For these studies, EMI surveys were either oriented in the cross-shore direction (Paine et al., 2004) or in the alongshore direction (Seijmonsbergen et al., 2004). The following section summarizes the advantages and drawbacks of using EMI techniques for coastal geologic framework research.

In the cross-shore direction, Paine et al. (2004) used a Geonics EM38™ at 15 kHz to measure changes in σ_a at an exploration depth of 0.8 m (horizontal dipole mode) and 1.5 m (vertical dipole mode) at 20 m station spacing. The objective of the study was to test whether a combination of EM and LiDAR data improve the accuracy and resolution of coastal wetland mapping that has traditionally been based on the analysis of aerial photographs and ground-based vegetation surveys. Two ~2.5 km transects were collected in December, 2003, across a variety of coastal sub-environments on Mustang Island (south Texas Gulf Coast). For example, the sub-environments that were mapped include the beach, dune, vegetated-barrier flat, fresh marsh, salt marsh, and wind-tidal flats. Paine et al. (2004) suggest that most coastal sub-environments have distinct average elevations, but relatively wide elevation ranges that potentially overlap other habitats and environments. Although LiDAR is useful for habitat classification from digital elevation models (DEM's), dense vegetation cover may produce anomalous elevations that may be significantly higher than

the ground elevation, thus leading to the misclassification of a particular habitat. If the difference between the top of the vegetation mass and the ground surface is known, these heights can be subtracted to produce a corrected ground-surface elevation profile. Comparing LiDAR data with EMI surveys, Paine et al. (2004) suggest that changes in conductivity measured by the EMI sensor are inversely correlated to LiDAR-derived elevations. However, the relationship to elevation in the cross-shore is simply a demonstration of how the sensor is able to detect sand content, which may be independent of topography (i.e., in the alongshore direction). They also found that conductivity closely tracked changes in salinity across each coastal sub-environment and proposed that EMI data can be used to distinguish habitats and geomorphic units to the same level achievable as ground-based vegetation surveys. However, they recommended that further investigation is needed to address seasonal changes in salinity across the barrier island.

In the alongshore direction, Seijmonsbergen et al. (2004) used a Geonics EM34™ oriented in the horizontal dipole mode with a coil separation and station spacing of 20 m, respectively. This configuration resulted in an exploration depth of ~ 15 m, which is a roughly-defined parameter. A continuous 14.5 km-length EMI transect was collected along the backbeach and across a former outlet of the Rhine River to test the sensor's ability to distinguish variations in subsurface lithology. The survey was conducted in an area that was previously characterized by drill hole data and these were used to validate the σ_a measurements. The results from their study suggest that coastal sediments can be classified according to their apparent conductivity. The range of σ_a values was categorized into three groups (i.e., low, medium and high). The first group of low σ_a

(20-45 mS/m) and low-variation amplitudes was interpreted as beach sands. The second group of medium σ_a values (20-90 mS/m) and large variability corresponded to clay and peat layers of varying thickness. A third group of high σ_a values (60-190 mS/m) and large variability was interpreted as clay rich brackish channel deposits. They further suggest that high σ_a values occur in areas where the conductive layer is thick and close to the surface. Although Seijmonsbergen et al. (2004) suggest that EMI surveys are a rapid, relatively inexpensive method to investigate subsurface lithology they also acknowledge that variations in salinity as a result of storm activity and/or sea-level change should be investigated in further detail (i.e., salinity vs. lithology tradeoff).

Demonstration of EMI in support of this review

To test the capability of a handheld portable EMI sensor in detecting subsurface changes in framework geology, a ~10 km alongshore EMI survey was collected Padre Island National Seashore, Texas (USA) to test how well the EMI sensor could detect a network of inferred (buried) Pleistocene streams identified by Fisk (1959). A multi-frequency GSSI Profiler EMP-400™ was used in the inline vertical dipole mode and used 3, 10 and 15 kHz frequencies corresponding to skin depths of ~ 5, 3 and 2 m, respectively. All of the EMI surveys were conducted in a region of previously identified Pleistocene fluvial paleo-channels and streams (Fisk, 1959) as determined from ~3000 deep drive-sampler, rotary-drill borings, near-surface cores and hand-dug surface pits. The study area is located within the central section of the National Seashore and is an ideal setting for testing the sensor because there is negligible infrastructure and cultural noise (e.g., no buildings, pipelines,

fences, railways, communication towers) to potentially interfere with the EM signal. Prior to collecting the data, the GSSI Profiler EMP-400™ sensor was calibrated independently to the surrounding environment and also with the operator. Calibrations were performed in the backbeach environment to reduce any noise from breaking waves, etc. in the swash zone. If operators switched between surveys, a new calibration was performed the same way every time, for consistency. For a detailed description of the calibration procedures please refer to the user manual, which is available online as a free download (Geophysical Survey Systems, 2007).

The 10 km-long EMI survey (Figure 2-3) traversed at least three previously inferred Pleistocene streams of varying width and presumably varying depth. Comparisons were made between the inferred channels by Fisk, measured σ_a values, and maximum dune height extracted from aerial LiDAR data. On Fig. 3C, the red curve indicates variations in σ_a, whereas the blue curve represents maximum dune height. On average, apparent conductivity decreases within the three interpreted paleo-channel regions. The lowest σ_a values are within the first channel and suggest a thicker sequence of valley fill material (i.e., more resistive beach sands). Comparisons of the locations of each paleo-channel as identified by the EMI sensor to those of Fisk (1959) are highlighted by the gray shaded regions on Figure 2-3. There is reasonable agreement between the locations for the first paleo-channel. There appears to be excellent agreement between the locations for the second channel shown by the minimum σ_a on the red curve. Conversely, there is a discrepancy between the locations

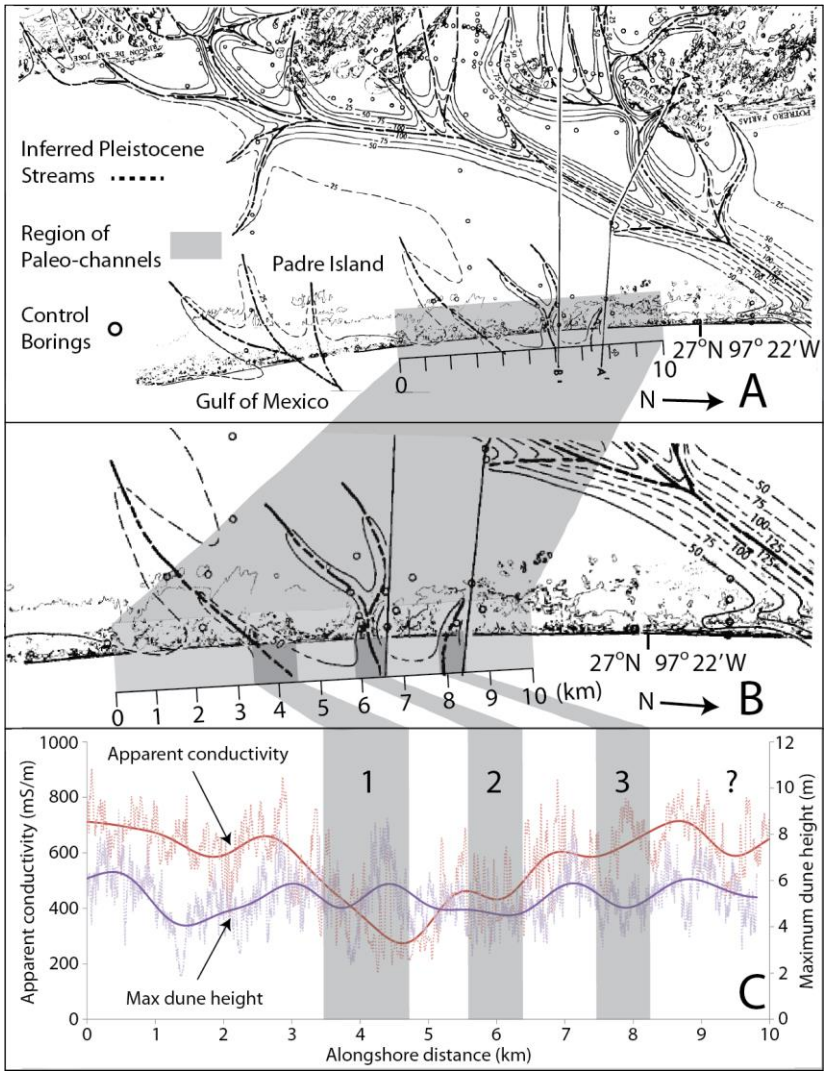

Figure 2-3. Location map of previously inferred Pleistocene streams identified by Fisk (1959). The regional distribution of the network of Pleistocene streams (dotted lines) that now lie beneath the modern barrier island system are shown in panel (A). The gray shaded region indicates the location of the 10 km alongshore EMI survey conducted in August 10, 2013 (B). A closer view (C) of the inferred paleo-channels (labeled 1-3) is compared to the alongshore variations in apparent conductivity (red curve) and maximum dune height (blue curve). A Savitzky-Golay smoothing filter (solid lines) was applied to the raw data (dotted lines) using AutoSignal™ V1.7. The smoothed lines are intended to highlight the long wavelengths in each data set. Maximum dune height was extracted from an aerial LiDAR survey (free online access) provided by the Army Corps of Engineers (USACE) and Joint Airborne LiDAR Bathymetry Technical Center of Expertise (JALBTCX) as part of the 2009 West Texas Aerial Survey project. A 25 m sampling window was used between consecutive points and the vertical and horizontal positional accuracy is 0.15 and 0.5 m, respectively (Weymer et al., 2015).

for the third channel suggesting that more surveys and coring are needed to confirm the exact location of the channel and the potential impacts on surface geomorphology.

EMI data are commonly displayed as apparent conductivity maps (2D contour plots), particularly for environmental and engineering coastal applications including saltwater intrusion, freshwater lens morphology and contaminant plume delineation (Stewart, 1982; Ruppel et al., 2000; Paine and Minty, 2005; Aziz et al., 2008; Triantafilis et al., 2011). However, EMI grids have not been collected to investigate the connections between geologic structures and alongshore variations in island morphology. An example of a 2D EMI grid survey is presented in Figure 4-2. Here, a 20 x 500 m grid survey was conducted in the backshore environment across a washover channel that was created during Tropical Storm Arlene, which made landfall (~ 64 km south of Corpus Christi, Texas, USA) near Padre Island on June 20th, 1993 (NOAA, 2014). Historical imagery from Google Earth© (1995, 2005, 2014) shows how the washover has recovered over the past two decades. Washovers can only recover in the absence of storm activity, which allows vegetation to establish and stabilize new foredunes (see Houser and Hamilton, 2009). This area was chosen to determine whether the EMI survey could reveal any relationship between subsurface σ_a and the location of the washover channel. Three frequencies were used by the sensor (3, 10, 15 kHz), providing a view into the conductivity structure at different depths, both within and outside the channel. Lower σ_a values observed inside the washover channel suggest a thicker layer of sand is present compared to the areas outside the channel where σ_a increases. Apparent conductivity increases at all three frequencies just outside of the channel (~100 m) suggesting a change in lithology. It is possible that the higher σ_a values indicate a

thinning of the sand layer such that a more conductive layer (e.g., clays/Pleistocene ravinement) is closer to the surface outside the channel. This hypothesis can be tested by taking cores within and outside the channel to validate the thickness of the sand layer that can control dune morphology (see Houser and Mathew, 2011). Regardless, the fact that a change in σ_a occurs within the channel suggests that the EMI sensor is capable of making reliable subsurface measurements to observed surface features.

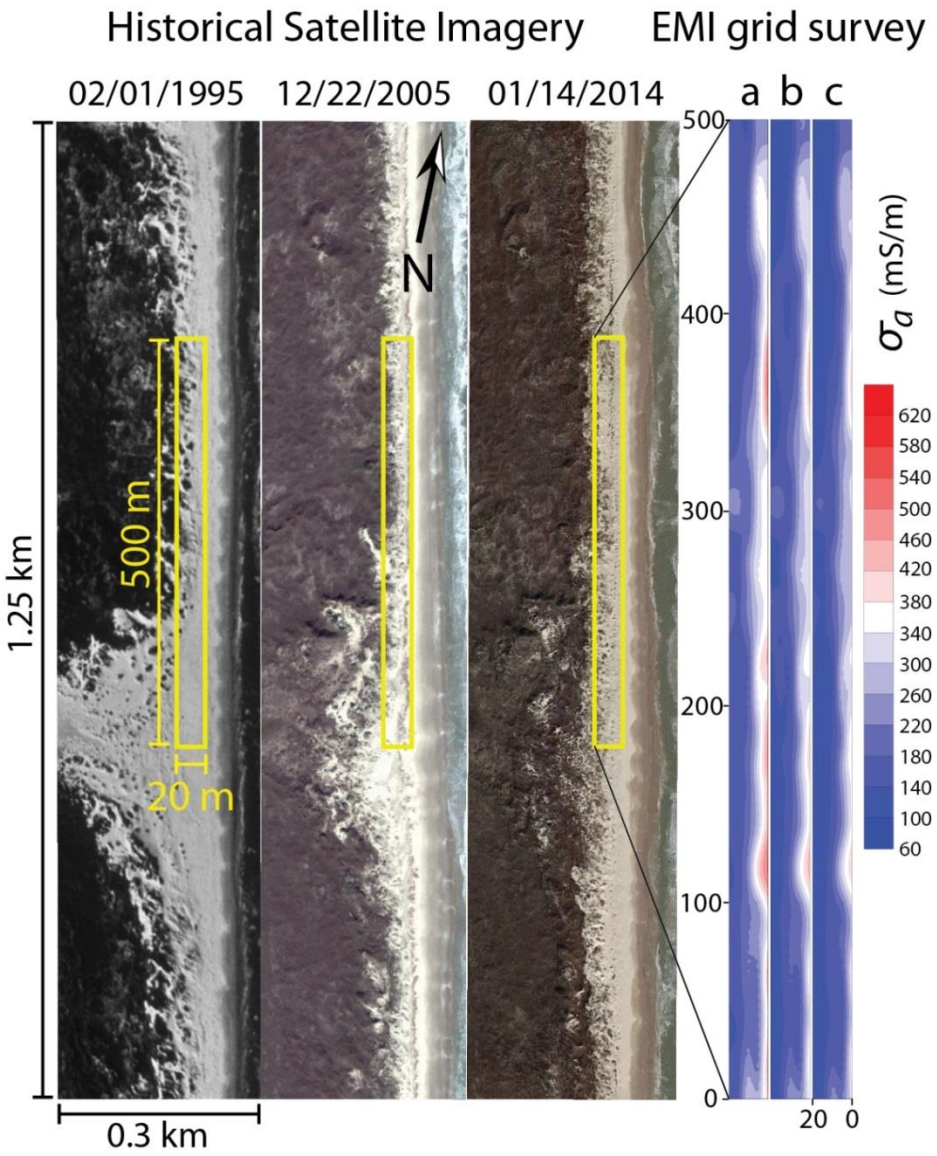

Figure 2-4. Example of an EMI grid survey across the beach-dune environment. The 10,000 m^2 survey was conducted with a GSSI Profiler EMP-400™ and was acquired in ~2 hours on November 29, 2013. Data was collected at 5 m line and station spacing and interpolated to a 1x1 m grid with ordinary kriging. Each panel represents a "depth slice" where the lowest frequency (3 kHz) corresponds to the deepest depth probed by the sensor. High σ_a values are in red, whereas low values are in blue. Shore-normal distance (m) starts at the backbeach (0 m) and traverses to the west (20 m). Satellite images courtesy of Google Earth©, 1995, 2005, 2014 (Weymer et al., 2015).

Conceptual model of groundwater effects on EMI signals

Since barrier island hydrology is dependent on the framework geology, the alongshore variation in groundwater can either exaggerate or partially mask paleo-channels in EMI surveys. For example, hydrology may have had an impact on the slight offset between the inferred paleo-channels and the lower σ_a values (see Figure 2-3). Although changing hydrology may alter EMI response parameters, it is still possible to make geologic interpretations so long as the hydrology is taken into consideration. The combined effects of each hydrologic factor on a hypothetical EMI signal are conceptualized in Figure 2-5. The hydrologic processes within a barrier island system are shown at two different length-scales, where Figures 2-5A-C represent hydrodynamics within the beach-dune system (tens of m) and Figures 2-5D-F illustrate larger-scale hydrologic variations across the entire barrier system (several km). In the swash zone, non-linear effects of waves, currents and tides combine to produce a landward-increasing superelevation of the mean freshwater water table (Nielsen, 1990). Nielsen observed that the mean water surface through the swash zone rises rapidly (Figure 2-5A), intersecting the beach face at a relatively high elevation (i.e., superelevation/overheight) before levelling off into the beach water table (Gourlay, 1992). Thus, the measured σ_a should be highest in the swash zone and decreases moving across the beach-dune system. Accounting for wave setup and tidal fluctuations (Figure 2-5B), the EMI signal likely varies over a tidal cycle where σ_a slightly increases during high tide and slightly decreases at low tide. The seasonal variations in precipitation (i.e., wet vs. dry conditions) have also been suggested to influence σ_a alongshore. During wet conditions the beach is saturated with rainwater, thereby increasing σ_a (Figure 2-5C). Conversely, during

dry conditions the water table lowers, resulting in lower σ_a and increasing the EMI sensor's ability to probe to greater depths.

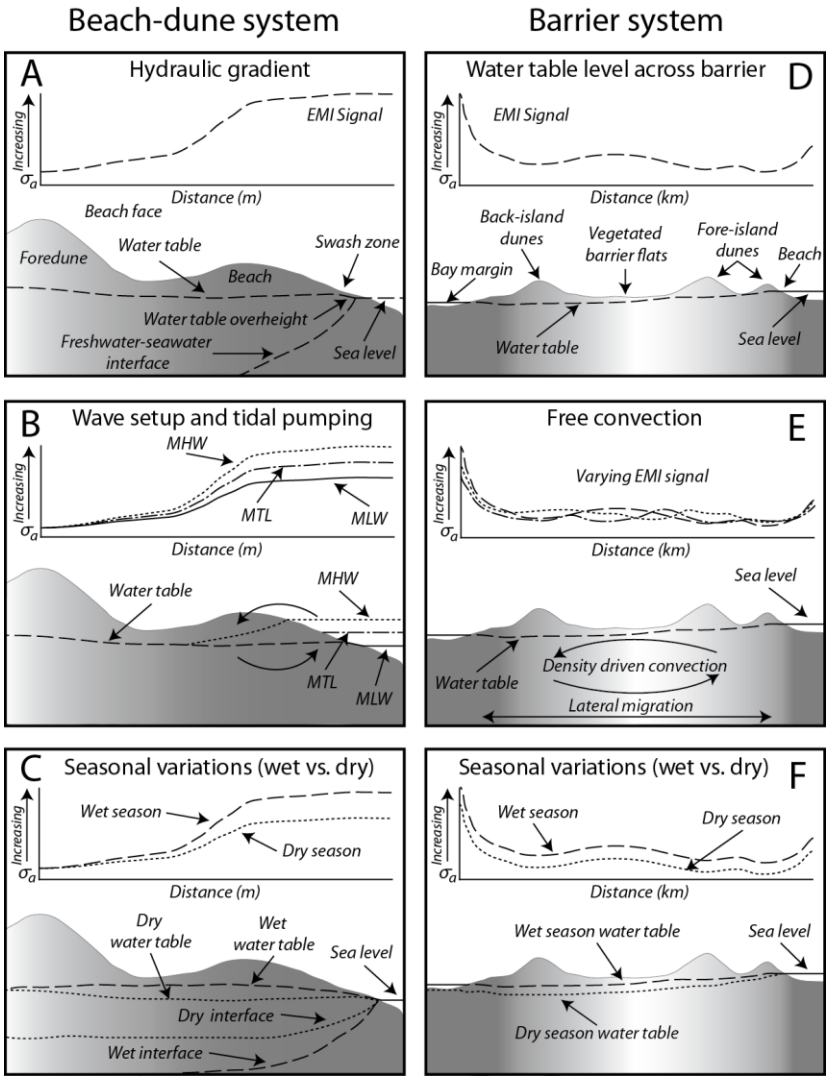

Figure 2-5. Conceptual model of groundwater dynamics in a barrier island and their effect on the EMI signal. The left panels represent meso-scale hydrodynamics within the beach-dune environment, whereas the right panels characterize large-scale hydrology across the larger barrier island system. The overall trend in changing salinity (all panels) is represented by the color gradient from gray to white, where gray is higher salinity (i.e., σ_a) and white is lower salinity (σ_a). Within the beach-dune system, hydrologic effects on the EMI signal include; hydraulic gradients (A), wave and tidal influences (B), and seasonal effects (C). Across the barrier island, large-scale hydrologic effects include; differences in the level of the water table (D), density-driven convection (E), and seasonal variations, which influence free convection (F) (Weymer et al., 2015).

Groundwater dynamics also vary across the barrier island system (Gourlay, 1992; Nielsen and Kang, 1996; Nielsen, 1997, 1999). It has been suggested that infiltration from wave runup in the swash zone is the main factor in creating a landward-dipping water table across the barrier (Nielsen, 1999). Theoretically, an EMI signal across a barrier island with little to no relief should gradually decrease landwards. However, most barriers have highly variable topography extending from the fore-island dunes, across the vegetated barrier-flats and into the back-island dunes and bay margin. Studies by Paine et al. (2004) suggest that σ_a is negatively correlated with topography, and therefore a more representative EMI signal across the barrier is shown in Figure 2-5D. Stevens et al. (2009) investigated density-driven free convection within the backbarrier/wind-tidal flats of Padre Island National Seashore. They found that in certain hydrological situations, instabilities created by denser saline fluid overlying less-dense fluid can drive saline water to descend into fresh water, thereby causing lateral migration of saline water across the barrier (Figure 2-5E). In arid environments (e.g., south Texas coast, Persian Gulf), tidal flats exist adjacent to back-barrier environments. During the summer, evaporation exceeds precipitation and the surface of the flats dry out. Conversely, during the winter, low-pressure systems pond bay/lagoon waters against the barrier, thus flooding the tidal flats. The seasonal cycles of wet/dry conditions significantly influence groundwater dynamics across the barrier, where σ_a slightly decreases as the flats continue to dry (Figure 2-5F). In summary, there are many hydrologic factors that influence the overall spatial distribution of saline and freshwater in barrier island systems some of which may be site specific. Therefore, EMI surveys should be conducted systematically and carefully to test the predictions depicted in Figure 2-5. Because EMI measurements respond

almost entirely to the bulk subsurface electrical conductivity, it is suggested that EMI sensors offer great potential to advance the current understanding of barrier groundwater dynamics.

Summary and future research

The relationships between geologic framework, hydrology and modern barrier island transgression are not well constrained by conventional geological methods. Antecedent geology has been shown in many studies to influence contemporary morphodynamics. However, groundwater dynamics also play a significant role in the evolution of the modern barrier island system. Previous studies have investigated these two controls on barrier island transgression independently, and it is argued that linkages between subsurface hydrogeology and surficial features must be understood to accurately predict future change. Traditional methods such as coring, seismic and GPR (to some extent) have proven useful to address these issues, nevertheless, these techniques are either invasive or cannot provide continuous subsurface information across the entire coastal tract (i.e., inner-shelf, nearshore, beach, barrier and lagoon).

EMI methods are a viable alternative to explore the geologic framework of barrier islands, because EMI sensors have a potential to provide subsurface information across the entire barrier island system. Traditional geological, geophysical and remote sensing methods work well within specific areas of the coast but these data sets must be integrated to give a complete picture of geologic framework across the entire coastal tract. In other words, it is argued herein that no other geophysical method besides EMI

can provide continuous subsurface coverage. EMI sensors provide high-resolution information regarding the complex feedbacks between antecedent geology and hydrologic conditions. When integrated with data from other methods, EMI techniques have direct implications for barrier island response to future storms and rising sea-level.

Although EMI methods show promise for future barrier island research, a number of key issues need to be resolved. Each cartoon depicted in Figure 2-5 illustrates the potentially confounding effects of changing hydrologic conditions on the EMI signal. Within the beach dune system, it is proposed that further work is needed to A) accurately characterize hydraulic gradients across the barrier island system, B) monitor wave and tidal effects on water table elevation, and C) understand seasonal hydrologic changes including precipitation and its influence on water table migration. Large-scale investigations across the barrier island system are also needed to D) monitor water elevations across the entire barrier, E) account for density-driven free-convection and lateral migration across the barrier island system, and F) monitor seasonal variations on large-scale barrier island groundwater dynamics. It is argued that subsurface hydrology is a proxy for framework geology. As the hydrologic effects on EMI sensors become better understood (i.e., Figures 2-5A-F) interpretations of framework geology will improve even further. In addition to these challenges, further study of decreases in exploration depth, breakdown of the LIN approximation and questions concerning a practical (absolute) calibration are crucial for improving our understanding of the limitations of EMI sensors in highly conductive coastal environments. Some of the emerging techniques for barrier island EMI studies include; inversion modeling for

multiple layers, geostatistical testing, and subsurface/surface integration with LiDAR morphometrics. It is proposed that EMI techniques are complementary to existing methods and can become a useful tool to study how subsurface hydrogeology governs modern barrier island transgression.

CHAPTER III

DIFFERENTIATING TIDAL AND GROUNDWATER DYNAMICS FROM BARRIER ISLAND FRAMEWORK GEOLOGY: TESTING THE UTILITY OF PORTABLE MULTI-FREQUENCY EMI PROFILERS

Introduction

Portable multi-frequency electromagnetic induction (EMI) profilers have become a popular tool for near-surface geophysical applications because they are non-invasive, cover large areas over a short period of time, and are relatively inexpensive compared to other geophysical techniques. EMI profiling is designed to measure lateral variations in electrical conductivity σ, along a traverse, as opposed to sounding techniques which detect vertical variations in σ with depth (Frischknecht et al., 1991). The most commonly used source for EMI prospecting is a small current carrying loop, which is essentially a magnetic dipole (West and Macnae, 1991). There is a variety of profilers available on the market including the Geonics; GSSI™, Geophex™, Dualem™, PROMIS™, GF Instruments™ and Stratagem™ systems. Most profiling techniques operate in the frequency domain; however, many acquisition and interpretation procedures are available in the time domain (Nabighian and Macnae, 1991). A significant application of dipolar source EMI profiling is the detection of highly conductive ore bodies for mining, and many instrumentation and interpretation techniques have been developed specifically for this purpose (Frischknecht et al., 1991). EMI profiling for other uses is rapidly increasing for applications such as: groundwater, environmental, and engineering

studies (see Huang and Won, 2000; Everett, 2013). In the coastal environment, the use of EMI has focused on imaging saltwater intrusion for groundwater resource management (e.g., Nenna et al., 2013). Coastal EMI surveys for other purposes have been underutilized for several reasons including: lack of awareness of the method by non-geophysicists, and data reliability (see George and Woodgate, 2002). We present a case study to assess the use of EMI profiling techniques for a coastal investigation, namely for characterizing large-scale barrier island hydrogeology at Padre Island National Seashore (PAIS), Texas in southeastern United States. The geological pattern along the island is of inherent interest not only for testing EMI methods, but also for informing coastal managers at the National Park and in the State of Texas.

Portable multi-frequency EMI systems

Portable multi-frequency EMI profilers provide users with the flexibility of choosing between several operating frequencies, as well as varying the instrument's orientation, height, and coil configuration (Won et al., 1996; Huang et al., 2008). Unless otherwise mentioned, "portable" means a lightweight sensor that is used by one person and can be operated in a continuous acquisition mode while walking. Unlike most traditional EMI sensors, which have separate transmitter (TX) and receiver (RX) coils connected by long cables, portable multi-frequency EMI profilers have a short, fixed separation between the TX and RX coils. For example, the GSSI Profiler EMP-400™ contains a TX coil that continuously emits a waveform containing multiple frequencies within the 1 – 16 kHz bandwidth, selectable at 1 kHz increments (Geophysical Survey

Systems, 2007; Huang et al., 2008). The RX coil measures the in-phase I and the quadrature (out-of-phase) Q components of the time-derivative of the secondary magnetic field (Won et al., 1996). The geometry of the GSSI Profiler EMP-400™ and an example of its use in the field is shown in Figure 3-1A. The coil separation *s* of the instrument is 1.21 m and the instrument height *h* used in this study is ~ 0.70 m. The system measures I and Q responses in parts per million (ppm), as well as σ_a in mS/m, which is a transform of the I and/or Q raw measurements (McNeill, 1980). The system sensor electronics are controlled by a wireless Bluetooth™ communications interface that is incorporated into a TDS RECON-400 Personal Digital Assistant (PDA). Additionally, GPS coordinates are recorded at each measurement location with a positional accuracy of ~ 1 m.

Conventionally, the separation distance, or offset, between TX and RX coils is important for determining the maximum depth at which a target can be detected. However, with newer fixed offset profilers, the maximum depth to the target is controlled by changing the operating frequencies. In other words, the depth of investigation (DOI) for the instrument used in this study is a function of frequency: the lower the frequency, the deeper the investigation. The DOI may be defined as the maximum depth probed by a geophysics sensor (Huang, 2005). Despite a fixed offset, EMI profilers record the Earth response at several frequencies (Huang, 2005), although frequencies below 16 KHz may be within the low frequency approximation and data at different frequencies will be redundant in resistive environments. The DOI is affected by many other factors such as: sensor sensitivity, operating frequencies, background noise

level (Huang, 2005), and the physical properties (see Everett, 2013) of the subsurface (e.g., porosity, moisture content, temperature, and salinity). Nearby lateral variations in subsurface σ also influence the effective DOI at any given location along the profile. Understanding how these factors relate to the DOI is important for survey design, but is also dependent on the geomorphological environment (fluvial, aeolian, glacial, and coastal, etc.) under investigation.

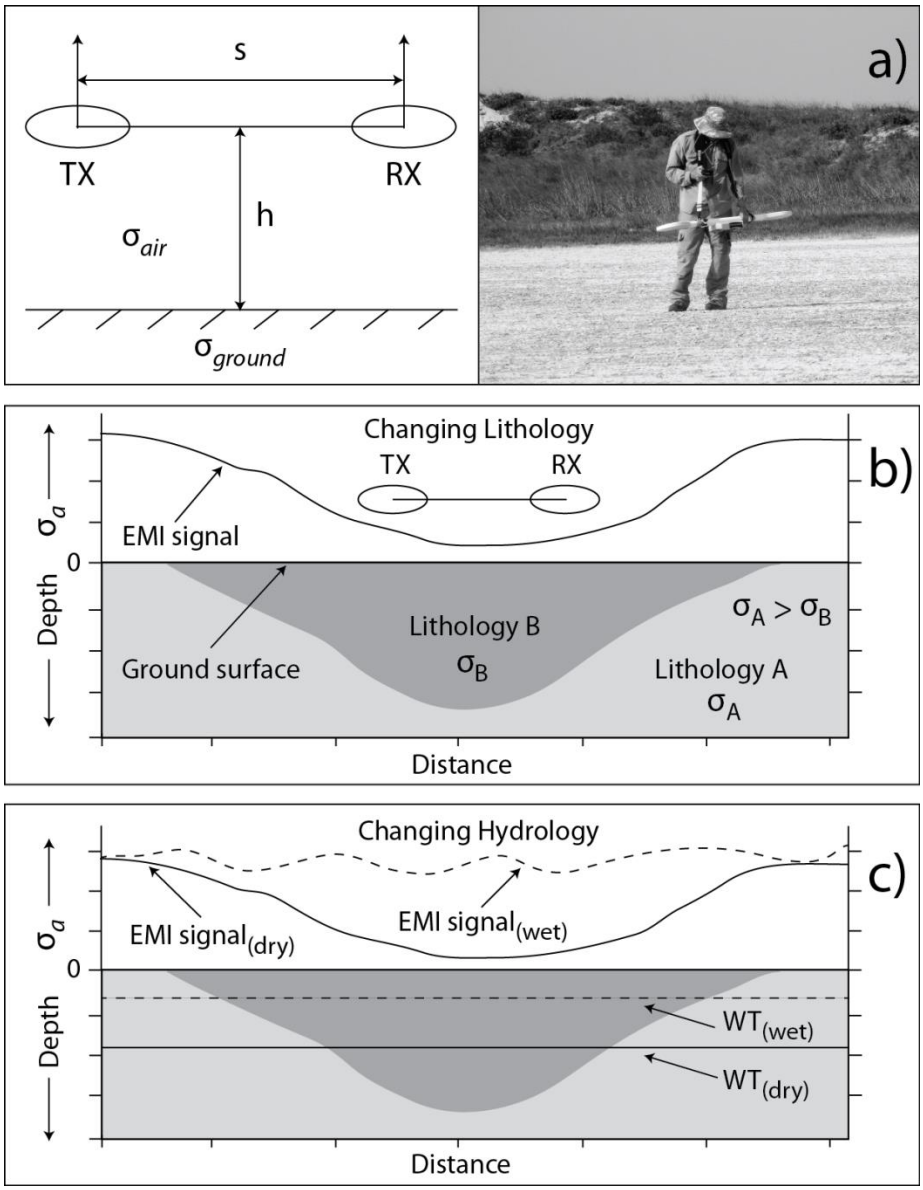

Figure 3-1. Overview of the EMI handheld profiler configuration and conceptual model of the relationships between varying hydrology, lithology, and apparent conductivity σ_a. (a) Profiler parameters (left panel) and the GSSI Profiler EMP-400™ being used in the field (right panel) where, TX = transmitter, RX = receiver, coil separation *s* = 1.21 m, height above ground *h* = 0.7 m, σ_{air} and σ_{ground} are the air and ground conductivities, respectively (after Huang et al., 2008). (b) Hypothetical EMI survey over changing lithology where lithology A σ_A is more conductive that lithology B σ_B. The EMI "signal" decreases across the less conductive sediments. (c) Generalized graph depicting variations in σ_a with respect to changes in hydrologic conditions. During dry conditions, the sensor is capable of probing greater depths. Conversely, during wet conditions σ_a is relatively homogenous, limiting the sensors ability to distinguish geologic features.

Interpretation of EMI data is commonly based on measurements at a single frequency (Huang and Won, 2000). Here we focus on apparent conductivity values measured at three frequencies to differentiate variations in σ at depth. Apparent conductivity σ_a is defined as the conductivity of a homogeneous half-space that would have produced the same response as that measured over the real Earth with the same sensor, and is transformed from either the I or Q response (Won et al., 1996). In this study we present only raw EMI σ_a data and have not applied any form of post-acquisition correction. In conductive environments, portable multi-frequency EMI sensors can be used for depth sounding since the frequency-dependent EM data are acquired at relatively high induction numbers

$$\theta = \sqrt{\frac{\omega\sigma\mu}{2}}s \tag{3.1}$$

where, θ is the induction number for a plane wave, $\omega = 2\pi f$ is the angular frequency, σ is the ground conductivity, μ is the magnetic permeability, and s is the TX – RX offset. The collection of multi-frequency data at high induction numbers enables mapping σ variations with depth (Huang et al., 2008). However, not all portable conductivity meters (e.g., Geonics EM31) are based on the high induction number assumption. EMI profilers have less capability to resolve depth variations at low induction numbers (low conductivity or resistive ground) as the S/N ratio is low in this case. It is important to note that Equation (9) involves a plane wave, but does have significant validity for the magnetic dipole-dipole configuration used in the present study.

A simple conceptual model (Figure 3-1B) illustrates how σ_a might vary with lithology along a barrier island. Figure 3-1B shows a sketch of the expected signals from

a hypothetical EMI survey over contrasting lithologies. Lithology A is more conductive than Lithology B and in a coastal environment, Lithology A could represent seawater-saturated sand/clay layer underlying a more resistive sand layer (B). Figure 3-1C gives examples of how the EMI response might change across such a contrast. Factors including tides, waves, the location of the fresh/saltwater interface, and soil moisture content influence the σ_a signal. Changes in contrast by the replacement of freshwater with saltwater can potentially reduce the DOI. During wet conditions, the EMI sensor does not probe very deeply because of high σ (e.g., salinity) that strongly attenuates the downward propagation of the EM field (dotted line). Conversely, during dry conditions σ is lower, therefore the sensor probes to greater depths (solid line) as the downward propagation is less attenuated.

As described above, attenuation increases with σ, thus reducing the DOI. The attenuation of penetrating EM fields with depth is known as the *skin effect*. EMI depth penetration is constrained by the conversion of the transmitted electromagnetic energy into kinetic energy of the mobilized subsurface charge carriers (Huang, 2005; Everett, 2013). A skin depth δ is the depth at which a plane wave vertically incident upon a half-space has an amplitude which is 1/*e* of its incident amplitude (see Huang, 2005; Everett, 2013), where

$$\delta = \sqrt{\frac{2}{\mu\sigma\omega}}. \tag{3.2}$$

The DOI can be less than a single skin depth in areas with complex geology and/or a considerable amount of cultural noise (Huang, 2005). The skin depths for the various frequencies used, over the range of conductivities likely present within the study area,

are presented in Table 3-1. Typical σ_a values measured along the beach within the study area range between ~ 50 – 800 mS/m (seawater is ~ 3,200 mS/m). For these σ_a values, the three main frequencies used in this study (i.e., 3, 10, and 15 kHz) correspond to skin depths ranging from ~ 41.1 – 4.6 m. However, assuming the DOI is approximately proportional to the square root of δ as suggested by Huang (2005), the lower bound for the DOI at 3, 10 and 15 kHz varies between ~ 6.4 – 2.1 m. It is important to note that the DOI is under the sensor, which is ~ 0.7 m above the ground in this study (see Figure 3-1A).

Table 3-1. Theoretical skin depths (δ) in meters over the frequency bandwidth of the GSSI Profiler EMP-400™ for a range of apparent conductivities encountered across the coastal environment. Note: the relative magnetic permeability (μ/μ_0) value of 1.0006 (typical of soil and sedimentary rock) used in this table follows that given in Nettleton (1940) and Scott (1983).

Frequency (kHz)	50	100	200	300	400	500	600	700	800	900	1000	1500	2000	2500	3000
1	71.2	50.3	35.6	29.0	25.2	22.5	20.5	19.0	17.8	16.8	15.9	13.0	11.3	10.1	9.2
2	50.3	35.6	25.2	20.6	17.8	15.9	14.5	13.4	12.6	11.9	11.3	9.2	8.0	7.1	6.5
3	41.1	29.0	20.6	16.8	14.5	13.0	11.9	11.0	10.3	9.7	9.2	7.5	6.5	5.8	5.3
4	35.6	25.2	17.8	14.6	12.6	11.3	10.3	9.5	8.9	8.4	8.0	6.5	5.6	5.0	4.6
5	31.8	22.5	16.0	13.0	11.3	10.1	9.2	8.5	8.0	7.5	7.1	5.8	5.0	4.5	4.1
6	29.0	20.5	14.6	11.9	10.3	9.2	8.4	7.8	7.3	6.8	6.5	5.3	4.6	4.1	3.8
7	26.9	19.0	13.5	11.0	9.5	8.5	7.8	7.2	6.7	6.3	6.0	4.9	4.3	3.8	3.5
8	25.2	17.8	12.6	10.3	8.9	8.0	7.3	6.7	6.3	5.9	5.6	4.6	4.0	3.6	3.2
9	23.7	16.8	11.9	9.7	8.4	7.5	6.8	6.3	5.9	5.6	5.3	4.3	3.8	3.4	3.1
10	22.5	15.9	11.3	9.2	8.0	7.1	6.5	6.0	5.6	5.3	5.0	4.1	3.6	3.2	2.9
11	21.5	15.2	10.8	8.8	7.6	6.8	6.2	5.7	5.4	5.1	4.8	3.9	3.4	3.0	2.8
12	20.5	14.5	10.3	8.4	7.3	6.5	5.9	5.5	5.1	4.8	4.6	3.8	3.2	2.9	2.7
13	19.7	14.0	9.9	8.1	7.0	6.2	5.7	5.3	4.9	4.7	4.4	3.6	3.1	2.8	2.5
14	19.0	13.4	9.5	7.8	6.7	6.0	5.5	5.1	4.8	4.5	4.3	3.5	3.0	2.7	2.5
15	18.4	13.0	9.2	7.5	6.5	5.8	5.3	4.9	4.6	4.3	4.1	3.4	2.9	2.6	2.4
16	17.8	12.6	8.9	7.3	6.3	5.6	5.1	4.8	4.4	4.2	4.0	3.2	2.8	2.5	2.3

Application of EMI methods in coastal studies

The literature on near-surface applied EM geophysics is far-ranging (see Everett and Farquharson, 2012), from modeling and inversion offerings (McNeill, 1980; Sasaki and Meju, 2006; Santos et al., 2010; Guillemoteau et al., 2015) to case studies in unexploded ordnance (UXO), soil science, and archeology (e.g., Sudduth et al., 2001; Benavides et al., 2009; de Smet et al., 2012; Pincus et al., 2013). Comparatively few studies have used EMI methods in coastal environments (e.g., Paine et al., 2004; Seijmonsbergen et al., 2004; Vrbancich, 2009; Nenna et al., 2013; Christensen and Halkjær, 2014; Delefortrie et al., 2014b), with the majority of these focusing on mapping saltwater intrusion. Most of these studies employ Geonics™ EM31, 34, 38 and similar frequency-domain sensors; Geonics™ EM47, 63 and similar time-domain electromagnetic (TDEM) sensors in addition to various airborne electromagnetic (AEM) systems. AEM surveys are important for coastal studies, but are beyond the scope of this paper. Previous coastal EMI studies have explored subsurface σ as it is related to geologic framework (Seijmonsbergen et al., 2004; Vrbancich, 2009), classification of coastal wetlands (Paine et al., 2004), and investigation of coastal groundwater dynamics and pollution (e.g., Goldman et al., 1991; Fitterman and Deszcz-Pan, 1998; Nenna et al., 2013; Christensen and Halkjær, 2014).

Seijmonsbergen et al. (2004) used the EM34 (albeit not a portable multi-frequency EMI profiler) at 20 m station spacing and 20 m coil separation to acquire a 14.5 km transect along a segment of the Dutch coast, Netherlands. Using this configuration, the DOI is ~15 m. Results from the study suggest that subsurface σ_a can

be used as a proxy to distinguish the spatial distribution of Holocene coastal deposits and previously identified pre-Holocene paleo-channels near a former outlet of the Rhine River. Paine et al. (2004) used the EM38 (a portable EMI profiler) with its ~1 m exploration depth at 20 m station spacing to collect two shore-normal transects at Mustang Island, Texas, USA. Their findings suggest that σ_a generally varies inversely with topography and that LiDAR and EMI data can be used together for characterizing different geomorphic environments to improve the accuracy of coastal habitat classification.

A number of coastal studies have investigated saltwater intrusion and contaminant plumes using EMI sensors other than portable multi-frequency instruments. For example, Nenna et al. (2013) tested the feasibility of TDEM methods to identify hydraulic communication between a confined freshwater aquifer and an unconfined saline aquifer using a Geonics PROTEM 47. Data were acquired using center-loop and offset receiver geometries. The results suggest that TDEM methods can be used to characterize saltwater intrusion in coastal aquifer systems and infer the continuity of confining layers between saturated layers with different water qualities. A different approach employing transient AEM was used by Christensen and Halkjær (2014) to map North Sea coastal hydrology at a heavily polluted site in western Jutland, Denmark, which suggests that transient AEM systems can be used to delineate the extent of the pollution plume, the fresh/saltwater boundary, and the complex pattern of subsurface preferential flow channels along the coast. While the above studies demonstrate the value of EMI sensors for coastal research, most have not examined in detail the effects

of changing hydrology as it is related to framework geology over different spatial-temporal scales.

Research objectives

The purpose of this study is to investigate the performance of a portable multi-frequency EMI profiler for mapping the hydrogeologic structure of a highly conductive barrier island/wind-tidal flat system at Padre Island National Seashore (PAIS), Texas, USA. Specifically, the calibration and measurement reproducibility of a GSSI Profiler EMP-400™ is assessed with respect to: 1) tidal influences on σ_a measurments, 2) detecting spatial variations in subsurface σ_a as it is related to geologic framework; 3) monitoring seasonal changes in groundwater conditions; 4) mapping the relationship between different coastal sub-environments and topography, both alongshore and across the barrier island/wind-tidal flat system. It is proposed that multi-frequency EMI profilers can be used for exploring quantitative performance characteristics with respect to fundamental issues in coastal geomorphology, such as interactions between antecedent geology and modern coastal processes.

Description of the study area

Padre Island National Seashore (PAIS) and the Laguna Madre wind-tidal flats are located within the south Texas Coastal Zone, ~ 40 km SSE of Corpus Christi, Texas, USA (Figure 3-2). This region has been the subject of numerous studies since the 1940's (e.g., Fisk, 1959; Brown and Macon, 1977; Morton and McGowen, 1980; Weise et al., 1980;

Amdurer and Land, 1982; Kocurek et al., 1992; Morton et al., 2000; Stevens et al., 2009; Weymer et al., 2015b) investigating various aspects regarding the origin, geologic history, hydrology, and/or morphodynamic processes of PAIS and adjacent wind-tidal flats. Geologic interpretations based on seismic, borehole data, cores, and hand-dug trenches provide a relative chronology of the geologic history of the island, spanning the majority of the Pleistocene (~1.8 Myr) through the present (Brown and Macon, 1977; Gradstein et al., 2008). Much of what is known about the geologic history of Padre Island is based on studies by Fisk (1959) and the Bureau of Economic Geology (Brown and Macon, 1977), and few attempts have since been made to further investigate the geomorphic evolution of the island and wind-tidal flats.

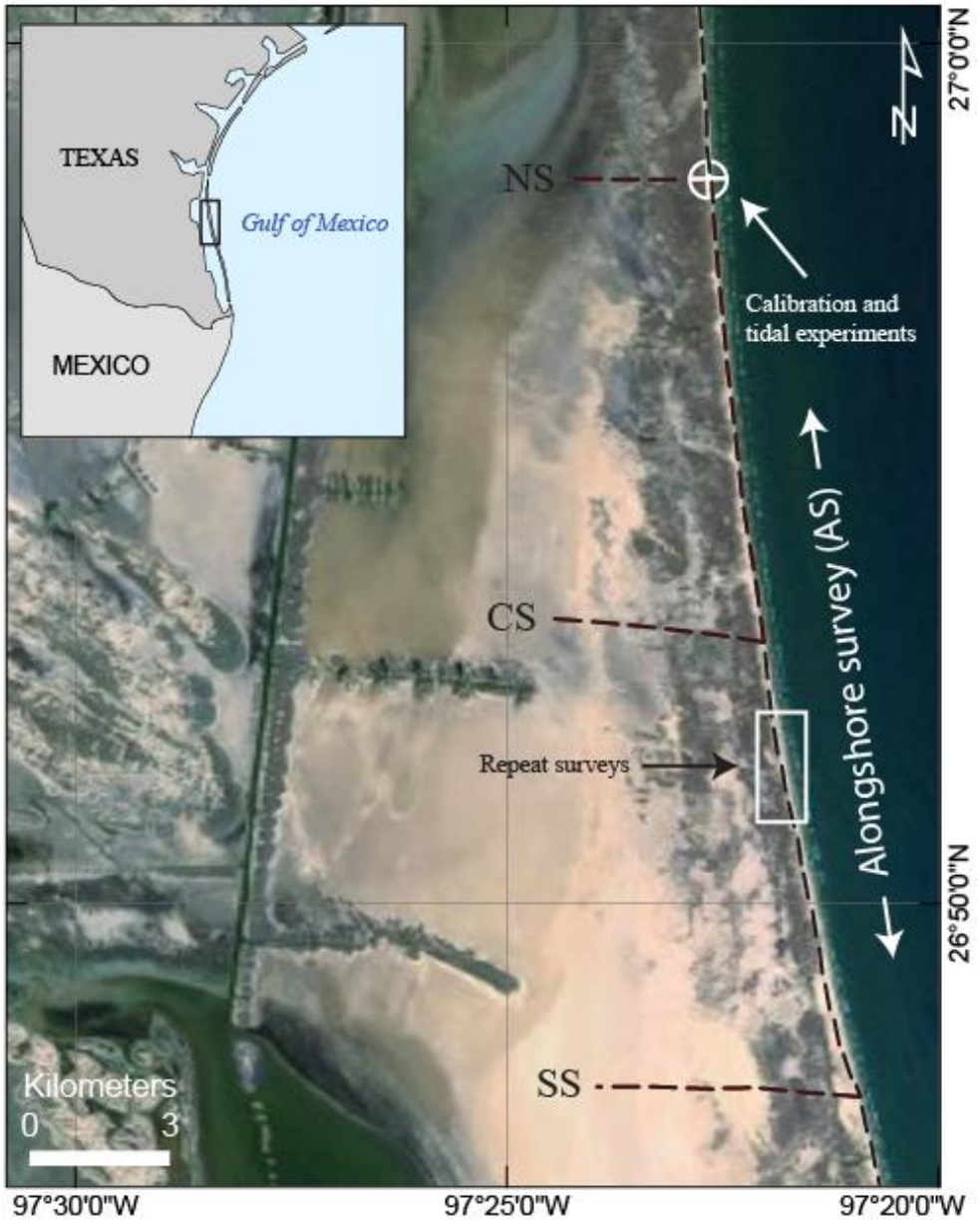

Figure 3-2. Location map of central PAIS and adjacent Laguna Madre wind-tidal flats in southern Texas, USA. EMI surveys are superimposed on satellite imagery. Shore-normal EMI transects are labeled as NS, CS, and SS corresponding to the northern, central and southern surveys, respectively. The entire 37 km alongshore survey (AS) crosses each of the shore-normal surveys. Repeat 2.5 km alongshore surveys are located ~ 2 km south of the CS, highlighted by the white box. Calibration and tidal experiments are positioned at the intersection of the AS and NS.

The existing premise is during the interglacial stages of the Pleistocene, when sea-level was approximately the same as it is today, inland rivers and streams were connected to a network of deltas within broad embayments along the shoreline (Brown and Macon, 1977). Fisk (1959) suggests that the Pleistocene ravinement surface in the region of the Laguna Madre Flats was deeply eroded by headwater tributaries of an entrenched valley system. Within the study area, there are as many as seven inferred late-Pleistocene streams that cut across the modern barrier island. Additionally, Pleistocene river deposits run parallel to the barrier, beneath the modern wind-tidal flats and may be part of the ancient delta system (Fisk, 1959).

Sea level rose through the Holocene, flooding the pre-existing Pleistocene stream and river valleys. Some of the valleys became bays and estuaries along the modern Texas coast and were partly filled with transgressive fluvial, deltaic, and/or estuarine deposits as well as wind-blown sand from the barrier, and by washover events during extreme storms (Hayes, 1974). When sea-level stabilized (~ 6 – 4 kya) sand shoals and offshore bars began to merge between the drowned-river valleys (Fisk, 1959). In the late Holocene, the shoals became a series of emergent, low discontinuous sandy islands that aligned parallel with the mainland shoreline (Brown and Macon, 1977). As the smaller proto-islands accreted they merged to form a large, arcuate system of barrier islands and spits extending ~ 600 km from modern-day Bolivar Peninsula to South Padre Island (Houser and Mathew, 2011). Stratigraphic units inferred from seismic surveys and borehole data suggest that the base of the barrier-lagoon system consists of Pleistocene sand and mud overlain by shoreface sand and mud, washover and aeolian deposits, and lagoonal muds (Brown and Macon, 1977). The

depth to the Pleistocene ravinement surface (known as the Beaumont formation) has been suggested to vary considerably along the length of the barrier island (Fisk, 1959). The sediment thickness of modern shoreface sands is estimated to be ~ 2 – 3 m, whereas the thickness of the shoreface sands and muds is ~ 10 m (see Brown and Macon, 1977; page 56, Figure 15) or greater within the paleo-channels (Fisk, 1959). Accordingly, approximate σ_a values in the current study range from > 400 mS/m outside the channels to < 200 mS/m within the sand-filled channels, which are likely more resistive.

Radiocarbon dates from shell samples suggest that the modern barrier and its hypersaline lagoon (Laguna Madre) began to form ~ 5 kya (Fisk, 1959), whereas Padre Island became a continuous barrier at ~ 3.7 kya (Brown and Macon, 1977). Laguna Madre became progressively isolated as Padre Island continued to grow, causing increased salinity in the lagoon and gradual development into a non-carbonate coastal sabkha (Amdurer and Land, 1982). The modern wind-tidal flats of Laguna Madre are anomalous compared to other coastal environments worldwide (Morton and Holmes, 2009). High evaporation rates, low rainfall, and isolation from tidal passes combine to produce a distinctive set of hydrologic and geomorphic conditions along the south Texas Coastal Zone. Wind is always an important factor in controlling coastal processes; however, the combination of low rainfall and high evaporation, prevailing southeasterly winds, and high temperatures in south Texas make aeolian processes even more important. Within the wind-tidal flats, sedimentation is dominated by aeolian and wind-tidal processes. Padre Island is microtidal and the mean and diurnal tidal levels within the study area are 0.38 m, 0.45 m, respectively (NOAA, 2015). Slight differences in elevation on the wind-tidal flats

markedly affect the frequency with which any given area is flooded, thus creating a complex of different sedimentary facies within the wind-tidal environment (Miller, 1975).

Methods

North Padre Island is the longest undeveloped barrier island in the world and is an ideal location for testing the performance of coastal EMI profiling techniques. With the exception of a few buildings at the northern entrance of the National Seashore, there is no urban development within PAIS. Thus, interference of EM signals by cultural noise (e.g., communication towers, railways, pipelines, fences, etc.) is minimal to non-existent. For this study, all surveys were conducted in the central segment of the island ~ 65 km south of the main park entrance. This area is accessible only by four-wheel drive vehicles and is one of the most remote sections of the island. Locations of the EMI surveys were chosen based on geologic maps by Fisk (1959) and Brown and Macon (1977) to allow for comparisons between σ_a measurements and previously interpreted geologic features. A series of surveys using a GSSI Profiler EMP-400™ were performed along three shore-normal transects in the southern (SS), central (CS) and northern (NS) segments of the study area (Figure 3-2). A 37-km-long alongshore survey (AS) was collected through the NS and SS. Additionally, repeat surveys over a period of ~ 1 year were taken within the AS to monitor the sensitivity of the profiler to seasonal changes in hydrologic conditions. Instrument calibration, measurement repeatability, and tests for the effect of tides on the EMI signal were performed

at the intersection (tie point) of the NS and AS and are described in detail in the following sections.

Calibration tests

Despite the growing interest in using EMI techniques for coastal studies, the importance of performing instrument calibrations is often overlooked. Along the beach factors such as; storms, tides, waves, currents, and precipitation regulate the position of the water table (see Lanyon et al., 1982; Nielsen, 1990), in turn altering subsurface σ. As a result, σ_a measurements by an EMI sensor are sensitive to fluctuations of the water table in response to these forcing mechanisms (Weymer et al., 2015b). The GSSI Profiler EMP-400™ requires two calibrations prior to each survey (Geophysical Survey Systems, 2007). The first is a field calibration where the operator stands a distance of ~ 4 m away from the instrument, placing the sensor on the ground to measure background noise/EM fields averaged over ~ 5 seconds at each frequency. Secondly, the instrument is calibrated with the operator holding it at a predetermined height above the ground (e.g., 0.7 m in this study). These "factory" calibrations must be performed before starting the survey, after changing batteries, and/or operators. However, other environmental factors and survey design unique to each study site should also be accounted for when calibrating the instrument. In the following discussion, we recommend several field calibrations that should be implemented for coastal surveys in addition to the existing standard GSSI calibration procedures.

Calibration tests were conducted on 03/30/2015 at various locations across the beach and at the NS and AS tie point (Figure 3-3). A diagram of the survey design is shown in Figure 3-3A. Based on the above-mentioned factors, there are three important calibrations necessary to determine measurement reliability. As will be demonstrated later in the results, σ_a varies significantly across the beach. Accordingly, the first calibration test examines how σ_a values change if the instrument is calibrated at different sub-environments across the beach (e.g., foreshore, backshore, beach-dune interface). For this test, the instrument was calibrated at 10 m intervals (e.g., C_0, C_{10}, C_{20}) starting at mean tide level (MTL = C_0) moving perpendicular to the shoreline and ending at the base of the foredunes (C_{50}). After each calibration (h = 0.7 m) measurements were taken at a 1 m step-size along the same 50 m transect, parallel to the shoreline ~ 25 m from MTL. The results of the survey are shown in Figure 3-3B. The highest σ_a values correspond to calibrations performed closest to MTL and generally decrease with distance away from the shoreline. However, σ_a values are slightly higher when the profiler was calibrated closer to the beach-dune interface (i.e., C_{40}, C_{50} m) than at C_{20} and C_{30}. The results suggest the profiler consistently measures the same trend in alongshore σ_a values, but there is a noticeable difference up to 100 mS/m between calibrations performed within 10 m of the MTL and calibrations performed ≥ 20 m from the MTL. To reduce the influence of high salinity and tides, it is suggested that calibrations be made > 25 m (or as far away as possible) from the MTL and that each subsequent calibration should be performed consistently the same distance away from the shoreline.

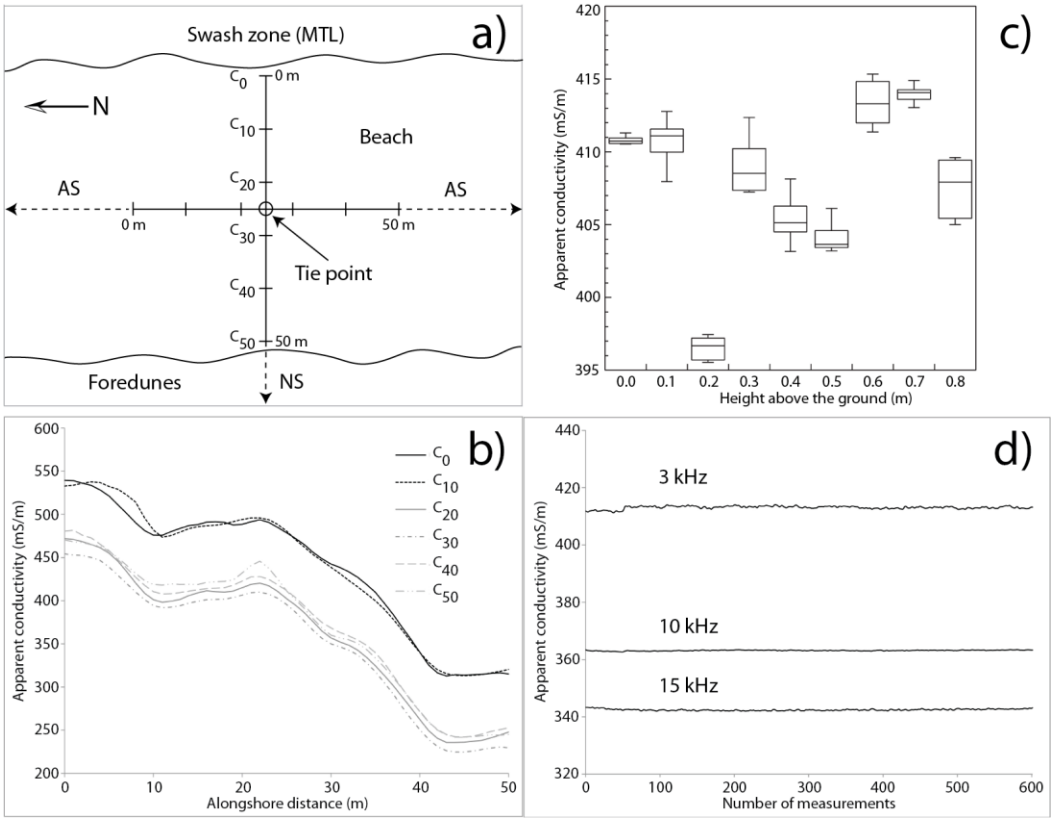

Figure 3-3. (a) Survey design for instrument calibration and tidal experiments at the intersection of the AS and NS. (b) Alongshore surveys following each calibration point (e.g., C_0 = 0 m landward from the MTL, C_{10} = 10 m from the MTL, and so on). The σ_a values are shown at 3 kHz for each survey. (c) Box and whisker plot of instrument drift measured at 0.1 m increments above the ground. (d) Time-series assessing instrument drift 0.7 m above the ground for each frequency at the tie point shown in 3a.

The second calibration test examines how measurements vary when calibrations are made at different heights above the ground. Prior to each survey, the operator can adjust the height of the instrument usually ranging from 0.0 – 0.8 m, where 0.8 m is the maximum position the profiler can be carried comfortably. A series of ten measurements was recorded every ten seconds at 0.1 m intervals to assess signal drift at each height (Figure 3-3C). Tidal variation is assumed to be negligible as each sequence of

measurements was acquired within minutes. The least amount of drift occurs when the sensor is placed closest to the ground surface (0.0 m), while the standard deviation increases with height between 0.1 – 0.6 m. Readings at 0.7 m are also reasonably stable (± 3 mS/m); however, stability decreases again at 0.8 m. For all surveys in this study, data was acquired 0.7 m because there is minimal drift at this height, and we wanted to avoid additional noise at the ground surface from trash and debris that unfortunately is prevalent along the beach at PAIS. It is suggested that for beach surveys the instrument should be carried at 0.7 m above the ground to avoid unwanted noise at the surface and to maximize the efficiency of data acquisition, especially for long (> 10 km) surveys.

The third calibration test examines signal drift over the battery life-cycle used to power the PDA. A continuous time-series of 600 measurements was acquired at ten second intervals over a period of ~ 100 minutes at each frequency (Figure 3-3D). Measurements were collected at the tie point (Figure 3-3A) 0.7 m above the ground to visualize signal drift at a stationary point. The drift at 3, 10, and 15 kHz frequencies varies between ~ 1 – 2 mS/m, which is at least an order of magnitude less than the variation of measurements collected for each survey in this study. Despite the small degree of noise at 3 kHz, the readings are reasonably stable at all frequencies and show no evidence of appreciable instrument drift. As noted by Abdu et al. (2007), error from signal drift is less significant in environments (e.g., coastal) where the S/N ratio is high. For coastal surveys covering a relatively small area, Delefortrie et al. (2014a) propose a drift-correction procedure using a calibration line that crosses the entire survey area over a short amount of time. Although useful, this procedure is not practical for the 37-km-

long alongshore survey in the present study because it takes ~ 4 – 5 hours to acquire 10 km of data. Along the beach, groundwater conditions can change over these timescales in response to tidal forcing. Thus, it is argued that a detailed account of tidal variation is more important for large-scale alongshore surveys than applying a drift correction to the spatial EMI data series. It is important to note that the calibrations described above are intended for walking surveys. Although beyond the scope of the present study, additional calibrations and drift corrections may be necessary if the instrument is being towed behind a vehicle (see Delefortrie et al., 2014a).

Instrument orientation testing

Test surveys were conducted on 05/18/2013 starting at the seaward side of the NS to determine: 1) consistency of σ_a measurements using different TX – RX boom orientations to check whether there is underlying 1D structure; 2) measurement reproducibility along the same transect acquired on the same day. Two vertical dipole (VD) orientations were tested: in-line (*P-mode*) with TX and RX coils aligned in the survey direction, and broadside (*T-mode*) with TX and RX coils aligned perpendicular to the survey direction. Differences between P-mode and T-mode signatures can be attributed to variations in the mutual electromagnetic coupling between the TX coil, the subsurface structure, and the RX coil. In other words, mutual coupling is affected by the relative geometry of the TX – RX configuration with respect to subsurface structure (Everett, 2013). Furthermore, the mutual coupling is the same for both modes if the subsurface is 1D. Both surveys were conducted at 0.5 m step-size along the same 100-m-

long shore-normal transect, starting at the backbeach and traversing the foredune ridge. Responses acquired in the different modes at each frequency were nearly identical. However, a slight mismatch between the two modes is visible between 50 – 70 m along the survey line at 1 and 5 kHz frequencies, but is not significant at 15 kHz (Figure 3-4). There is a considerable amount of noise at 1 kHz; therefore 3 kHz was used as the lowest frequency for the remainder of the study. The anomaly is more noticeable with decreasing frequency and is more pronounced for the T-mode. This effect could be caused by a discontinuity from a shallow feature along the profile and should be more detectable at the lowest frequency because the EMI sensor has a larger sensitivity pattern (i.e., larger illuminated volume) at low frequency. The 3D sensitivity pattern also has larger extent in the direction parallel to the coil-coil line. Therefore, the 3D anomaly should be more pronounced on data acquired with the T-mode configuration (see Pérez-Flores et al., 2012; Guillemoteau and Tronicke, 2015). The small quantified difference over this limited area justifies collecting data in one orientation, thus all subsequent surveys in this study were executed in P-mode. The small 3D effects from these tests suggest that geoelectrically the beach can be approximated as a 1D environment along a single transect.

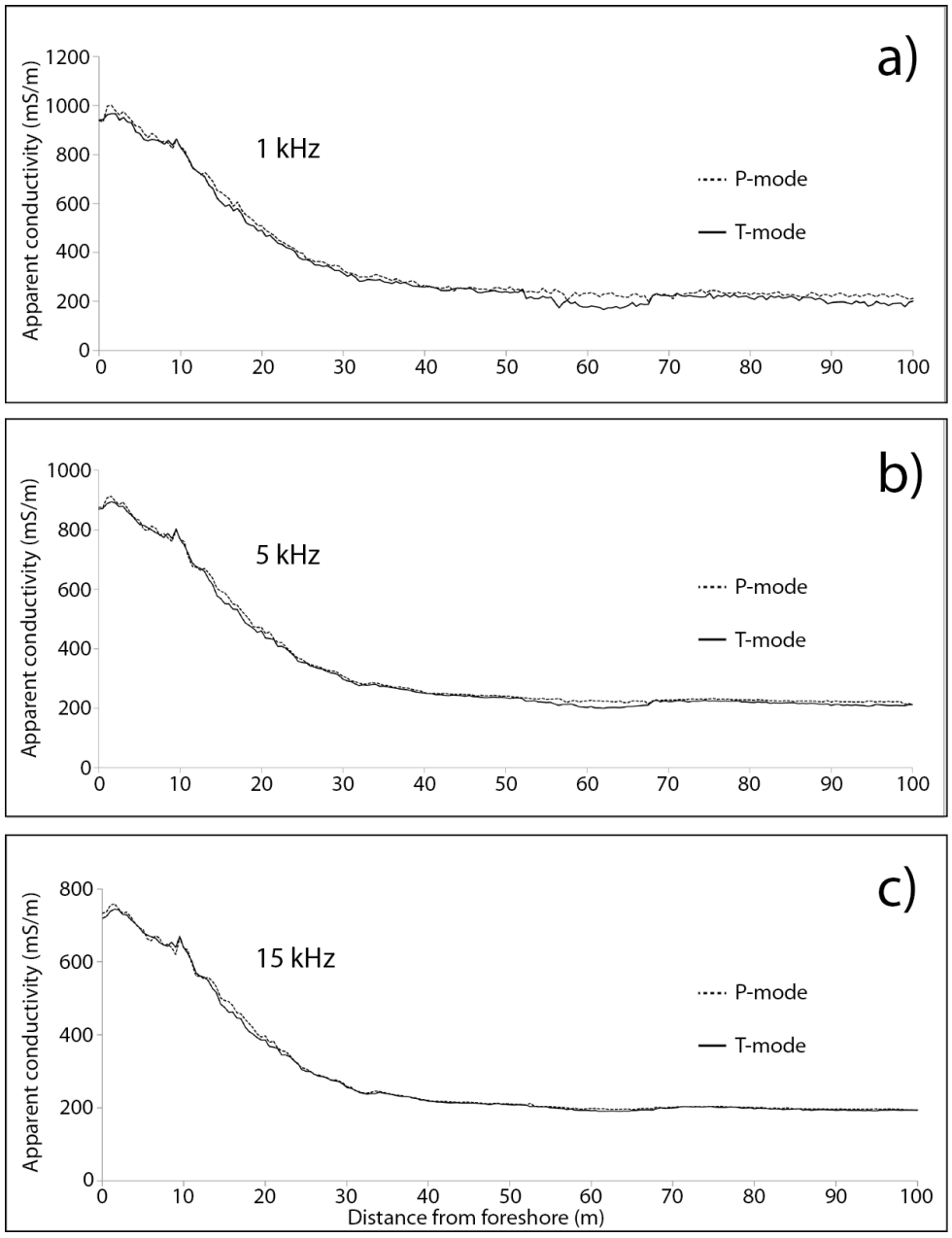

Figure 3-4. Comparison of σ_a measurements taken with different profiler orientations: P-mode and T-mode. Each survey at 1 kHz (a), 5 kHz (b), and 15 kHz (c) was conducted along the same shore-normal transect starting from the backbeach (0 m) and moving west across the foredune ridge (100 m). Step-size for each survey was 0.5 m.

Repeatability tests

Measurement repeatability tests were performed at PAIS and off-site at Texas A&M University campus, College Station, Texas. At PAIS, repeat measurements were recorded at the intersection (i.e., tie points) of the CS and NS sites with the AS survey. The values and relative difference of σ_a measurements between the tie points (Table 3-2) show good agreement at each recorded frequency. The relative difference in σ_a values (d_{ac}) was calculated by:

$$d_{ac} = (\frac{A_x - A_y}{A_y}) x\ 100 \tag{3.3}$$

where, A_x is σ_a at the point where the two surveys intersect in the alongshore, or x-dimension, and A_y is σ_a at the point where the two intersect in the shore-normal direction, or y-dimension. It is possible that the mismatch between values at each tie point can be attributed to measurement error because the positional accuracy of the EMI sensor's GPS is ~ 1 m. Nonetheless, the overall agreement of σ_a values at each tie point provides further evidence that same-day measurements by the EMI sensor are reproducible.

Table 3-2. Tie points and relative difference of measured σ_a values between the alongshore and shore-normal surveys collected in August, 2013. The σ_a values in the upper rows are the tie points between the start of the 10 km alongshore survey (0 km) and the start of the central shore-normal survey (CS). The σ_a values in the lower rows are the tie points between the end of the 10 km alongshore survey (10 km) and the start of the northern shore-normal survey (NS).

	3 kHz	**10 kHz**	**15 kHz**
Alongshore (0 km)	677.657	573.961	519.914
Central (0 km)	676.731	573.363	520.865
Relative difference (%)	0.137	0.104	-0.183
Alongshore (10 km)	619.374	536.981	481.833
Northern (0 km)	600.619	517.821	473.218
Relative difference (%)	3.12	3.70	1.82

In addition to testing the profiler in a coastal environment, where the subsurface hydrology is both complex and dynamic, repeat surveys were performed on the campus at Texas A&M University in a loamy soil environment where the hydrology is presumably less spatially and temporally variable. Two surveys were conducted on 11/11/2014 and 11/19/2014 along a 30 m transect at a 1 m step-size (Figure 3-5). The first survey was performed during dry conditions, whereas the second survey was taken a week later a few days after a rain event. A buried object (irrigation pipe) is visible between 12 – 15 m along the transect and allows a detailed comparison between each set of survey data. The approximate depth of the pipe is 2 – 3 m and the DOI is ~ 6.4 – 2.7 m for the range of σ_a values measured at 3, 10, and 15 kHz (see Table 3-1). The spatial coherence of the signals at each frequency provides an indication of the quality and the repeatability of the measurements. Apparent conductivity is computed from the

measured secondary magnetic field. For a constant offset and a given homogeneous half-space, the expected Im(Hs/Hp) response decreases as the frequency decreases. In this case, the theoretical response is too weak in comparison to the noise level from environmental effects. Nonetheless, the results suggest that the sensor is capable of taking reliable measurements at higher frequencies across different acquisition dates.

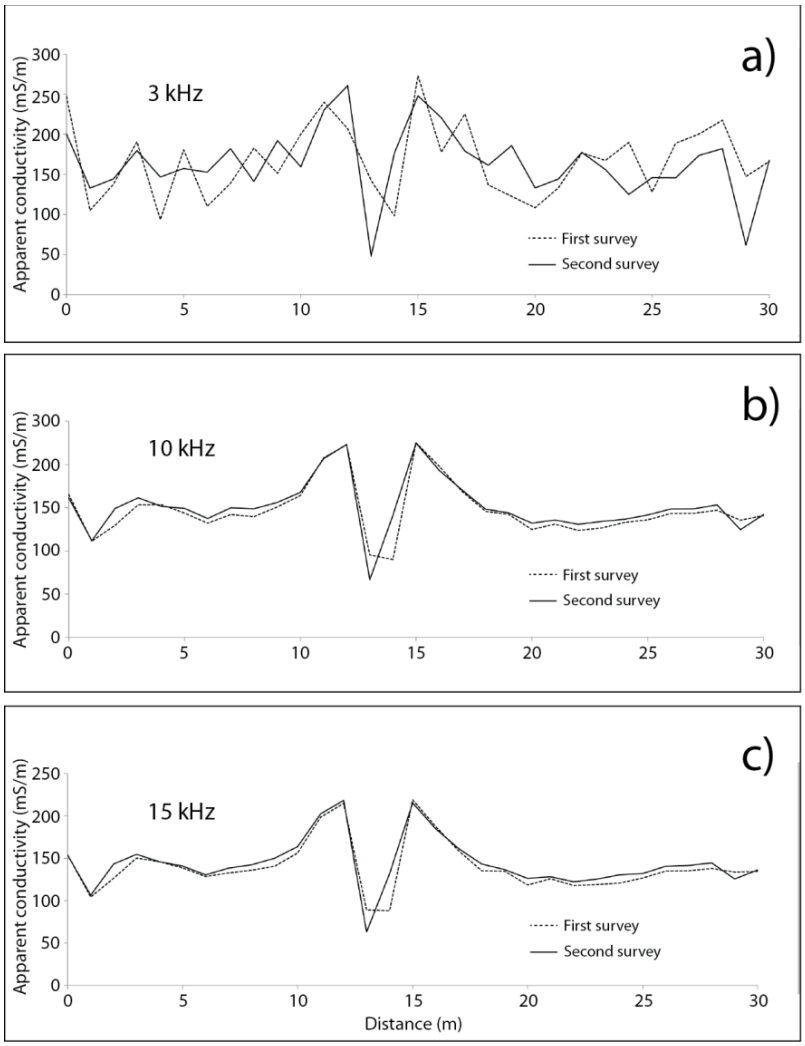

Figure 3-5. Off-site repeatability tests performed on campus at Texas A&M University in College Station, Texas. The same frequencies (i.e., 3, 10, 15 kHz) were used at the off-site location as what was measured for all subsequent surveys in the study site (except Figure 3-4).

Results

Tidal cycle experiments

Previous studies suggest that tidal motions play a substantial role in the position and fluctuation of the water table in sandy beaches (e.g., Lanyon et al., 1982; Nielsen, 1990). Rising and falling tides should cause fluctuations in subsurface σ with respect to variations in the exchange of fresh and salt water over the course of the tidal cycle. It is reasonable to assume that this "tidal effect" influences the EMI response depending on when a survey is performed (i.e., during low or high tide). What is not known is the manner in which σ_a changes in response to tidal dynamics and how far inland this effect persists. Here, we present the results of three experiments investigating the behavior of EMI data over a 12-hour tidal cycle both alongshore and across the beach at the intersection of the NS and AS (see Figure 3-3A).

The tests were conducted on 03/30/2015 at 08:00, ~ 75 minutes after low tide at the tie point between NS and AS. Measurements were recorded (h = 0.7 m) every hour, for 12 hours, to monitor changes in σ_a (Figure 3-6). Tidal data were downloaded from the NOAA Tsunami Capable Tide Stations database (http://tidesandcurrents.noaa.gov/tsunami/). The closest ocean-facing tide station is the Bob Hall Pier, Corpus Christi, Texas (Station ID: 8775870) located ~ 70 km NNE of the study site. At the tidal station, water level data are referenced to mean lower low water (MLLW) and measurements are recorded at 1 minute intervals.

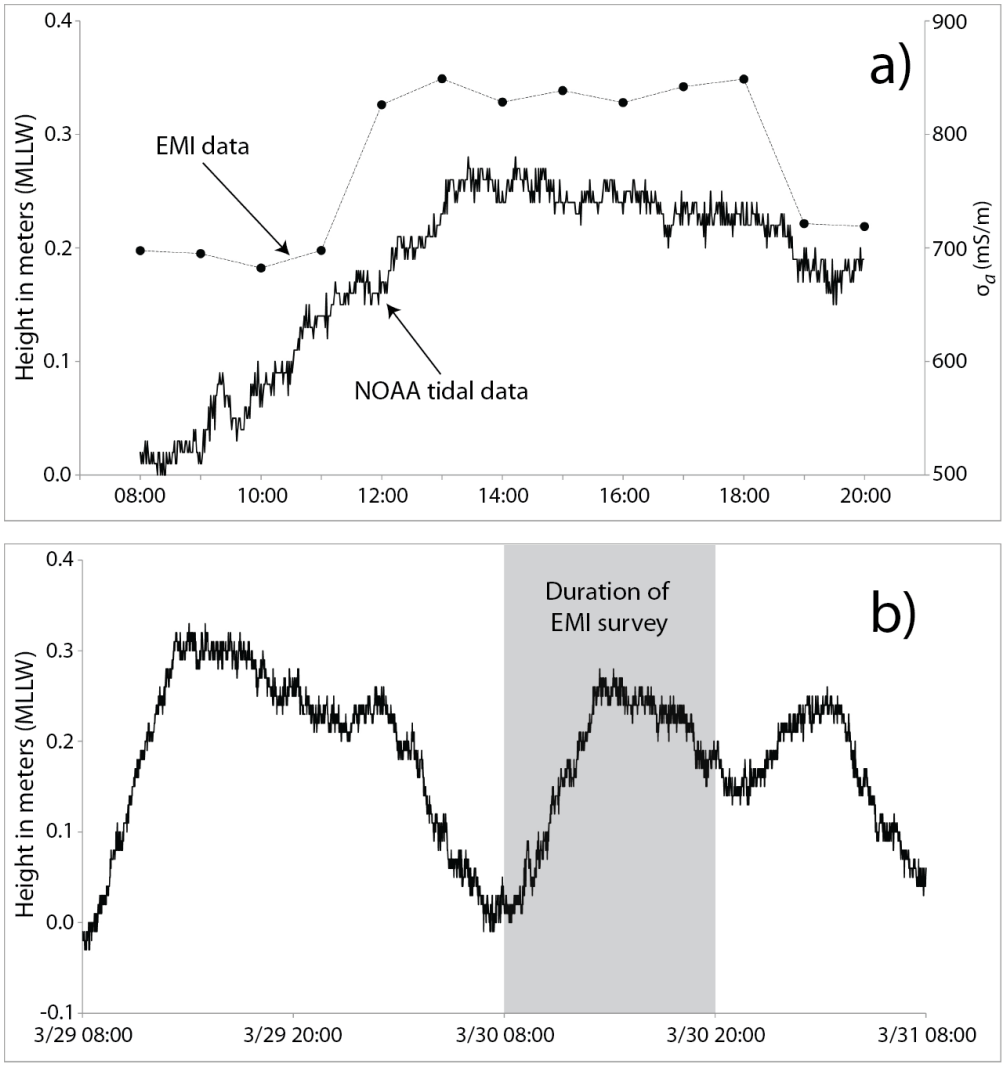

Figure 3-6. (a) Tidal cycle and step-function 3 kHz EMI response over a 12-hr sampling interval at the tie-point between the AS and NS. Tidal data was downloaded on October 18th, 2015 from the NOAA website at: http://tidesandcurrents.noaa.gov/tsunami/#. The closest NOAA tidal station to the study site is the Bob Hall Pier, Corpus Christi, TX (Station ID: 8775870). Water level records are recorded at 1-minute intervals. (b) 48-hour tidal cycle data prior to, during, and after the 12-hour EMI survey. Note: all water level data is referenced to mean lower low water (MLLW).

The tidal data exhibit the mixed semidiurnal pattern that is characteristic of the region. The 12-hour survey captured two low tides of varying magnitude (~ 06:42 and

20:02), and one high tide (~ 14:39). Although the tidal signal exhibits a periodic trend, the EMI signal follows a more step-function-like pattern. At low tide, the σ_a values (~ 695 mS/m) remain fairly constant for 4 hours and then suddenly jump to ~ 830 mS/m at 12:00, preceding high tide by nearly 3 hours. The σ_a values remain consistently high up to 3 hours after high tide and suddenly drop to ~ 720 mS/m at 19:00. The EMI signal exhibits a lead/lag step-response that increases rapidly preceding the high tide then drops off slowly during falling tide. The σ_a values at the higher low tide (20:00) are on average ~ 30 mS/m higher than values recorded at the lowest low tide (08:00).

The aforementioned effect can also be seen in two additional surveys that were performed over a 50 m alongshore transect and 50 m shore-normal transect (Figure 3-7). Both surveys were collected at 1 m step-size at the same location as the repeatability tests, i.e., at the intersection of NS and AS (refer to Figure 3-3A). The objective of these tests was to examine measurement repeatability along each transect during different stages of the 12-hour tidal cycle to better understand the effect of changing hydrologic conditions on the EMI signal. Each survey was repeated every hour for twelve hours, starting at 08:00 and ending the same day at 20:00. Both the alongshore and shore-normal surveys were acquired in approximately five minutes, respectively. Two low

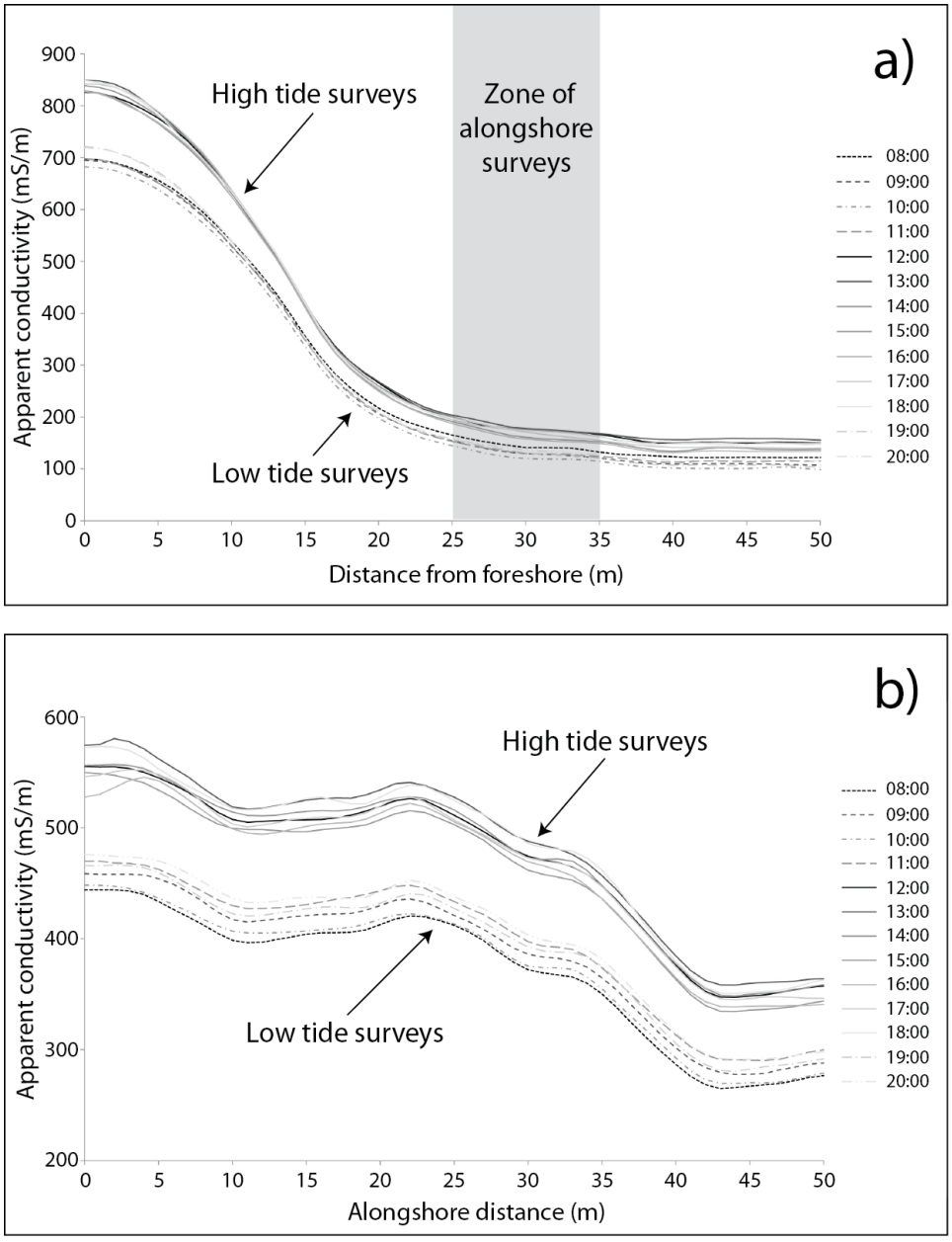

Figure 3-7. Shore-normal (a) and alongshore (b) 3 kHz repeat surveys measured over the course of a 12-hour tidal cycle. The profiler was oriented in P-mode for each survey and was calibrated at the same tie-point location (see Figure 3a) prior to each hourly survey. The dotted lines in both surveys correspond to measurements taken during low tide, whereas solid lines represent measurements made during high tide. The darkest lines represent the onset of high and low tides and gradually decrease in intensity with time.

tides and one high tide were captured during the surveys and the difference in water levels between the tides was ~ 0.3 m. Similar to the results shown in Figure 3-6, both the alongshore and shore-normal surveys suggest that there is a tide-dependent step response in σ_a. For example, σ_a values measured at both high and low tides are clustered together, delineated by the solid and dotted lines in the figure, respectively. With respect to the shore-normal surveys, the separation between high and low tide responses becomes smaller with distance inland. Nonetheless, a difference of up to ~ 50 mS/m occurs at the base of the foredune ridge. The highlighted area in Figure 3-7A delineates the zone where each alongshore survey was performed, where the difference- in σ_a values is ~ 80 mS/m between high and low tides. Although σ_a values varied over the course of the tidal cycle, the overall trend in the data for each survey is consistent.

Shore-normal EMI surveys

Shore-normal EMI transects were performed across the barrier/wind-tidal flats at the southern (SS), central (CS) and northern (NS) sites in August, 2013. Each transect was collected at a 10 m step-size at 3, 10 and 15 kHz frequencies (Figure 3-8). The length of each transect for the NS, CS and SS sites are 1.9, 3.2, and 4.6 km, respectively. For each profile, the highest σ_a values correspond to the lowest elevations (i.e., beach, salt marsh and wind-tidal flats). Conversely, the highest elevations correspond to the lowest σ_a values (i.e., dunes and back-barrier dunes). Here we adopt terminology used

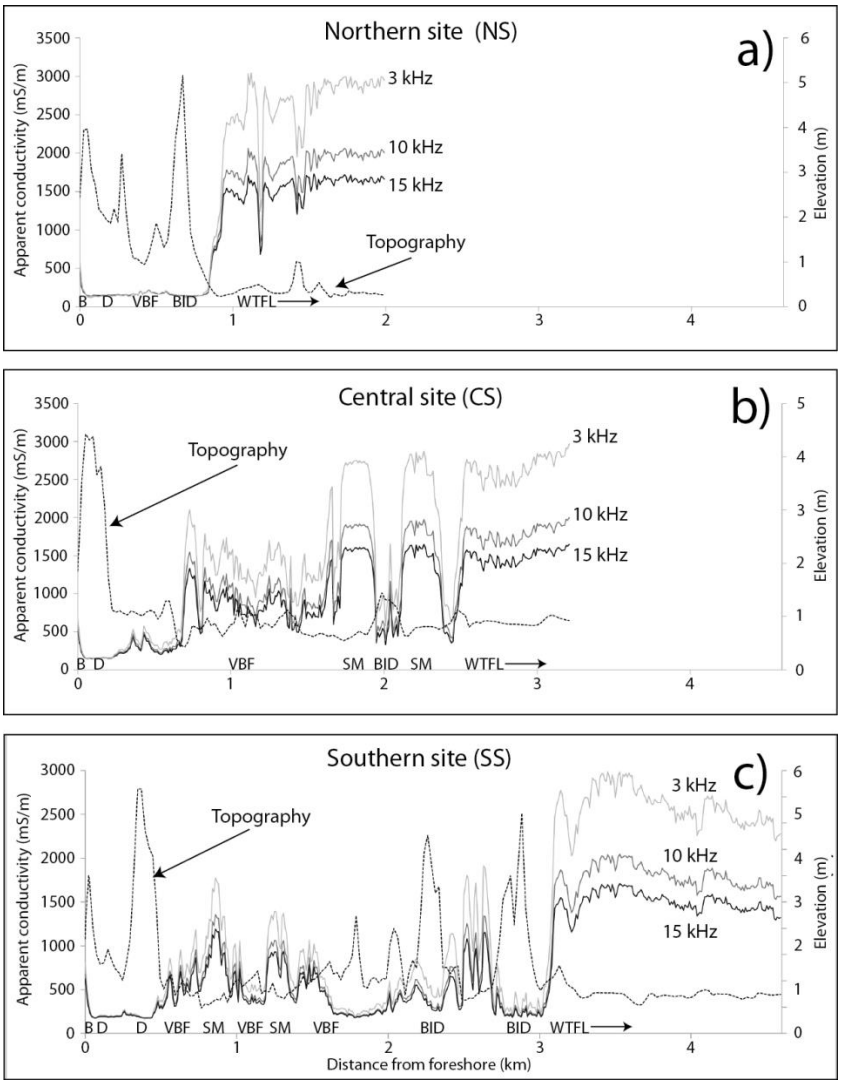

Figure 3-8. Shore-normal surveys and classification of each sub-environment for the northern (a), central (b), and southern (c) sites collected between August 7, 8 and 9, 2013, respectively. Abbreviated labels for each environment are as follows: beach (B), dunes (D), vegetated-barrier flats (VBF), back-island dunes (BID), wind-tidal flats (WTFL), and salt marsh (SM). For each survey, the light gray, dark gray and black lines correspond to σ_a values measured at 3, 10 and 15 kHz, respectively. The step-size for each survey was 10 m. Topography data (dotted lines) was extracted from an open access dataset provided by the Army Corps of Engineers (USACE) and Joint Airborne LiDAR Bathymetry Technical Center of Expertise (JALBTCX) as part of the 2009 West Texas Aerial Survey project. The LiDAR data can be accessed through the NOAA Digital Coast Data Access Viewer at: http://coast.noaa.gov/digitalcoast/data/coastallidar. Topographic elevation was extracted from the LiDAR-derived DEM every 25 m along the northern, central and southern transect. The horizontal and vertical positional accuracy of the LiDAR is 0.15 and 0.5 m, respectively.

by Paine et al. (2004) for classifying different coastal sub-environments across the barrier island system. Distinct sub-environments are labeled for each survey in Figure 3-8 and are defined in the figure caption. The width of the island generally increases from north to south and the variety of coastal habitats also increases with island width. As a result, variations in the EMI signal related to changes in geomorphic environments become more pronounced from the NS to SS. For all surveys, σ_a measurements increase with decreasing frequency.

In addition to σ_a measurements, topographic information was extracted from aerial LiDAR datasets for comparison with the EMI data. The aerial LiDAR survey was performed in 2009 by the Army Corps of Engineers (USACE) and Joint Airborne LiDAR Bathymetry Technical Center of Expertise (JALBTCX) as part of the West Texas Aerial Survey project to assess post-hurricane conditions of the beaches, barrier islands, and lakeshores along the Texas coast. The 2009 LiDAR dataset is the most recent one publicly available. Although there is a 4-year interval between the LiDAR and EMI surveys, Padre Island has not been directly impacted by a hurricane since 2008, when Hurricane Dolly struck south Padre Island as a Category 1 storm (NOAA, 2015). As a result, Padre Island currently is more stable than other islands along the Texas coast (i.e., Galveston, Matagorda, Bolivar Peninsula) which have been recently impacted by Hurricanes Rita and Ike (NOAA, 2015). The 1 meter resolution LiDAR-derived digital elevation model (DEM) used in this study was generated using an ordinary kriging algorithm at Texas A&M University. The entire study area was processed by dividing the entire point cloud into tiles approximately 8 km by 8 km. There was no single

semivariogram used in processing the LiDAR point cloud tiles because the exact semivariogram parameters are tile-dependent. The DEM was broken into tiles in order to facilitate processing and because the morphology of each tile is different, the semivariogram parameters will vary slightly between tiles. The processed DEM tiles were subsequently merged to produce the final DEM covering the entire study area.

Alongshore EMI surveys

Alongshore surveys (Figures 3-9, 3-10) were performed between November 2013 through March 2015 to investigate the profiler's ability to detect variations in framework geology and the location of previously inferred Pleistocene paleo-valleys/paleo-channels (see Fisk, 1959; Brown and Macon, 1977). These paleo-channels lie between the CS and NS sites of the present study. The alongshore surveys are located within a 10-km section of the beach and intersect the CS and NS transects (see Figure 3-2). Each survey was performed in the backbeach environment, ~ 25 – 35 m inland from the MTL (as indicated by wrack-line deposits), where the beach is drier and presumably less affected by the dynamic hydrology. Similarly to the shore-normal surveys, each transect was collected at a 10 m step-size at 3, 10 and 15 kHz frequencies. For comparison, the previously identified paleo-channels were digitized from Fisk (1959) using ArcGIS™ software and superimposed on satellite imagery (Figure 3-9). There is a high degree of variability in σ_a along the 10-km-long transect with values ranging from ~ 50 – 800 mS/m. Average alongshore σ_a values are ~ 400 mS/m, consistent with

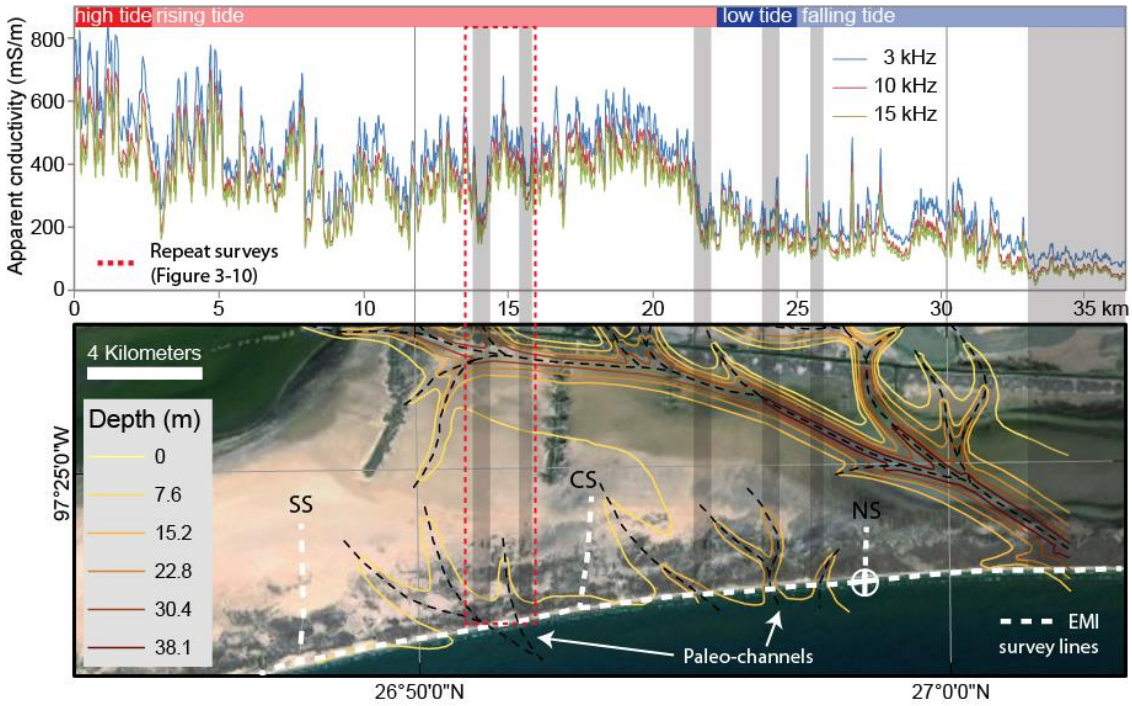

Figure 3-9. Alongshore EMI comparison with previously interpreted paleo-channels by Fisk (1959) and the approximate tidal states during data acquisition. The EMI survey was collected on October 11th, 2014. Distance in kilometers on the x-axis of the EMI survey. The gray shaded regions highlight the intersections of the paleo-channels corresponding (on average) to low σ_a values. Depth contours were manually digitized using ArcGIS™. Inferred Pleistocene streams are indicated by black-dotted lines and the EMI surveys are represented by the white-dotted lines. The repeat alongshore surveys (Figure 3-10) are denoted by the red-dotted lines.

seawater-saturated beach sand. However, σ_a values decrease in certain places to < 200 mS/m, indicating a change in lithology and/or groundwater conditions. The decrease in σ_a occurs roughly within the same areas where Fisk (1959) inferred the location of Pleistocene paleo-valleys/channels from seismic and core data.

A comparison of three repeat surveys taken within a smaller 2.5 km segment of the AS (see Figure 3-9) shows the seasonal effects on the EMI signal over a period of ~

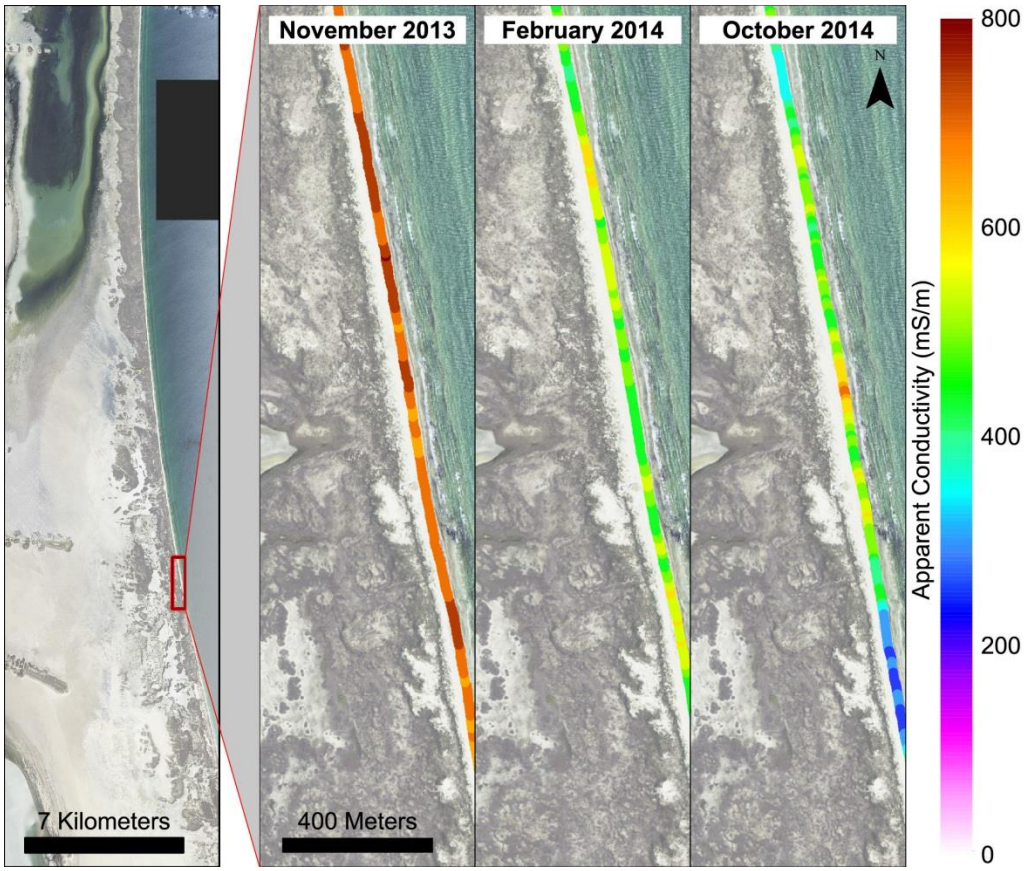

Figure 3-10. Comparison of 3 kHz repeat alongshore surveys within the AS collected on November 28th, 2013, February 2nd, 2014 and October 11th, 2014. Apparent conductivity values for each survey are superimposed on satellite imagery from National Agricultural Imagery Program (NAIP), 2012. Note: each image has the same scale, and σ_a is displayed using the same range in values (0 – 800 mS/m).

one year between November 2013 and October 2014. All of the surveys are located within the boundaries of the interpreted paleo-channel region. The 3 kHz σ_a values in each panel are displayed using GPS positions recorded by the sensor. The tidal state during each survey was approximately at low tide and is assumed to be less significant

than the seasonal variation within the signal (Table 3-3). Figure 3-10 illustrates how σ_a varies between seasons (i.e., during wet and dry conditions). The σ_a values are highest in November 2013, a few days after a rainy period and elevated storm surge, resulting in a signal consistent with homogenous saturated substratum. Conversely, the lowest σ_a values correspond to the October 2014 survey when the beach was considerably drier. Here the σ_a signal shows more heterogeneity that is hypothesized to reflect the framework geology of the island. In general, the results suggest that the sensor probes deeper and is able to detect variations in geologic structure when the beach is drier.

Table 3-3. Daily tidal variations during each EMI survey. Survey times are listed relative to the high and low tides. Data was recorded by NOAA at the Padre Island (south end) tide station #4471 (26º 04.1'N, 97º 09.4'W). Note: reported times and heights correspond to high and low waters. Historical tidal data downloaded from NOAA's Tides and Currents website: (http://tidesandcurrents.noaa.gov/historic_tide_tables.html) on April 15, 2015.

Date (Time of survey)	Time **h m**	Tide	Height **ft**	**cm**	Survey direction
18 May, 2013	01:34	Low	0.5	15	NS test survey (Figure 3-4)
(~10:00 – 11:00)	09:53	Hi	1.4	43	
	17:21	Low	0.8	24	
	20:51	Hi	0.9	27	
7 August, 2013	05:05	Hi	1.3	40	NS (Figure 3-8)
(~15:00 – 20:00)	09:53	Low	1.1	34	
	12:50	Hi	1.2	37	
	21:10	Low	0.1	03	
8 August, 2013	05:07	Hi	1.2	37	SS (Figure 3-8)
(~11:00 – 15:00)	10:09	Low	1.0	30	
	14:04	Hi	1.1	34	
	21:42	Low	0.2	06	
9 August, 2013	05:08	Hi	1.2	37	CS (Figure 3-8)
(~10:00 – 16:00)	10:34	Low	0.8	24	
	15:21	Hi	1.1	34	
	22:18	Low	0.3	09	
29 November, 2013	05:41	Low	0.3	09	Repeat AS (Figure 3-10)
(~09:00 – 10:00)	14:13	Hi	1.6	49	
2 February, 2014	03:40	Hi	1.0	30	Repeat AS (Figure 3-10)
(~10:00 -12:00)	10:53	Low	-0.2	-06	
	17:32	Hi	0.9	27	
	23:31	Low	0.3	09	
11 October, 2014	11:14	Low	0.1	03	AS (Figures 3-9 and 3-10)
(~08:00 – 20:00)	20:11	Hi	2.1	64	
30 March, 2015	06:42	Low	0.3	09	Tidal and calibration experiments
(~8:00 – 20:00)	14:39	Hi	1.3	40	(Figures 3-3, 3-6, and 3-7)
	20:02	Low	1.0	30	

Discussion

Groundwater dynamics within sandy beaches and barrier islands have been studied in detail (e.g., Nielsen, 1990; Nielsen and Kang, 1996; Nielsen, 1999; Horn, 2002; Stevens et al., 2009) and have important implications for EMI investigations. Understanding the interaction between surface and groundwater flows is not only important quantifying beach profile evolution (Horn, 2002), but also has been shown in this study to influence σ_a measurements, complicating geologic framework interpretations. Nielsen (1999) suggests that the watertable under coastal barriers will be highest on the seaward side of the island because of wave action and tides. Nonlinear effects within the beach combined with wave and tidal forcing creates a landward-increasing superelevation of the mean water table level, resulting in a net landward flow of subsurface groundwater and thinning of the freshwater lens in the backbarrier (Nielsen and Kang, 1996). It follows that fluctuations in the watertable alongshore and across the island should to some extent regulate EMI signals, however, this effect is suggested to be more pronounced for alongshore surveys in this study. Therefore, we choose to focus on the results of the alongshore surveys in the following discussion as the results of the shore-normal surveys are similar to findings by Paine et al. (2004) and have previously been discussed in depth.

Results from the tidal experiments (see Figures 3-6 and 3-7) suggest that there is a tide-dependent step response in σ_a over a 12-hour tidal cycle. This phenomenon has also been observed by Nielsen (and others) in several studies along the eastern coast of Australia. Using 11 stilling wells to monitor the movement of the water table at

Barrenjoey Beach, north of Sydney, Australia, Nielsen (1990) observed three characteristics at one of the wells landward of the high water mark: 1) the minimum water level was substantially higher than the low tide level; 2) the variation of the water table was not sinusoidal, despite the near sinusoidal (semidiurnal) nature of the tides, and 3) the maximum water level was a few centimeters higher than the high tide level. Nielsen (1990) suggests the resulting response of the water table level is a function of three mechanisms: formation of a seepage face around low tide, asymmetry of the boundary condition at the sloping beach face and the nonlinearity of the governing equations (Darcy's law, continuity equation, and Boussinesq's equation). In other words, the beach slope acts as a nonlinear filter such that water enters the porous medium across the beachface more easily than it leaves, because the infiltration at high tide is more efficient than draining at low tide Nielsen and Kang (1996). This effect is also observed in the current study and may explain the similar lead/lag step-like response in σ_a during the tidal cycle.

The fluctuation of the water table with respect to storms, waves, and tides is a significant problem to consider when performing EMI surveys in the coastal environment, especially for alongshore surveys. For large-scale transects, σ_a measurements will vary at different locations across the beach and depend on the state of the tidal cycle when the surveys were performed. It is argued that a detailed account of tidal dynamics (e.g, low, rising, high, falling) is required for comparison with each EMI survey for data processing and reliable geologic interpretation (see Figure 3-9). Combining the tidal experiments demonstrated in this study with a detailed account of

tidal states provides an avenue forward in separating the complex groundwater vs. geologic signals embedded in the EMI spatial data series. There are free, publically available online resources for downloading accurate tidal information such as; the NOAA Tsunami Capable Tide Stations database. For example, the tidal variability for each survey during the study is given in Table 3-3, showing the time of the survey with respect to the tidal cycle. By knowing the difference in σ_a between high and low tides, the location across the beach in which the survey was performed, and the tidal state during the time of the survey, it is suggested that σ_a values can be adjusted to low tide values to remove the tidal effect. This effect is lowest closest to the dune line, however, at PAIS there is a considerable amount of topographic variation fronting the dunes that may alter the EMI signal as well as reduce the efficiency of data acquisition. Therefore, the optimal zone for alongshore profiling is ~ 25 – 35 m (Figure 3-7A), where the difference in σ_a between high and low tide is roughly the same as at the base of the dunes and there is insignificant topographic variability. Figure 3-7 shows that for both the alongshore and shore-normal repeat surveys the overall trend in the EMI signal is the same over the 12-hour tidal cycle. This suggests that signal processing techniques (e.g., transform functions) and time-series analysis can be used to model the variability of the EMI signal with respect to tidal forcing. This concept will be explored in future studies and has potentially important implications for understanding the complex interactions of groundwater with framework geology.

Results from repeat alongshore EMI surveys demonstrate that σ_a varies considerably when measured during different seasons. Alongshore surveys during wet vs.

dry conditions show noticeably different σ_a values, but may also be masked by tidal effects and/or changing beach states following stormy or calm periods. The wet profile shows more evidence of fine-scale geological heterogeneity, whereas the dry profile shows a larger range between maximum and minimum σ_a values. During wet conditions, σ_a readings are consistently uniform and higher than during dry conditions, limiting the DOI and the sensor's ability to detect changes in lithology. Conversely, during dry conditions the profiler can probe deeper into the resistive surface and is able to better detect lateral variations in the underlying geologic structure. This is because lithological σ contrasts are greater if the lithology is not water saturated. The effect of changing groundwater conditions on EMI signals is suggested to be more dominant at smaller spatial scales (<< 10 km), but is not as important when looking at large-scale (> 10 km) geologic framework geology (see Weymer et al., 2015b). As mentioned previously, small-scale fluctuations of the EMI signal along a profile that result from dynamic hydrology can be statistically corrected. It is argued that geologic interpretations can be made for large-scale barrier island investigations by removing the nonlinearities of the tidal effect.

Conclusions

The results of this study suggest that portable multi-frequency EMI profilers should be used with caution for geologic framework investigations in highly conductive barrier islands. Changing hydrologic conditions over different spatiotemporal scales influence EMI signals both alongshore and across the island, however, are suggested to be more significant for alongshore profiling. It is suggested measurements should be

acquired 0.7 m above the ground and that alongshore surveys be performed ~ 25 – 35 m inland from the MTL in order to maximize data acquisition time and to reduce the influence of changing tides. We recommend combining the instrument calibration and tidal protocol used in this study with detailed tidal records to separate the effects of hydrology and geology on the σ_a signal.

Repeat alongshore surveys during different seasons show different σ_a values, but may also be masked by tidal effects and/or changing beach states. During wet conditions, subsurface σ is relatively uniform, limiting the DOI and the ability of the EMI sensor to detect subsurface variations in lithology. Conversely, during dry conditions the profiler probes deeper and is better able to detect variations in the underlying geologic framework. The effect of changing groundwater dynamics on EMI signals is suggested to be more significant at smaller spatial scales (<< 10 km), but is not as important when looking at large-scale (> 10 km) framework geology. In other words, σ_a measurements are best viewed in a relative sense for mapping the geologic framework of a particular coastline. Future studies investigating the rich statistical information contained within the EMI spatial data series will provide further insight into understanding the variation within the signal and interpreting the complex coastal processes that causes it. We propose that multiple EMI surveys are required along the same transect to account for the confounding effects of changing hydrologic conditions on EMI responses. For geologic framework investigations, EMI surveys should be performed in the backbeach environment during dry conditions when the water table is lower.

CHAPTER IV

LONG-RANGE DEPENDENCE IN COASTAL-BARRIER ELECTROMAGNETIC INDUCTION SPATIAL DATA SERIES

Introduction

It has long been known that many aspects of geophysical observables will exhibit similar statistical properties regardless of the length or time scale over which the observations are sampled (Burrough, 1981). A famous example is the length L of a rugged coastline (Mandelbrot, 1967), which increases without bound as the length G of the ruler used to measure it decreases, in rough accord with the formula $L(G) \backsim G^{1-D}$, where $D \geq 1$ is termed the fractal dimension of the coastline. Andrle (1996), however has identified limitations of the self-similar coastline concept, suggesting that a coastline may contain information that clusters at certain characteristic length-scales pertaining to local processes or structural controls. Recent evidence from Padre Island (Houser and Mathew, 2011), Fire Island (Hapke et al., 2010), and Santa Rosa Island (Houser et al., 2008) suggests that the geomorphology of barrier islands is affected to varying degrees by the underlying framework geology and that this geology varies over multiple length-scales and can be repeating. Little known about the large-scale geologic structure of barrier islands including the important length-scales of subsurface features that may influence alongshore variations in surface morphology, which in turn affects island response to storms and sea level rise.

Some of the geological factors that lead to the self-similarity of natural terrain variations, or lack of it, are reviewed by Xu et al. (1993). In essence, competing and complex morphodynamic processes operate over different spatiotemporal scales, such that the actual terrain becomes a complex superposition of the various effects of these processes (see Lazarus et al., 2011). Although landscapes are not continuously self-similar (i.e., self-affine), it has been suggested that fractal dimensions capture some aspect of surface roughness over a limited range of scales that are not directly evident in conventional morphometric measures (e.g., slope gradient, profile curvature) (see Baas, 2002). In coastal settings, there exist morphodynamic processes that lead to regular (non-fractal) terrain variations. For example, swash zone processes govern the size and spatial distribution of regularly spaced, small-scale (~ 10^1 m) beach cusps. Over larger scales (~ 10^2 – 10^3 m), complex interactions between incident wave energy and nearshore ridge and swale bathymetric features can generate periodic alongshore variations in beach-dune morphology (e.g., McNinch, 2004; Houser, 2012) that are superimposed on larger-scale transport gradients (Tebbens et al., 2002). While coastal terrains might not be exactly or even statistically self-similar, it is reasonable to expect they should exhibit some degree of long-range dependence (LRD). Long-range dependence affects phenomena in which correlations between observations that are far apart (in space or time) decay like a power law, much slower than one would expect from independent data or data following a short-memory process such as autoregressive-moving-average (ARMA) (Beran, 1994; Doukhan et al., 2003).

The framework geology of a barrier system is the result of a long, complex and ongoing geologic history, characterized by sea level fluctuations and episodes of deposition and erosion. The framework geology may be self-similar exhibiting LRD, or approximately so, but methods to ascertain the alongshore variability of the buried framework geology are difficult to implement and can be costly. Geophysical data provide an avenue forward. Acoustic methods provide valuable information offshore, but are problematic onshore because of inefficient coupling of seismic sources with unconsolidated beach sands. Similarly, ground-penetrating radar (GPR) exhibits poor depth penetration in highly conductive seawater-saturated sediments. Herein we examine electromagnetic induction (EMI) geophysical datasets that can probe, to tens of meters depth, the long-range-dependent structure of the framework geology underlying modern barrier systems (see Weymer et al., 2015b).

This study at Padre Island National Seashore (PAIS), Texas, USA demonstrates how EMI data can be used to map subsurface electrical conductivity σ as it is related to variations in the subsurface framework geology. Two alongshore EMI surveys at different spatial scales (~ 100 and 10 km) were performed to test the hypothesis that, similar to changes in surface-exposed barrier island morphology, subsurface framework geology exhibits self-similarity and LRD. The survey design allows for detailed comparisons of the long-range-dependent structure within the framework geology over several orders of magnitude. We also explore the benefits of using the family of autoregressive integrated moving-average (ARIMA) processes in statistically modeling EMI data. It is argued that these models offer a compact way of capturing the entire

hydrogeological complexity of a barrier island with only three parameters that cannot be achieved by other signal processing techniques. This approach offers significant advantages over other statistical techniques used to quantify the underlying processes that give rise to the long-range-dependent structure of large-scale barrier island framework geology.

Study area

Padre Island is part of a large arcuate barrier island system located along the southern Texas coastline and is the longest undeveloped barrier island in the world. The National Seashore is ~ 129 km in length, and is an ideal setting for performing EMI surveys because there is minimal cultural noise to interfere with the EMI signal of the framework geology. Furthermore, the island is continuous for > 100 km and is not dissected by tidal inlets or navigation channels that can interfere with or dominate the underlying framework geology. Modern beach sands depth ranges between ~ 2 – 3 m alongshore and are underlain by a Pleistocene sand/mud ravinement surface of varying thickness that was subsequently buried during the Holocene transgression (Brown and Macon, 1977). Fisk (1959) interpreted a network of Pleistocene (or older) paleo-channels within the central segment of the island from seismic surveys and ~ 3,000 drive-sampler and/or rotary-drill borings. This evidence provides a frame of reference to test the capability of the EMI sensor to map changes in subsurface apparent conductivity (σ_a) with respect to variations in the framework geology.

A handheld multi-frequency GSSI Profiler EMP-400™ was used in the in-line (*P-mode*) configuration with the transmitter (TX) and receiver (RX) coils aligned parallel to the survey direction. The profiler records apparent conductivity σ_a at up to three frequencies simultaneously within the 1 – 16 kHz bandwidth, selectable at 1 kHz increments (Geophysical Survey Systems, 2007). GPS coordinates were recorded for each measurement at ~ 1 m positional accuracy. For all surveys σ_a increases with depth, however, the trend in the signal is roughly the same at each frequency. Herein, we focus on measurements at 3 kHz representing the greatest depth of investigation (DOI) of ~ 6.4 – 3.5 m over the range of conductivities (~ 50 – 600 mS/m) encountered in the study area (Weymer et al., *accepted*). Surveys were performed in the backbeach environment, ~ 25 m inland from the swash zone to reduce the effect of temporally variable hydrology (e.g., tides), and to avoid topographic variations (e.g., coppice dunes) fronting the foredune ridge that can alter the EMI signal. The duration and approximate tidal states of each survey were documented to compare with the EMI signal. Tidal data were accessed from NOAA's Tides and Currents database (https://tidesandcurrents.noaa.gov). Padre Island is microtidal and the mean and diurnal tidal ranges within the study area are 0.38 m, 0.45 m, respectively (NOAA, 2015).

Field methods and EMI spatial data series

Profiles of EMI σ_a responses typically are irregular and each datum represents a spatial averaging of the bulk conductivity σ, which in turn is a function of a number of physical properties (e.g., porosity, lithology, water content, salinity, etc.). The "sensor

footprint", or surface area beneath which the spatial averaging is performed, is dependent on the separation between the TX – RX coils (1.21 m in this study), the operating frequency, and can be less than the step-size between subsequent measurements along the profile. In other words, the sensor footprint determines the volume of ground the instrument measures at each acquisition point, and as will be discussed later, the radius of the footprint has important implications for analyzing LRD. Two different station-spacings were used to examine the correlation structure of σ_a at various spatial scales. An island-scale alongshore survey of 100 km was performed using a 10 m station spacing (station spacing >> footprint radius) such that each σ_a measurement was recorded over an independent volume of ground. Additionally, a nearly continuous sequence of σ_a was collected at a 1 m spacing (station spacing< footprint radius) for 10 km within the paleo-channel region of the island. The survey design allows for detailed comparisons of the long-range-dependent structure within the framework geology over several orders of magnitude ($10^0 – 10^5$ m).

The 100 km EMI survey (Figure 4-1) represents, to our knowledge, the longest continuous EMI survey ever completed, resulting in a sufficiently large sample size n = 10,783 (97 km) for accurately modeling LRD of barrier island geology (see Beran, 1992; Taqqu et al., 1995). A total of 21 segments were collected during three field campaigns: October 9 – 12th, 2014, November 15 – 16th, 2014, and March 28th, 2015. The EMI files were stitched together by importing GPS coordinates from each measurement into ArcGIS™ to create the composite spatial data series. The unprocessed (raw) data shows a high degree of variability along the island. To reduce the effect of drift, a linear trend

removal was applied to the data (Figure 4-1b), following which the mean was subtracted. High-amplitude responses within the EMI signal generally exhibit a higher degree of variability compared to smaller, low amplitude responses. Higher σ_a readings correspond to a smaller sensor footprint and most likely are capable of detecting small-scale near-surface heterogeneities (see Guillemoteau and Tronicke, 2015). Low σ_a readings suggest the sensor is probing greater depths and averaging over a larger footprint. The differenced dataset (Figure 4-1c) shows that the increments of $\Delta\sigma_a$ are Gaussian distributed, but exhibit epochs of high variation, or 'burstiness' in some of the areas of high σ_a readings. These anomalies correspond to surveys that were collected in November, 2014, a few days following a rain event. Although it is reasonable to expect that some of the variations in the signal measured under wet conditions are caused by the framework geology, the bursty intervals are likely affected enough by the wet conditions to mask the underlying geological signature (Weymer et al., *accepted*). Each segment collected in November, 2014 represents a small length (~ 5 km) compared to that of the entire data series.

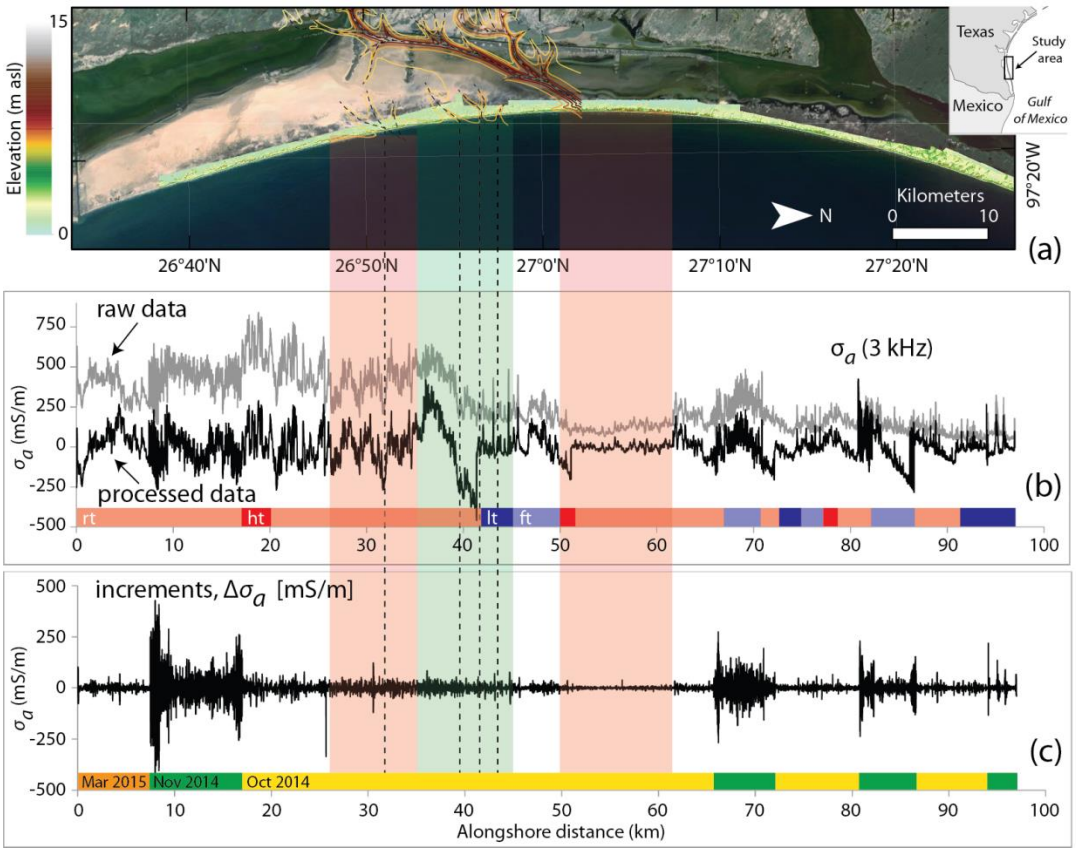

Figure 4-1. 100 km alongshore EMI survey. (a): DEM of study area and previously identified paleo-channel region by Fisk (1959). Channels are highlighted in red and green, where the green region indicates the location of the 10 km survey. 25 ft (7.6 m) contour intervals are highlighted with depths increasing from yellow to red and the center of the channels are represented by the black-dotted lines. (b): Raw σ_a (gray) and drift-corrected (black) EMI responses. Tidal conditions during each EMI acquisition segment are shown below. Low (lt) and falling tides (ft) are indicated by blue and light blue shades, respectively. High (ht) and rising tides (rt) are highlighted in red and light red, respectively. (c): Differenced increments of $\Delta\sigma_a$ shown in (b). Survey dates are highlighted below, corresponding to different hydrologic conditions.

The 10 km survey (Figure 4-2) was performed in one day on March 29th, 2015, so that variable hydrologic conditions should not play a significant role. The composite data series consists of 8 stitched segments. This alongshore survey is located within the

inferred paleo-channel region of the study area, providing some geologic constraints for understanding the variability within the EMI signal (Figure 4-2a). Here, the sample size is n = 10,176, permitting analogous statistical comparisons between the two data series with approximately the same sample size at both low and high spatial resolution. Unlike the 100 km survey, the footprint of the sensor overlapped each subsequent measurement, enabling a more detailed characterization of the underlying σ structure because the separation between the TX – RX coils (1.21 m), a good lower-bound approximation of the footprint, is greater than the step-size (1 m).

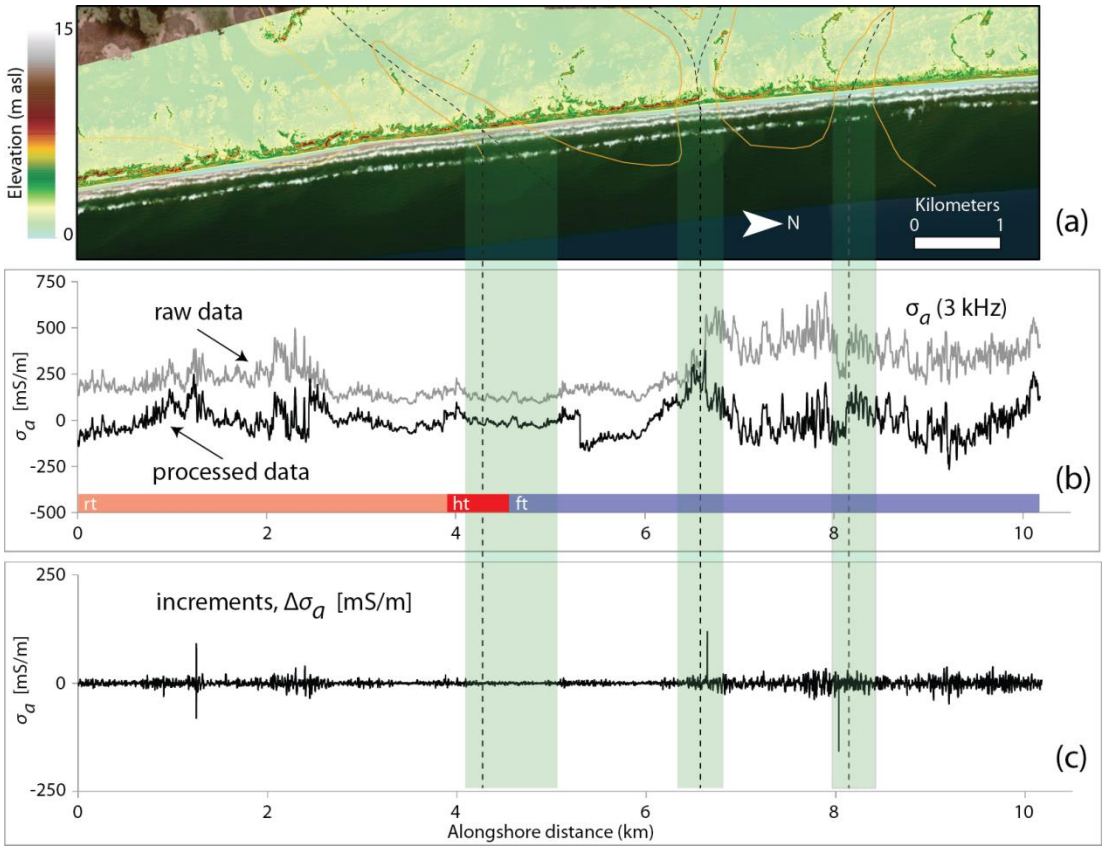

Figure 4-2. 10 km alongshore EMI survey within the previously interpreted paleo-channel region (highlighted in green) by Fisk (1959). (a): DEM and northern segment of paleo-channels superimposed in yellow with the center of the channels represented by the black-dotted lines. (b): Raw σ_a (gray) and drift-corrected (black) EMI responses. Tidal conditions are shown below using the same color scheme as in Figure 4-1. (c): Differenced increments of $\Delta\sigma_a$ shown in (b).

The overall trend in σ_a measurements is comparable to the 100 km survey, where high amplitude and low amplitude signals correspond to high and low variability, respectively (Figure 4-2b). The decrease in σ_a that persists between ~ 2.5 – 6 km coincide with two large inferred paleo-channels, whereas a sharp reduction in σ_a is observed at ~ 8.2 km in close proximity to a smaller channel. It is hypothesized that the

geometry of each channel is directly related to the variation in the EMI signal, such that long, gradual minima in σ_a are indicative of large, deep channels and short, abrupt minima in σ_a represent smaller, shallow channels. The differenced data in Figure 4-2c shows smaller-amplitude bursts of variability compared to the 100 km survey because there is less of a hydrologic and/or seasonal effect on the signal. The small amplitude bursts generally occur outside the paleo-channels. It is supposed that reduced variability in the signal is related to the framework geology. Most of the known paleo-channels are located within the 10 km transect and likely contain resistive infilled sands resulting in lower and relatively consistent σ_a readings (Weymer et al., *accepted*).

Tests for long-range dependence

The plots of both spatial data series appear nonstationary where parts of the signal have local linear trends and periodicities. However, a closer evaluation of the entire signal reveals that cycles at many different frequencies occur, superimposed in a random sequence with a constant mean overall (see Beran, 1994). This behavior is typical for stationary processes with LRD, and is often observed for a variety of geophysical phenomena (Beran, 1992). A common first order approach for determining whether a data series has LRD is through inspection of the autocorrelation function, which is important for determining an appropriate statistical model to fit the data (Figure 4-3a, 4-3d). Large correlations at small lags can easily be detected by models with short-memory (e.g., ARMA, Markov processes) (Beran, 1994). Conversely, when correlations slowly tend to zero like a power function, the data contain long-memory effects and

either fractional Gaussian noise (fGn), or fractional ARIMA (FARIMA) models are useful (Taqqu et al., 1995). Both EMI signals in this study exhibit large correlations for large lags, suggesting the data have LRD that is closely linked to long memory effects. The intensity of LRD is related to the scaling exponent, or Hurst parameter H of a self-similar process, where $1/2 < H \leq 1$ indicates an increasing tendency towards such an effect (Taqqu, 2003). Results from a rescaled range R/S analysis (Figure 4-3b, 4-3e) show very high H-values of 0.99 and 0.97 for the 100 km and 10 km surveys, respectively.

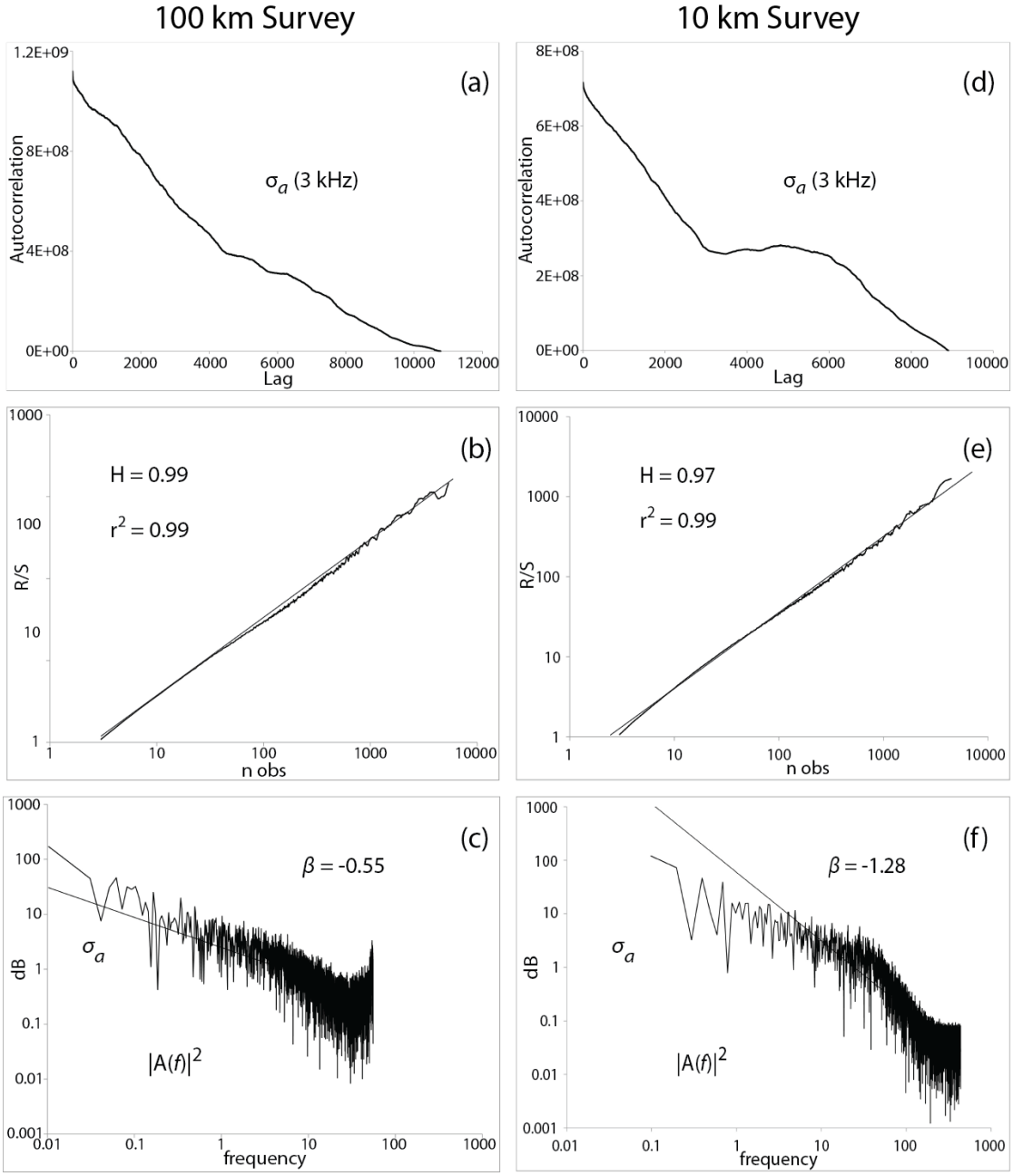

Figure 4-3. Autocorrelations of measured σ_a values for the 100 km (a) and 10 km EMI surveys (d). *R/S* analysis for the 100 km (b) and 10 km surveys (e). The calculated Hurst coefficients *H* are 0.99 and 0.97 for the 100 km and 10 km surveys, respectively. PSD plots for the 100 km (c) and 10 km surveys (f).

The manner in which different frequencies (or herein, spatial wavenumbers; we use these terms interchangeably) are superposed within an EMI signal has been suggested to contain information related to geologic features over a variety of length scales (Weymer et al., 2015b). For example, the lowest-wavenumber contributions are associated with geologic features that occur over the longest length scales. The distribution of frequency components can be examined by plotting the power spectrum where the slope β provides a quantitative measure of heterogeneity in a fractal signal (Figure 4-3c, 4-3f). An increase in $|\beta|$ indicates the series is influenced more by long-range correlations and less by small-scale fluctuations (Everett and Weiss, 2002). The power spectral density (PSD) for the 100 km survey has more small-scale variability than the 10 km survey because, 1) changing hydrologic conditions can vary over longer spatial scales, and 2) the data were acquired over a longer time span (months vs. one day). Thus, the slope of β = -1.28 is steeper for the 10 km survey indicating long-memory effects are more dominant within the paleo-channel region compared to the entire island. It is possible that the variability within the signal and the degree of long-range persistence is also a function of the sensor footprint (step-size), which is critically examined below.

FARIMA statistical modeling and interpretation

Results from preliminary tests for estimating the self-similarity parameter *H* strongly suggest that both EMI spatial data series, and by inference the underlying framework geology, exhibit LRD. The two simplest statistical models accounting for

LRD are fGn, and FARIMA models. In the former case, fGn and its "parent" fractional Brownian motion fBm are used to evaluate stationary and nonstationary fractal signals, respectively (see Eke et al., 2000; Everett and Weiss, 2002). Both fGn and fBm are governed by two parameters, variance σ^2 and the low-frequency scaling parameter, *H* (Eke et al., 2000). A more comprehensive class of models that have similar low-frequency properties as fGn and fBm is FARIMA. Because fGn and fBm models have only two parameters, it is not possible to model the high-frequency components that additional parameters in FARIMA models are designed to handle. FARIMA is a generalization of the ARIMA (*p*,*d*,*q*) process where the degree of differencing *d* is permitted to take on fractional values to better model LRD (see Hosking, 1981). Both classes of models are intrinsically dependent on *H* and are discussed in detail by Taqqu et al. (1995). Because the EMI data series presumably contain both short and long-memory effects, we chose to use FARIMA as the analyzing technique.

An ARIMA model of a data series is defined by three terms (*p*,*d*,*q*), where the goal is to determine the integer values (e.g., 0, 1, 2, etc.) of *p* and *q*, and either the integer or the fractional values of *d* that most accurately model the patterns contained within the original data series. Different combinations of (*p*,*d*,*q*) provide important information on how the various length-scales within the framework geology relate to each other. As mentioned above, *d* is the differencing term that models LRD and it is normally inspected before *p* and *q* to identify whether the process is stationary (i.e., constant mean and σ^2). If the series is nonstationary, it is differenced to remove either linear ($d = 1$) or quadratic ($d = 2$) trends, thereby making the mean of the series

stationary and invertible (Cimino et al., 1999). This allows determination of the *p* and *q* parameters, which indicate the order of the autoregressive (AR) and moving-average (MA) components, respectively. For the analysis, we used the 'arfima' and 'forecast' statistical packages in R to fit a series of ARIMA (*p*,*d*,*q*) models to the observed EMI signals (see Hyndman and Khandakar, 2007; Veenstra, 2012; Hyndman, 2015).

The results of six realizations for the family of ARIMA (*p*,*d*,*q*) models and their residuals (RMSE) are shown for each survey (Figures 4-4, 4-5). Based on the residuals and visual inspection of each model iteration, two observations immediately become apparent: 1) the data are most accurately modeled as an ARIMA (0,*d*,0) process for both surveys, and 2) the mismatch between the data and models is considerably less for the 10 km survey. The first observation suggests that our data are most appropriately modeled by a FARIMA process that is stationary (i.e., $0<d<1/2$) and has long-memory, where the spectral density is concentrated at low frequencies (see Hosking, 1981). This implies that variations in the framework geology at the broadest scales dominate the EMI signal and that the small-scale fluctuations in σ_a caused, for example, by changing hydrological conditions are not statistically significant. Moreover, there is a stronger tendency towards LRD within the paleo-channel region in the 10 km survey, indicating a stronger geologic control compared to the rest of the island.

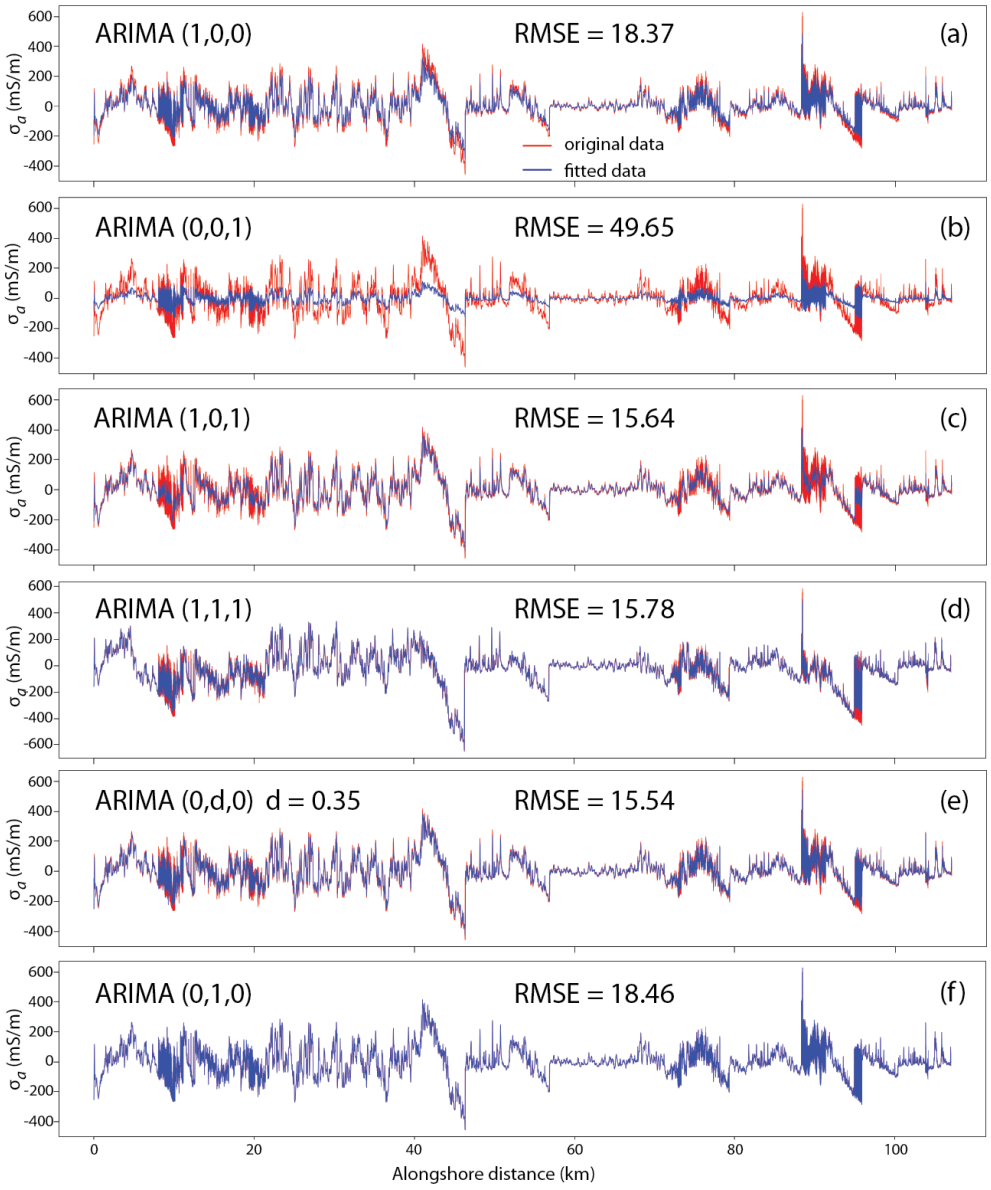

Figure 4-4. Family of ARIMA models for the 100 km EMI survey. Model results are shown for the processed (drift-corrected) σ_a data. The residuals (RMSE) listed for each model gives the standard deviation of the model prediction error. The first three plots allow for more flexible modeling of short-range properties where (a) is an AR process, (b) is an MA process, and (c) is an ARMA process. An example of the general ARIMA (*p*,*d*,*q*) process to model both short and long-range correlations is shown in panel (d). Two special cases of an ARIMA (0,*d*,0) process are shown in panels (e-f), and represent a stationary process with long memory. For each plot the original (real) data is shown in red and the fitted (model) data is highlighted in blue.

Regarding the second observation, the results suggest that a densely-spaced step-size (i.e., 1 m) is preferred to accurately model both short and long-range contributions within the signal. This presents an obvious logistical challenge, because it increases the amount of data acquisition time in the field if the surveys are to be collected at a constant step-size. ARIMA models require that the data must be taken at equal time or spatial intervals (see Cimino et al., 1999). The EMI profiler used in this study can also acquire data at continuous time intervals on the order or seconds. A recent study by Delefortrie et al. (2014a) demonstrates that portable EMI profilers can be towed behind a vehicle, thus it is reasonable to expect that island-scale surveys can still be efficiently performed by collecting data in continuous acquisition mode. This concept will be explored in future studies.

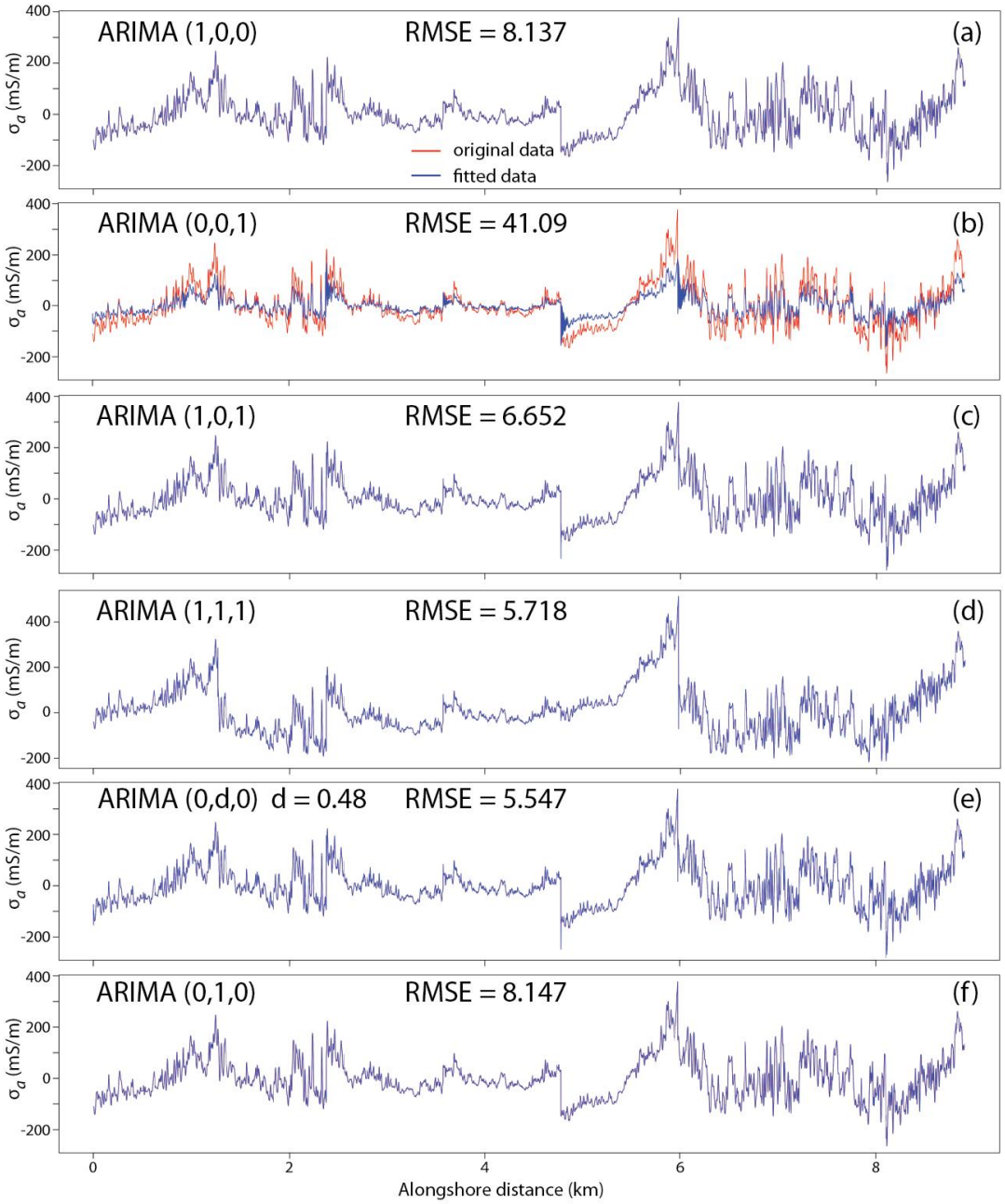

Figure 4-5. Family of ARIMA models for the 10 km EMI survey. Model results are shown for both the processed (drift-corrected) σ_a data. The parameters used for each model follow the same progression as listed in Figure 4-4.

Conclusions

This research demonstrates that the large-scale framework geology of a barrier island, as detected by EMI geophysical methods, has LRD that can be accurately and efficiently modeled by a FARIMA process. An important finding from this study is that FARIMA provides a robust and novel way for fitting a statistical model to the framework geology of a barrier island. It is argued that FARIMA models offer a compact way of capturing the entire hydrogeological complexity of a barrier island with only three parameters (p,d,q) that cannot be achieved by other signal processing techniques. Moreover, EMI profiling can rapidly characterize the entire island and is considerably more cost-effective compared to other geologic and/or geophysical techniques. With respect to large-scale framework geology investigations, we recommend a densely-spaced EMI survey is preferred. This provides a better representation of varying framework geology as well as ensuring a better model fit to the data.

CHAPTER V

FRAMEWORK GEOLOGY CONTROLS ON LARGE-SCALE BARRIER ISLAND TRANSGRESSION

Introduction

Despite the inherent risks of living on barrier islands, the United States is experiencing continued population growth along its coast (Zhang and Leatherman, 2011). According to 2000 census data there are more than 1.4 million people living on barrier islands in the U.S., where population has increased by 14% from 1990 to 2000. With the continued threat of sea level rise, extreme storms and coastal flooding, there are considerable challenges for coastal scientists, engineers, policy makers, and the public for developing sustainable management strategies that support resilient coastal communities. Part of the problem in understanding the susceptibility of barrier response to sea level rise and storms is that few studies have investigated the large-scale evolution of entire islands. This urgency, both to humans and to terrestrial and aquatic ecosystems, makes it imperative that we understand the processes and interactions between geology and surface morphology in these dynamic and vulnerable coastal environments (see Talley et al., 2003).

Previous studies demonstrate that the underlying geology, otherwise termed *framework geology*, of barrier islands plays a significant role in the evolution of coastal landscapes (Kraft et al., 1982; Belknap and Kraft, 1985; Evans et al., 1985; Riggs et al., 1995; Short, 2010). For example, antecedent structures such as paleo-channels, offshore ridge and swale bathymetry, and relict transgressive features have been suggested to

influence barrier island geomorphology to varying degrees and over a wide range of scales (see McNinch, 2004; Hapke et al., 2010; Lentz and Hapke, 2011; Houser, 2012). At the **coastal plain scale** (~ 10^2 km), framework geology influences the structure of the coastal plain, that may include glacial, fluvial, tidal, and/or inlet paleo-valleys and channels (Belknap and Kraft, 1985; Demarest and Leatherman, 1985; Colman et al., 1990), and paleo-deltaic systems offshore or beneath the modern coastal plain (Coleman and Gagliano, 1964; Frazier, 1967; Otvos and Giardino, 2004; Twichell et al., 2013; Miselis et al., 2014). At the **shelf scale** (~ 10^1 km), framework geology consists of feedbacks between geologic features and relict sediments within the littoral system (e.g., Riggs et al., 1995; Schwab et al., 2000; Rodriguez et al., 2001; Honeycutt and Krantz, 2003) and is an important control on dune formation (Houser et al., 2008) and shelf features, including sand ridges (e.g., Browder and McNinch, 2006; Schwab et al., 2013). At the **shoreface scale** (< 1 km), framework geology involves meso to micro-scale sedimentological changes (e.g., Murray and Thieler, 2004; Schupp et al., 2006), variations in thickness of shoreface sediments (Miselis and McNinch, 2006), and spatial variations in sediment transport across the island (Houser and Mathew, 2011; Lentz and Hapke, 2011; Houser, 2012). However, most of what is known regarding barrier island framework geology is based on studies at relatively small spatial-scales (e.g., McNinch, 2004; Hapke et al., 2010; Lentz and Hapke, 2011).

There are detailed local studies that have investigated the importance of framework geology (e.g., McNinch, 2004; Hapke et al., 2010; Lentz and Hapke, 2011), but not entire islands with a few notable exceptions (e.g., Houser, 2012). Little is known about the large-

scale ($10^1 – 10^2$ km) framework geology of barrier islands and the important length-scales of subsurface features that may control alongshore variations in surface morphology, which in turn affects island response to storms and sea-level rise (i.e., transgression). Riggs et al. (1995) state that: *"It is essential to understand this geologic framework before attempting to model the large-scale behavior of these types of coastal systems.... we must understand the detailed geologic framework underlying the shoreface and the inner shelf, as well as the physical dynamics operating within and upon regional segments of the shoreface system."* Assessments of large-scale framework geology are critical for coastal management and risk evaluation for both natural and anthropogenically-modified barrier islands (Hapke et al., 2010; Lentz and Hapke, 2011; Lentz et al., 2013) in order to better understand the connections (or lack thereof) between geology and surface morphology.

Island transgression in response to storms and sea-level rise has been suggested to be dependent (to varying degrees) by pre-existing geologic features which complicates models that assume uniform sand at depth and alongshore (e.g., Belknap and Kraft, 1985; Riggs et al., 1995; Lazarus et al., 2011; Lentz and Hapke, 2011). Models need to compare the degree to which the evolution is free (large sand body) or forced by the geology. In a free system, small-scale undulations in the dune line reinforce natural randomness within a free system that is not influenced by underlying geologic features (Houser, *pers. comm.*). Any variation in the dune line will have an impact on the entire transgression of the island because this process is accomplished primarily by relative sea-level rise and extreme storms that are capable of breaching the dunes and depositing sediment to the backbarrier in the form of

blowouts, washover fans and terraces (Morton and Sallenger, 2003; Stone et al., 2004; Houser, 2012). Houser (2012) suggests that the threshold storm surge required for foredunes to be overtopped or breached decreases as sea-level rises, and subsequently the probability of island overwash and island transgression increases.

Part of the difficulty in examining the relationships between framework geology and island morphology is we cannot directly observe the large-scale framework geology below the surface using traditional labor intensive, low-resolution techniques such as coring. Thus, coastal scientists have turned to geophysical techniques including seismic imaging (e.g., Emery, 1969; Swift, 1975; Penland et al., 1985; Panageotou and Leatherman, 1986; Simms et al., 2006), ground-penetrating radar (GPR) (e.g., Leatherman, 1987; Jol et al., 1996; Heteren et al., 1998; Neal and Roberts, 2000; Buynevich and Fitzgerald, 2003), and more recently, electromagnetic induction (EMI) (e.g., Seijmonsbergen et al., 2004; Vrbancich, 2009; Weymer et al., 2015b) to characterize the underlying geology along the coast. For example, Seijmonsbergen et al. (2004) used an EM34 system at 20 m station spacing and 20 m coil separation to acquire a 14.5 km transect along a segment of the Dutch coast, Netherlands. Using this configuration, the depth of exploration (DOI) is ~15 m. Results from the study suggest that subsurface apparent conductivity σ_a (mS/m) measured by the EMI sensor can be used as a proxy to distinguish the spatial distribution of Holocene coastal deposits and previously identified pre-Holocene paleo-channels near a former outlet of the Rhine River. EMI sensors are becoming an attractive alternative to conventional methods used for barrier island geological research, because they are non-invasive, provide continuous subsurface

information, are capable of characterizing large areas in a short time, and are considerably more cost-effective than the abovementioned traditional geologic and/or geophysical techniques (Weymer et al., 2015b).

This study makes a connection between the large-scale structure of barrier island framework geology and island geomorphology using multivariate analysis and ARIMA statistical modeling of subsurface EMI and LiDAR-derived DEM metrics along Padre Island National Seashore (PAIS), Texas, USA. This approach allows statistical comparisons between subsurface/surface features at a variety of spatial scales and is unique in its attempt to integrate high resolution subsurface/surface datasets for an improved understanding on the geologic controls that force barrier island transgression to varying degrees.

Study area

Padre Island National Seashore (PAIS) is a protected barrier island located ~ 40 km SSE of Corpus Christi, Texas, USA (Figure 5-1). The barrier is one of the southernmost links in a chain of islands and peninsulas along the Texas coastline (Weise et al., 1980). The national seashore is 129 km in length and is the longest undeveloped barrier island in the world. This makes the study area an ideal location for investigating the relationships between large-scale framework geology and surface morphology because the island is not dissected by inlets or navigation channels (excluding Mansfield Channel), or modified by engineered structures (e.g., groynes, jetties, etc.) that interrupt natural morphodyamic processes across the coastal zone (see Talley et al., 2003).

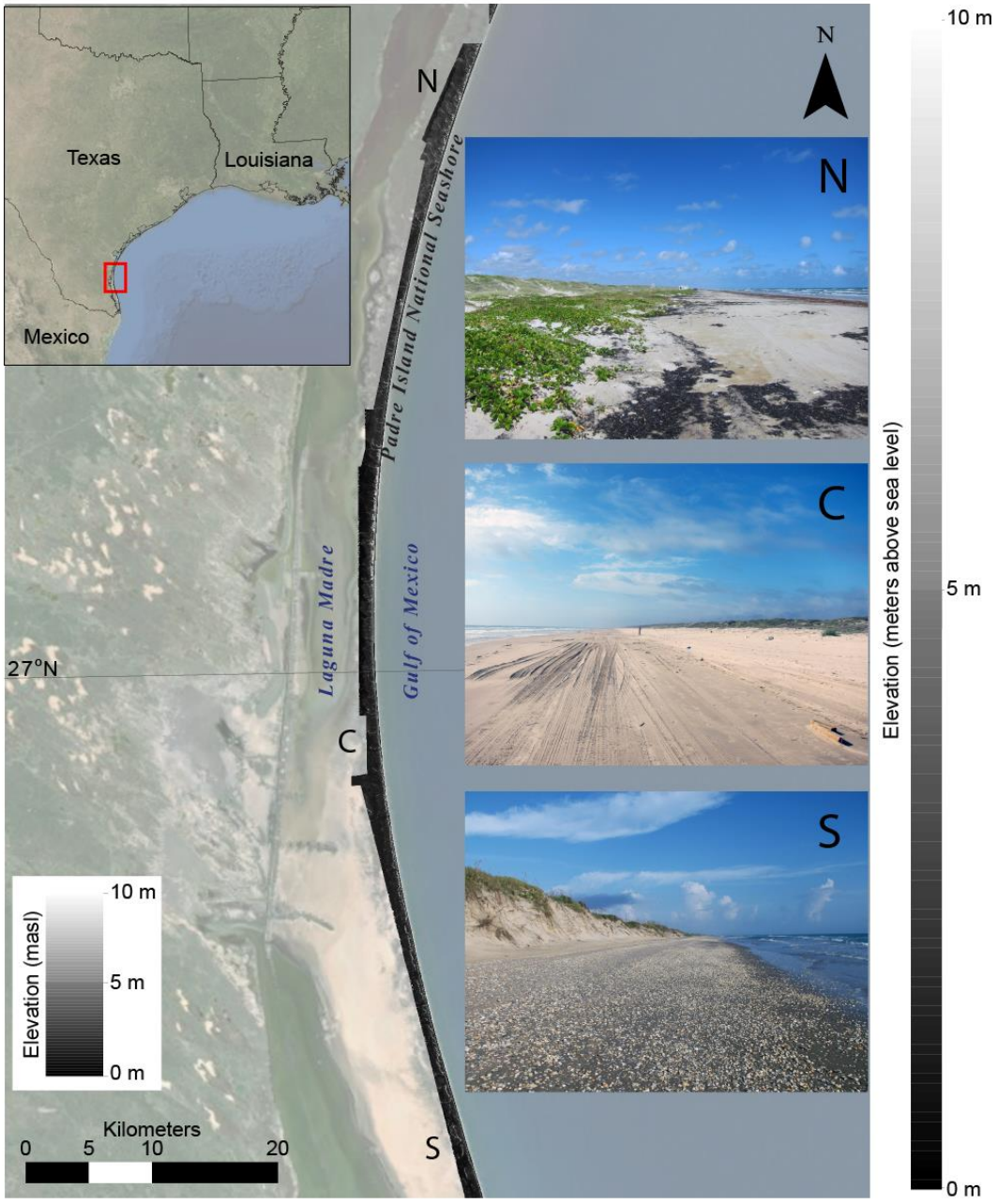

Figure 5-1. Location map of the study area in Padre Island National Seashore (PAIS), Texas, USA. Field images from the northern (N), central (C), and southern (S) regions of the island showing alongshore differences in beach-dune morphology. Images taken in October, 2014.

Relatively little is known about the framework geology along the island. A notable exception is a series of coring and seismic surveys conducted by Fisk (1959) in the central region of Padre Island (~ 27º N). This area is where opposing longshore currents converge, adjacent to the Sand Bulge in the hypersaline wind-tidal flat region of Laguna Madre (see Brown and Macon, 1977). Geologic interpretations based on these data suggests that the thickness of modern beach sands is ~ 2 – 3 m, and are underlain by Holocene shoreface sands and muds to a depth of ~ 10 – 15 m (Fisk, 1959). The Holocene deposits are perched upon a Pleistocene ravinement surface of fluvial-deltaic sands and muds. A network of buried valleys and paleo-channels exhibiting a dendritic, tributary pattern have been interpreted by Fisk (1959) in the vicinity of the 27º N convergence zone. The depths of these valleys inferred from seismic surveys have been suggested to range from ~ 25 – 40 m (Brown and Macon, 1977). However, the exact location and cross-sectional area of each valley and paleo-channel alongshore is not well-constrained. It is possible that other channels exist outside the surveyed area by Fisk (1959), which presents a unique opportunity for using EMI to compare known and unidentified geologic features alongshore.

Methods

Field EMI survey

A 100-km-long alongshore EMI survey was performed during a series of field campaigns between October, 2014 – March, 2015. This represents the longest EMI transect ever performed (to our knowledge), covering nearly the entire length of PAIS. A

multi-frequency GSSI Profiler EMP-400™ was used for each segment (~ 4 – 5 km) along the transect, which was located in the backbeach environment ~ 25 m inland from the mean tide level (MTL). This was done to reduce the effect of changing groundwater conditions in response to nonlinear tidal forcing (Weymer et al., *accepted*). For all surveys, a vertical dipole orientation was used in the in-line (P-mode) direction parallel to the profile line. Measurements were made at a 10 m step-size because ARIMA models require that the data must be stationary and taken at equal time or spatial intervals (see Cimino et al., 1999). The instrument was carried at a height of ~ 0.7 m above the ground to avoid unwanted noise from debris on the beach that unfortunately is prevalent along the island. Although the sensor is capable of recording three frequencies simultaneously (see Geophysical Survey Systems, 2007), we chose to focus on data collected at the 3 kHz bandwidth, which is optimal frequency for maximizing the depth of investigation (DOI), resulting in a DOI of ~ 6.4 – 3.5 m over the range of conductivities (~ 50 – 600 mS/m) in the study area (Weymer et al., *accepted*). Because the depth of the modern beach sands is ~ 2 – 3 m (see Brown and Macon, 1977; page 56, Figure 15), variations in the depth to shoreface sands and muds (i.e., framework geology) is within the detection limits of the profiler. A total of 21 segments were stitched together by importing GPS coordinates from each measurement into ArcGIS™ to create the composite spatial data series. A linear trend removal, following which the mean was subtracted, was applied to reduce drift and precondition the data series for statistical modeling.

Geomorphometry

Topographic information was extracted from aerial LiDAR data that was collected by the Army Corps of Engineers (USACE) in 2009 as part of the West Texas Aerial Survey project assessing post-hurricane conditions of beaches, barrier islands, and lakeshores along the Texas coastline. This dataset is the most recent publicly available LiDAR survey of PAIS that provides the greatest coverage of the island. Despite the time discrepancy between LiDAR and EMI surveys, Padre Island has not been impacted by a hurricane since 2008, when Hurricane Dolly struck nearby at South Padre Island on July 23rd, as a category 1 storm (NOAA, 2015). It is assumed that the surface morphology across the island did not change considerably between 2009 and 2015, because the island is more stable than other islands along the Texas coast (e.g., Galveston) that have been more recently and directly impacted by Hurricane Ike, September 13th, 2008 (NOAA, 2015). A 1-m resolution digital elevation model (DEM) was created using an ordinary kriging algorithm (Weymer et al., *accepted*). The processed DEM tiles were merged to produce the combined DEM of the entire island within the park boundaries of PAIS. The data was processed using SAGA GIS, which is freely available open-source software and subsequent terrain analysis was conducted using an automated approach developed at Texas A&M University (Wernette et al., 2016).

Several metrics including beach width, dune height, and island width were extracted from the DEM using a recently developed automated multi-scale approach (see Wernette et al., 2016). This technique extracts the shoreline and backbarrier shoreline

based on elevation thresholds to calculate beach and island width referenced to mean sea-level (MSL). Dune metrics including dune crest, dune heal, and dune toe are calculated based on the average relative relief (RR) to determine dune height alongshore. Relative relief is a measure of topographic position of the center pixel within a given computational window. A detailed description of the procedure for extracting each metric is discussed in Wernette et al. (2016). Each feature was extracted by averaging the RR values across window sizes of 21, 23, and 25 m, based on *a priori* knowledge of the observed geomorphic features in the study area. These large window sizes better capture general features, reducing the sensitivity to fine-scale variability inherent in LiDAR-derived DEM's (Wernette et al., 2016). Each DEM series is paired with the σ_a data by GPS coordinates (latitude) recorded in the field by the EMI sensor. Cross-sectional slices were taken every 10 m (y-coordinate) perpendicular to the shoreline, where each point along the profile is summed to calculate beach and island volume based on the elevation thresholds mentioned above. Dune volume is calculated by summing the pixel elevations starting at the dune toe (stoss), traversing the dune crest, and ending at the dune heal (lee). In total, six DEM morphometrics were extracted as spatial data series paired with the EMI data, each having an identical sample size (n = 9,694), which is sufficiently large enough for accurately modeling the data (see Cimino et al., 1999).

Statistical methods

Although the procedures for creating each dataset in this study are considerably different, the intended goal is the same; to produce multiple spatial data series containing an identical number of data points that can be analyzed using a combination of signal processing and statistical modeling techniques. The workflow for processing both subsurface (EMI) and surface (DEM metrics) is given in Figure 5-2. The resulting signal from each data series represents a spatial averaging of a geophysical parameter that contains information about the important processes-form relationships between geologic features and island geomorphology. Because we are interested in evaluating these connections (or lack thereof) at large spatial scales, a common approach is to first determine the autocorrelation function and Hurst coefficient (self-similarity parameter) *H* to verify whether the data series contains short and/or long-range memory (Beran, 1994; Taqqu et al., 1995). The R/S statistic is the quotient of the range of values in a data series and the standard deviation. When plotted on a log/log plot, the resulting slope of the line gives the value of *H,* which is useful as a diagnostic tool for estimating the degree of LRD (see Beran, 1994). For a given number of observations X_i, X_2, … X_n, a partial sum sequence is defined by $S_m = X_1 + \ldots + X_m$, for $m = 0,1,\ldots$ (with $S_0 = 0$). The Hurst statistic is calculated by (see Samorodnitsky, 2007):

$$\frac{R}{S}(X_1, \ldots, X_n) = \frac{max_{0\le i\le n}\left(S_i - \frac{1}{n}S_n\right) - min_{0\le i\le n}\left(S_i - \frac{i}{n}S_n\right)}{\sqrt{\left(\frac{1}{n}\sum_{i=1}^{n}\left(x_i - \frac{1}{n}S_n\right)^2\right)}} \qquad (5.1)$$

where, S_n/n is the sample mean of the data. The R/S analysis in this study was performed in AutoSignal™. An *H*-value > 0.5 indicates a tendency towards LRD, whereas values close to 1.0 indicate an increase in such an effect. If the signal has LRD, a special class of ARIMA models known as fractional ARIMA, or FARIMA, is specifically designed to model the long and short-range correlations within a particular data series. An ARIMA series is formally defined as (Taqqu et al., 1995):

$$X_i = \Delta^{-d}\varepsilon_i, i \geq 1 \tag{5.2}$$

where, ε_i are independent, identically distributed normal random variables with mean 0 and variance 1, and where Δ is the differencing operator $\Delta\varepsilon_i = \varepsilon_i - \varepsilon_{i-1}$. The way to interpret $X_i = \Delta^{-d}\varepsilon_i, i \geq 1$with a fractional value of *d* is as a moving average (see Hosking, 1981). The parametric family of ARIMA (*p*,*d*,*q*) models is defined by the following (see Samorodnitsky and Taqqu, 1994):

$$\Phi(B)X_i = \theta(B)\Delta^{-d}\varepsilon_i \tag{5.3}$$

where, $\Phi(B)$ and $\theta(B)$ involve the autoregressive (AR) and moving average (MA) coefficients, respectively.

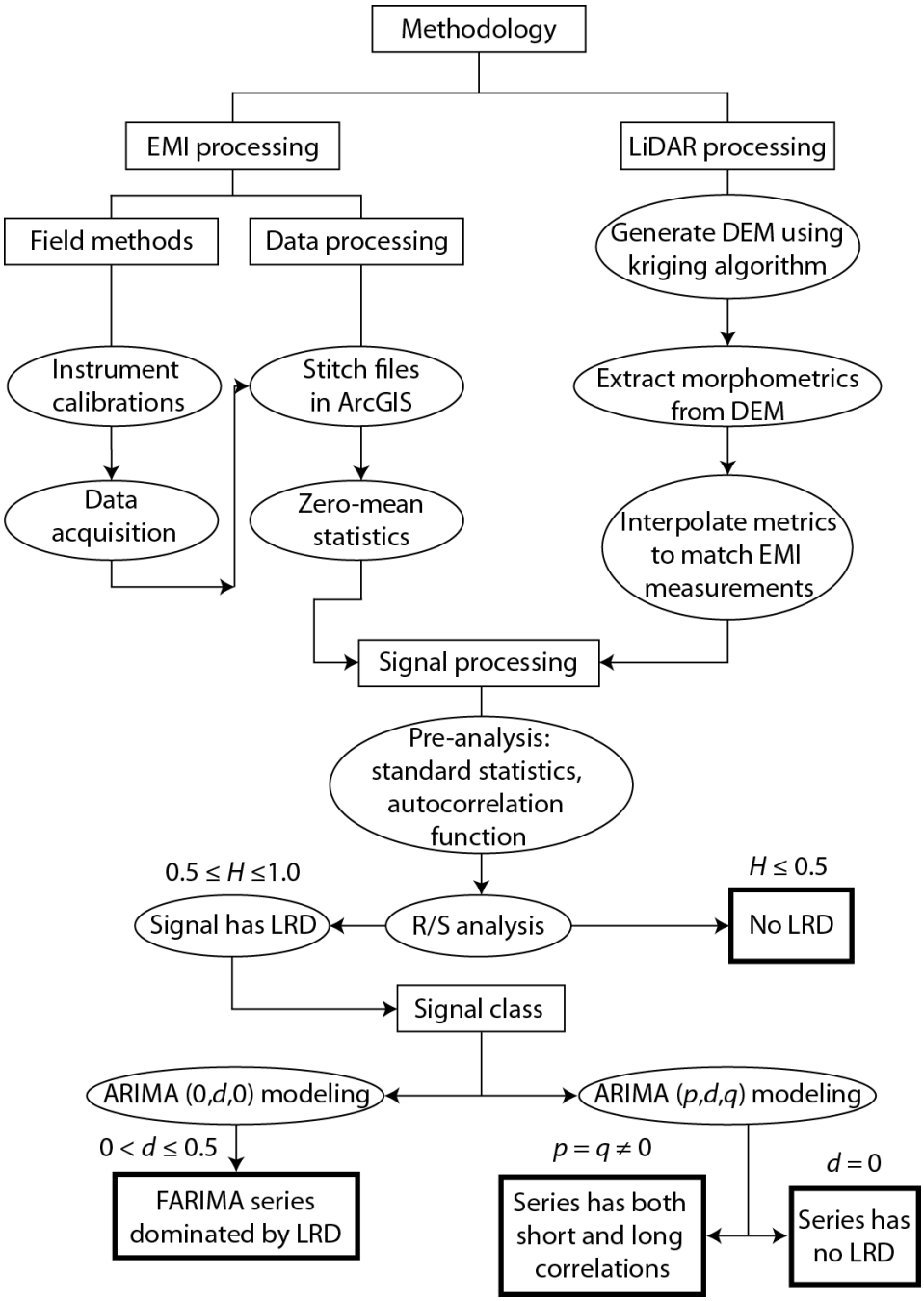

Figure 5-2. Flow chart illustrating the methods for collecting, processing and analyzing the EMI and LiDAR data presented in this study. Rectangles denote the theme of each process, whereas each step in the process is shown in ellipses. Bold rectangles designate the end of each process.

ARIMA models are used across a wide range of disciplines and have broad applicability for understanding the statistical structure of a given time or spatial data series as it is related to some physical form or process (see Granger and Joyeux, 1980; Hosking, 1981; Beran, 1992; Taqqu et al., 1995; Cimino et al., 1999). An ARIMA process represents a time or spatial data series as realizations of *stochastic* processes that can be generated from a linear combination of random shocks (Cimino et al., 1999). The model of a data series is defined by three terms (p,d,q), where p and q indicate the order of the autoregressive (AR) and moving-average (MA) components, respectively. A more generalized form of ARIMA allows the degree of differencing d to take any real value including fractional values (e.g., $0 < d \leq 0.5$), whereas p and q can only be integer values (e.g., 0, 1, 2). The AR element, p, represents the lingering effects of preceding scores or values. The integrated element, d, represents trends in the data, and the MA element, q, represents the lingering effects of preceding random shocks (see De Jong and Penzer, 1998; Cimino et al., 1999).

Identification of an appropriate model is accomplished by finding small values of p,d,q (usually between 0 – 2) that most accurately fit patterns in the data. When a value is 0, the element is not needed. For example, if $d = 0$ the series has no long-memory, whereas if $p = q = 0$, the model has no short-memory. If $p,d,q \neq 0$, the model contains a combination of both short and long-memory effects. Generally, the model results are used for either forecasting future or missing values within the data series. In the present study, we are interested in determining the orders of p,d,q not for forecasting, but rather for understanding the physical meaning of each parameter with respect to framework

geology. For the analysis, the ‘arfima’ and ‘forecast’ statistical packages in R were used to fit a family of ARIMA (*p*,*d*,*q*) models to the actual EMI data and island metrics (see Hyndman and Khandakar, 2007; Veenstra, 2012; Hyndman, 2015).

Each representative spatial data series is collated with the LiDAR-derived DEM of the study area. Superimposed is the network of inferred paleo-channels by Fisk (1959), allowing comparison of relationships between the paleo-channels, subsurface σ_a, and surface morphology for the entire barrier island (gray shaded regions). A Savitzky-Golay smoothing filter was applied (darker lines in the signals) to all data series using a moving window of $n = 250$. This procedure generates a sequence of internal smoothing passes to improve the signal-to-noise (S/N) ratio, thereby enabling comparisons of the lower-frequency signals over larger spatial scales with respect to framework geology.

Results

Spatial data series

Each spatial data series (Figure 5-3) represents the superposition of many different wavelengths (or wavenumbers) that are assumed to be caused by physical processes operating across different scales (see Weymer et al., 2015b). High frequency signals characterize small-scale heterogeneities, whereas low-frequency components capture variations in each metric at the broadest scales. There is a high degree of variability within each signal that is directly related to the complex geological and geomorphological patterns along the island. Within and outside the paleo-channel region, general associations (or lack thereof) between EMI and DEM metrics can be

made. Based on the overall low-frequency trends in each signal, the island is divided into three zones (red vertical lines) corresponding to the northern (~ 64 – 97 km), central (~ 27 – 64 km), and southern (~ 0 – 27 km) regions. The central zone corresponds to the paleo-channel region.

The morphology of the beach-dune system, as well as island width varies substantially from north to south. In the southern zone of the island, the beach is generally narrower, which may be influenced by a disruption in longshore currents by the Mansfield Channel (i.e., shadow zone). In the paleo-channel region, beach width decreases considerably and is more variable. Beach width increases towards the northern section of the island, overall. The volume of the beach tends to be lowest in the northern zone, varies considerably in the central part of the island, then stabilizes and gradually decreases towards the south. Alongshore dune heights are greater in the south, become more variable in the paleo-channel region, and decrease overall except for the area adjacent to Baffin Bay. Dune volume is lowest in the northern section, intermittently increases in the central zone and slightly decreases towards the south. The island is considerably narrower from the Mansfield Channel to roughly Baffin Bay and increases significantly in the northern zone. Island volume follows a similar trend. Overall, σ_a values are low north of the paleo-channel region compared to the southern zone where σ_a increases substantially. However, the lowest σ_a values are located within the inferred paleo-channels by (Fisk, 1959).

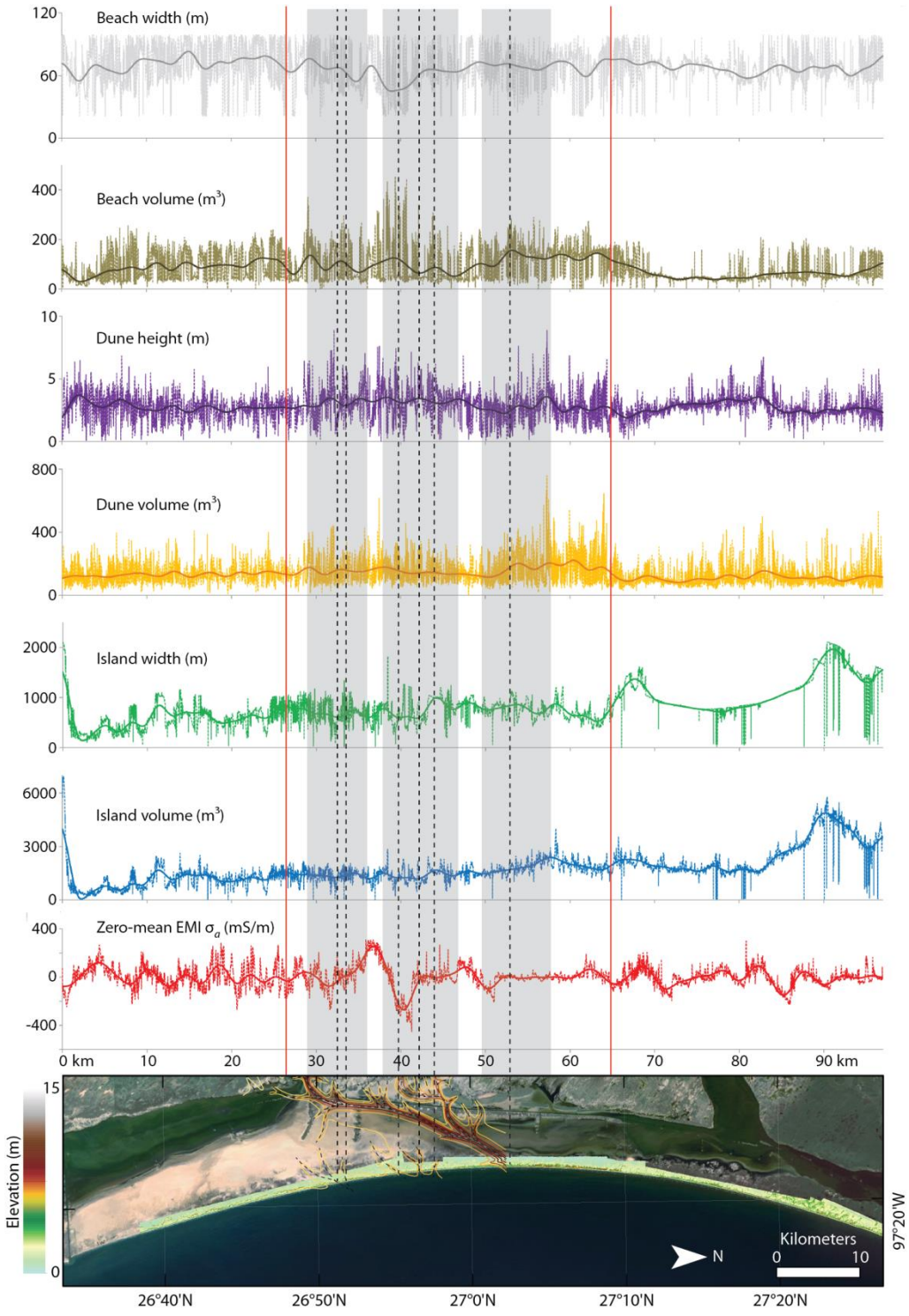

Figure 5-3. EMI survey and DEM metrics extracted from the aerial LiDAR data. The sampling interval (step-size) for each data series is 10 m. The island is divided into three zones (red lines) based on the overall trends of each signal.

Tests for LRD

As noted, the Hurst coefficient *H* defines the autocorrelation, the fractal dimension *D*, and provides a measure of the degree of LRD for a given time or spatial data series (see Beran, 1994; Taqqu et al., 1995; Eke et al., 2000). Recall that LRD is defined by *H*-values > 0.5, where *H* near 1.0 indicates a high degree of smoothness or close correlation within the data series. *H* near zero indicates a high degree of roughness, or anticorrelation, and $H = 0.5$, is uncorrelated white noise (see Eke et al., 2000). The calculated *H*-values for the EMI signal and DEM metrics are given in Figure 5-4. Estimated *H* coefficients for each signal range between 0.80 – 0.95, indicating a strong tendency towards LRD ($H > 0.5$). The beach and dune data series have lower *H*-values of 0.82 and 0.83, respectively. Island width has the highest *H*-value (0.95), whereas the EMI series has the next highest ($H = 0.86$). The R/S plots of island width and volume show the strongest trend towards LRD compared to the other DEM metrics. The beach and dune metrics have similar *H*-values when compared to the EMI signal. Because each data series shows evidence of LRD, a more robust way of determining the persistence of short and/or long-range memory between each signal can be achieved by fitting a series of ARIMA models to each data set.

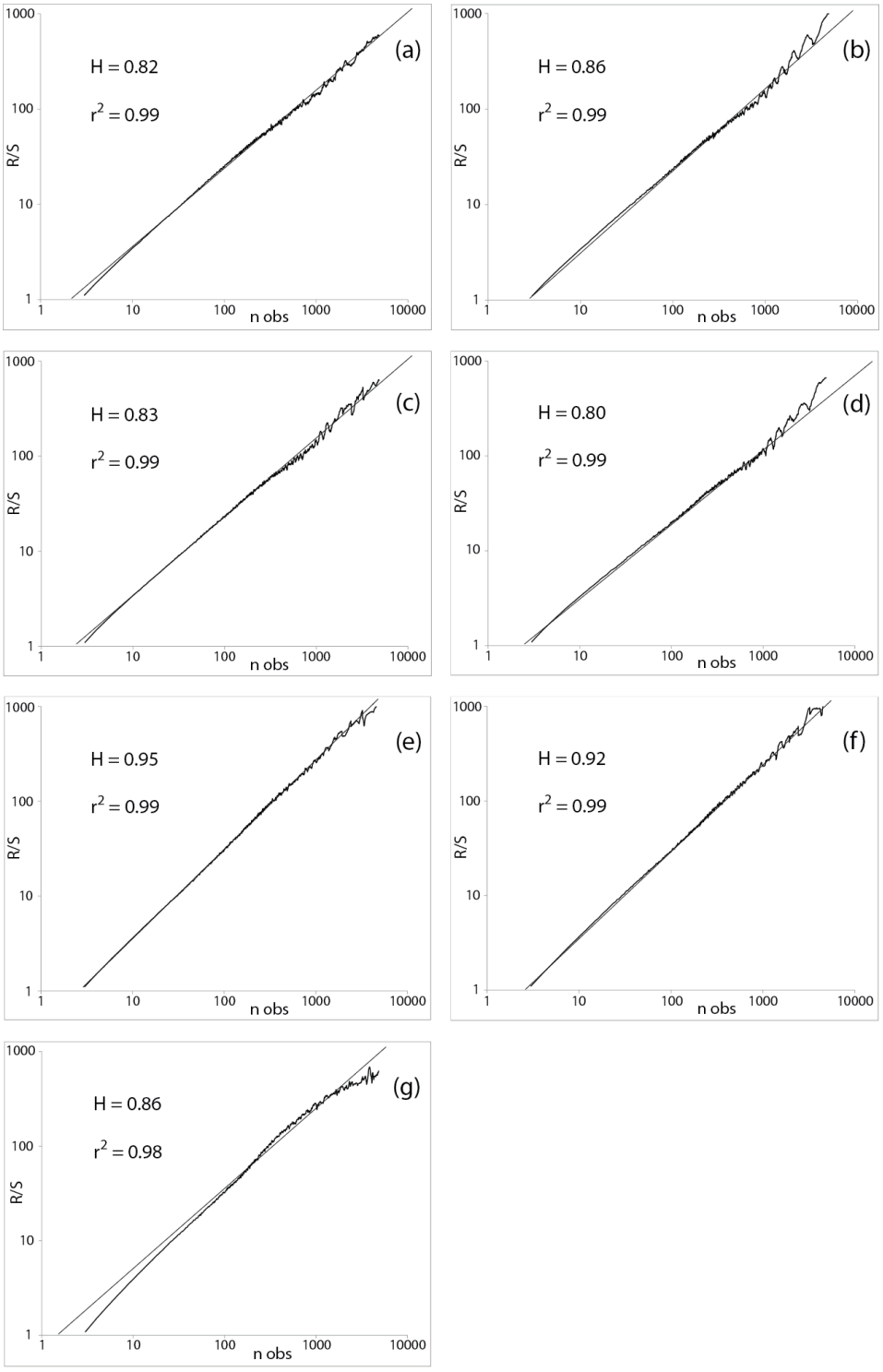

Figure 5-4. R/S analysis for determining the degree of LRD (Hurst coefficient *H*) for each island metric and the EMI signal. a) beach width, b) beach volume, c) dune height, d) dune volume, e) island width, f) island volume, and g) EMI σ_a.

ARIMA (p,d,q) model results and multivariate analysis

A sequence of ARIMA (*p*,*d*,*q*) model iterations was conducted for every data series using an iterative process for each model parameter to find the best fit to the data. For the analysis, the models include different combinations of *p*,*d*,*q* that model either short: ARIMA (100; 001; 101), long: ARIMA (010; 0*d*0), or both short and long-memory processes: ARIMA (111). Six realizations of each data series were performed resulting in a total of 42 models, which not only provide information on the best model fit, but also enables physical interpretations of *p*,*d*,*q* at the largest "global" spatial scales (100 km). Determining the best model fit is usually achieved by comparing the residuals, or root-mean-square error (RMSE) of each model, where the lowest RMSE values indicate lower residual variance. The RMSE values for each data series and model iteration is given in Table 5-1.

Table 5-1. Comparison of residuals (RMSE) for each ARIMA model iteration used in this study.

	ARIMA (1,0,0)	**ARIMA** (0,0,1)	**ARIMA** (1,0,1)	**ARIMA** (1,1,1)	**ARIMA** (0,1,0)	**ARIMA** (0,*d*,0)
Beach width	13.4	14.9	13.0	13.1	14.8	13.0
Beach volume	44.8	50.5	43.1	43.1	49.1	42.7
Dune height	0.7	0.8	0.7	0.7	0.8	0.7
Dune volume	60.6	63.9	59.7	59.2	69.03	58.9
Island width	138.4	253.2	121.3	121.1	140.8	120.9
Island volume	271.3	611.4	244.3	244.1	273.9	243.3
EMI σ_a	18.4	49.7	15.6	15.8	18.5	15.5

The RMSE values reveal several characteristics about each signal: 1) all data series are best fit by an ARIMA (0,*d*,0) or FARIMA process, 2) the ARIMA models most accurately fit the EMI data, and 3) in all cases, the poorest fit to each series is by the ARIMA (0,0,1) MA process. The results suggest that FARIMA best models the statistical structure of each data series, which means that a single differencing parameter *d* is the most significant parameter in this study that describes LRD across multiple spatial scales. It is important to note that different values of *d* were used in each FARIMA model (Table 5-2).

Table 5-2. Summary table showing the computed "global" *d* parameters that most appropriately model each ARIMA (0,*d*,0) iteration. The difference between each metric with respect to EMI is listed as absolute magnitudes for comparison. Close matches are shaded in gray.

	***d* parameter**	**difference**
Beach width	0.38	0.03
Beach volume	0.42	0.07
Dune height	0.34	0.01
Dune volume	0.32	0.03
Island width	0.13	0.22
Island volume	~ 0.00	0.35
EMI σ_a	0.35	-----

These values were calculated using the 'FitARMA' statistical package in R and is necessary to determine the degree of differencing required to accurately model the long-range contributions within the data (see Mandelbrot, 1967; McLeod and Zhang, 2008; McLeod et al., 2011). A graphical representation of the FARIMA models for each data series is shown in Figure 5-5 as an example allowing visual inspection of each model fit

to the actual data. Because each data series is scale dependent, it is not possible to compare RMSE results without normalizing the data. The range in values for each data series can differ by several orders of magnitude. Instead of normalizing the data, an alternative approach is to calculate the difference between *d*-values for each metric with respect to the EMI data series to examine the statistical relationships (or lack thereof) between island metrics and EMI. The absolute value of the differences between framework geology (EMI) and surface morphometrics is shown in Table 5-2. The results demonstrate that EMI is most closely related to dune height with a relative difference of 0.0054. Beach width and dune volume are the next closest matches to the EMI signal, whereas island width and volume exhibit the poorest relationship. As mentioned above, these values represent the "global" values of *d* and provide an indication of the LRD-structure at the largest spatial scales (~ 100 km). It is reasonable to assume that the degree of LRD may change over smaller "regional" (e.g., ~ every 30 km) and/or "local" (e.g., ~ every 10 km) scales.

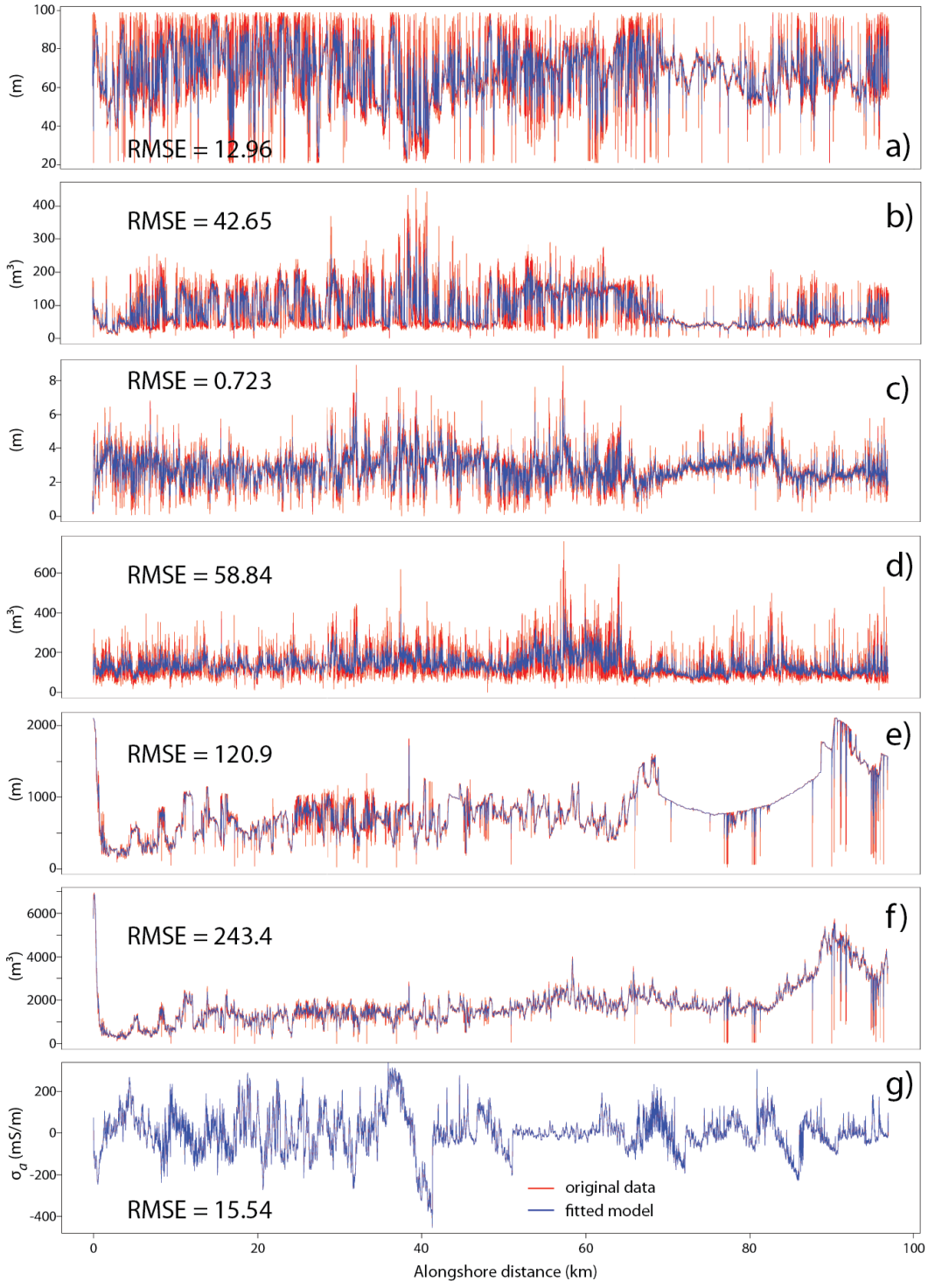

Figure 5-5. Example of the best fit ARIMA (0,*d*,0) models for each signal: a) beach width, b) beach volume, c) dune height, d) dune volume, e) island width, f) island volume, and g) EMI σ_a.

A series of 21 FARIMA model iterations was performed by dividing the island into ~ 30 km segments, roughly corresponding to the southern (0 – 30 km), central (30 – 60 km), and northern (60 – 100 km) zones (Table 5-3). This allows regional comparisons of each FARIMA model both inside the known paleo-channel region (~ 30 – 60 km) and outside the region where the framework geology is not well-constrained. The results vary considerably within each zone and for each spatial data series. Within the paleo-channel region, the strongest tendency towards LRD is island volume (d = 0.42), whereas the lowest d-value is EMI σ_a (d = 0.11). The other metrics have comparable values d ~ 0.3, where beach width and dune height exhibit a higher tendency towards LRD. In the southern zone, EMI σ_a and beach volume have very similar d-values (~ 0.44). Conversely, beach width has the smallest d-value (~ 0) and the other metrics range between ~ 0.03 – 0.2. In the northern zone, EMI and island volume have nearly identical d-values, whereas the lowest value corresponds to island width (~ 0). The difference in d-values between EMI and each metric is shown in Table 5-4 to allow comparisons between the framework geology controls on surface morphology at the regional scale. There is a statistically significant relationship between EMI and beach volume in the southern zone of the island. There does not appear to be any appreciable relationship between EMI and each metric within the paleo-channel region. However, there is a statistically significant relationship between EMI, beach volume, dune volume, and island volume in the northern zone. The FARIMA model results at the regional scale are somewhat contrary to the global scale models and warrant further analysis at the local scale (10 km).

Table 5-3. Summary table showing the computed "regional" *d* parameters that most appropriately model each ARIMA (0,*d*,0) iteration.

Alongshore distance	Beach width	Beach volume	Dune height	Dune volume	Island width	Island volume	EMI σ_a
0-30 km	~ 0.00	0.44	0.13	0.20	0.03	0.18	0.44
30-60 km	0.37	0.30	0.36	0.31	0.30	0.42	0.11
60-100 km	0.26	0.41	0.35	0.46	~ 0.00	0.50	0.49

Table 5-4. Summary table showing the difference between each metric with respect to EMI listed as absolute magnitudes for comparison. Close matches are shaded in gray.

Alongshore distance	Beach width	Beach volume	Dune height	Dune volume	Island width	Island volume
0-30 km	0.44	0.006	0.30	0.24	0.41	0.25
30-60 km	0.26	0.19	0.26	0.20	0.19	0.32
60-100 km	0.23	0.09	0.14	0.04	0.49	0.004

FARIMA models were conducted at the local scale by dividing the island into 10 km segments, starting at the southern zone (0 – 10 km) and ending at the northern zone of the island (90 – 100 km). A total of 70 FARIMA model iterations were run and the results of each differencing parameter *d* represent trends towards LRD at an order of magnitude less than the global (100 km) scale (Table 5-5). As expected, there is a high degree of variability in *d* for each data series within each 10 km segment. The *d*-values for the EMI data series show a stronger tendency towards LRD (> 0.4) within the paleo-channel region, however, also show high values towards the northern segment (90 – 100 km). To facilitate easier comparisons between EMI and metrics within each 10 km

segment, the differences are shown in Table 5-6. The closest matches between the metrics and EMI are shaded in gray, enabling associations between framework geology and surface morphology at smaller, local scales. The smallest differences in *d* are within the 20 – 30 and 30 – 40 km segments, corresponding to dune height, dune volume, island volume, and beach volume, respectively. Within the paleo-channel region, the local *d*-values are similar to the regional *d*-values ranging between ~ 0.14 – 4.7 overall, suggesting that framework geology controls on island morphology vary within different locations of the island and also over different spatial scales. By comparing how the *d* parameter varies over several spatial scales (i.e., global, regional, and local), it is possible to determine, statistically, the important connections between framework geology and island geomorphology, which is discussed below.

Table 5-5. Summary table showing the computed "local" *d* parameters that most appropriately model each ARIMA (0,*d*,0) iteration.

Alongshore distance (km)	Beach width	Beach volume	Dune height	Dune volume	Island width	Island volume	EMI σ_a
0-10	0.41	0.39	0.20	0.21	0.09	0.18	0.36
10-20	0.30	0.42	0.20	0.26	0.37	~ 0.00	0.36
20-30	0.26	0.40	~ 0.00	~ 0.00	0.49	~ 0.00	~ 0.00
30-40	0.47	~ 0.00	0.41	0.25	0.29	0.28	~ 0.00
40-50	0.28	0.21	0.21	0.19	0.30	0.02	0.44
50-60	0.03	0.31	0.23	0.32	~ 0.00	0.33	0.48
60-70	0.16	0.37	0.29	0.34	~ 0.00	0.30	0.40
70-80	0.47	0.34	0.43	0.26	~ 0.00	0.42	0.49
80-90	0.27	0.19	0.42	0.39	0.01	0.02	~ 0.00
90-100	0.13	0.13	~ 0.00	0.06	0.44	0.47	0.41

Table 5-6. Summary table showing the difference between each metric with respect to EMI listed as absolute magnitudes for comparison. Close matches are shaded in gray.

Alongshore distance	Beach width	Beach volume	Dune height	Dune volume	Island width	Island volume
0-10 km	0.05	0.03	0.16	0.15	0.27	0.18
10-20 km	0.06	0.06	0.16	0.10	0.02	0.36
20-30 km	0.26	0.40	~ 0.00	~ 0.00	0.49	~ 0.00
30-40 km	0.47	~ 0.00	0.41	0.25	0.29	0.28
40-50 km	0.16	0.23	0.23	0.25	0.14	0.42
50-60 km	0.45	0.17	0.26	0.16	0.48	0.15
60-70 km	0.24	0.04	0.11	0.06	0.40	0.10
70-80 km	0.03	0.16	0.06	0.23	0.49	0.07
80-90 km	0.27	0.19	0.42	0.39	0.01	0.02
90-100 km	0.28	0.28	0.41	0.35	0.03	0.06

Discussion

The results of the FARIMA models suggest there is a statistically significant connection between framework geology and dune height "globally" along the entire length of the island. At the *regional scale*, there is a statistically significant connection between EMI and beach volume in the southern zone and between beach volume, dune volume, and island volume within the northern zone. At the *local scale*, relationships between EMI and each metric vary considerably and are highly localized. All data series are most accurately modeled by a single parameter *d*, suggesting LRD persists (to varying degrees) in both island geology and geomorphology across multiple spatial scales. Although it has long been known that LRD and self-similar processes exist along coastlines that can be described by power laws and fractal dimensions (see Mandelbrot, 1967; Tebbens et al., 2002; Lazarus et al., 2011), this behavior has not been previously

shown to exist in the subsurface geology of a barrier island. For the first time, this study demonstrates the utility of EMI for mapping barrier island framework geology as well as using FARIMA as a new analyzing technique for understanding the spatial connections between barrier island framework geology and geomorphology.

Different values of the *d* parameter provide further insight into the type of process each data series exhibits. When *d* is < 0.5, the series is a stationary process, which has an infinite moving average MA (*local*) representation. Conversely, when $d > -0.5$, the series is invertible and has an infinite autoregressive AR (*directional*) representation (see Hosking, 1981). In the case where $0 < d < 0.5$ (in this study), the ARIMA (0,*d*,0) process is stationary and contains LRD that increases as *d* approaches 0.5. Here, the autocorrelations within the data series decay to zero as the lag increases and the spectral density is concentrated at low frequencies (Hosking, 1981). For each model in our study, the *d*-values range between {~ 0 – 0.49}, which not only provides an indication of the degree of LRD and self-similarity, but also enables physical interpretation of what each *d*-value means. Values closer to 0.5 represent a MA process (stronger LRD), whereas values approaching 0 represent an AR/white noise process (weaker LRD).

The similar statistical behavior (quantified by a small difference in *d*-values) between framework geology and dune height provides evidence of a geologic control on dune morphology at the largest spatial scales (Table 5-2). At the regional scale (i.e., southern, central, and northern zones), the data suggest that framework geology is more closely related to beach volume, which in turn controls dune height. At the local scale,

(smaller 10 km sections of the island) there seems to be a weak statistical connection between EMI and all metrics within the paleo-channel region. However, the statistical relationships become stronger within the southern and northern zones of the island because these areas are less controlled by the framework geology and are governed more by contemporary morphodynamic processes. These results provide further evidence that although framework geology influences island geomorphology to varying degrees at different locations along the island, it becomes more important at the global scale. It is hypothesized that over the largest spatial scales, framework geology initially sets up alongshore variations in dune height, which is then modified by smaller-scale morphodynamic processes. The balance between framework geology and contemporary morphodynamics is dependent on the local strength of the framework geology and varies along the length of the island. This is one possible explanation for why the *d*-values are different across multiple spatial scales. These findings support previous framework geology studies from the Outer Banks, NC (e.g., Riggs et al., 1995; McNinch, 2004; Browder and McNinch, 2006), Fire Island, NY (e.g., Hapke et al., 2010; Lentz and Hapke, 2011), and Pensacola, FL (e.g, Houser, 2012). Nonetheless, these studies mainly focus on offshore controls on shoreface and/or beach-dune dynamics. Additionally, most of these studies investigated framework geology controls at local or regional scales because few islands are as long and/or continuous as Padre Island. The current study improves existing literature in that 1) it provides a large-scale survey of framework geology onshore, and 2) it demonstrates the utility of a "new" geophysical EMI

instrument and FARIMA statistical methods for modeling the spatial connections between framework geology and barrier island geomorphology.

Alongshore variations in beach width and dune height are not uniform in PAIS and exhibit different characteristics within and outside the paleo-channel region (Figure 5-3). These differences may be forced by the framework geology within the central zone of the island and may be further influenced by smaller-scale morphodynamic processes outside the paleo-channel region. EMI σ_a is considerably lower within (or in close proximity to) the inferred paleo-channels, which is likely a result of more resistive infilled sands (see Seijmonsbergen et al., 2004; Weymer et al., *accepted*). It is hypothesized that the geometry of each channel is directly related to the variation in the EMI signal, such that long, gradual minima in σ_a are indicative of large, deep channels and short, abrupt minima in σ_a represent smaller, shallow channels. Dune height and volume increase within this region, suggesting that the increased accommodation space within the channels acts as an internal sediment source enabling the dunes to become larger, which is reinforced by local storm surge that varies at nearshore scales (<< 10 km). Once the dunes are initialized by the framework geology, stabilizing vegetation may act as another important control on dune evolution (e.g, Hesp, 1988) that may be represented by the higher-frequency signals embedded within the spatial data series. Beach and dune morphology in areas that are not significantly controlled by framework geology (e.g., southern and northern zones) exhibit a more random behavior that represent a free system that is primarily controlled by contemporary morphodynamics (e.g., wave action, storm surge, wind, etc.).

As mentioned previously, the overall configuration and geometry of the beach-dune system controls island response to storm surge and rising sea level where low-lying dunes are more susceptible to overwash processes that redistribute sediment landwards in the form of washover fans and terraces (Morton and Sallenger, 2003; Stone et al., 2004; Houser, 2012). Because variations in dune height act as an important control on storm impacts and ultimately large-scale island transgression, it is argued that the framework geology in PAIS acts as a first order control on large-scale island transgression and is more significant than contemporary morphodynamics. This challenges existing models that consider small-scale undulations in the dune line as natural randomness within the system. Rather, we propose that the dunes are forced by the framework geology, which is related to the thickness of the modern shoreface sands beneath the beach as detected by the EMI sensor and highlighted using the statistical analysis.

Conclusions

This study demonstrates the utility of EMI as a new tool for mapping barrier island framework geology and statistically modeling geophysical and geomorphological spatial data series by a FARIMA process to better understand the important geologic controls on large-scale barrier island transgression. Because each data series contains LRD, each series is most accurately modeled by a single parameter *d*, which allows direct statistical comparisons between the framework geology and surface geomorphology. At the *global scale* (100 km), there is a strong statistical connection between framework geology and dune

height (d = 0.0054), suggesting that the framework geology initially forces the development of the dunes, which in turn forces the island as it transgresses in response to storms and sea-level rise. The difference in d-values between EMI and beach width is significantly small (0.0292), also suggesting a geologic control, but may be modified by morhodynamic processes including; wind, wave action, tides, currents, and sediment transport. At the *regional scale* (~ 30 km), there is a statistical connection between EMI and beach volume, which controls dune height. At the *local scale* (10 km), there is a considerable degree of variability between EMI and each metric that is highly localized and exhibits weak statistical connections within the paleo-channel region, suggesting that the southern and northern zones outside the paleo-channels are controlled more modern morphodynamics. These findings suggest that the framework geology controls on barrier island geomorphology are strongest at the global scale. FARIMA models offer a compact way of capturing the entire geological complexity of a barrier island that is contained in a single parameter d that cannot be achieved by other signal processing techniques. It is argued that these statistical models provide a compact an efficient way for understanding the geologic controls on large-scale island transgression that can be applied across field sites and potentially in different geomorphic environments.

CHAPTER VI

CONCLUSIONS

This dissertation quantifies the important length-scales of framework geology as an important control in alongshore variations in surface geomorphology, which in turn affects island response to storms and sea-level rise (i.e., transgression). A series of shore-normal and alongshore EMI surveys were conducted in Padre Island National Seashore (PAIS), Texas, USA to test the quantitative performance characteristics of a GSSI Profiler EMP-400™ for detecting changes in subsurface electrical conductivity σ as it is related to variations in geology. Extracted DEM metrics from aerial LiDAR paired with each EMI measurement enables comparisons between surface morphology and framework geology using multivariate analysis and ARIMA statistical modeling. This study represents the first attempt in using EMI methods for characterizing the large-scale framework geology controls (or lack thereof) on island morphology along the world's longest undeveloped barrier island. Results demonstrate that EMI profiling is a viable alternative to conventional methods such as coring and GPR for exploring barrier island framework geology. While traditional geological and geophysical techniques work well within specific areas of the coast, there is a need to integrate these data sets to build a complete picture of the framework geology. In other words, it is argued herein that no other geophysical method besides EMI can provide continuous subsurface coverage across the barrier island system. EMI sensors provide high-resolution information regarding the complex feedbacks between framework geology and hydrology. However,

these sensors require several calibrations and accurate records of changing tidal states in order to separate the effects of changing hydrology and geology from the EMI σ_a signal. Moreover, EMI data should be acquired within a period of several days, during similar hydrologic conditions in order to reduce seasonal effects. When combined with data from other methods, EMI techniques have direct implications for improving our understanding of barrier island transgression in response to storms and rising sea-level, which is summarized below.

Hypothesis 1: *Electromagnetic induction (EMI) is a viable method for investigating subsurface barrier island framework geology*

In order to test the utility of EMI profiling as a viable method for investigating barrier island framework geology (**Hypothesis 1**), a series of field experiments were performed at PAIS establishing the advantages and limitations of these sensors (Chapters II and III).The results of this study suggest that portable multi-frequency EMI profilers should be used with caution for geologic framework investigations in highly conductive barrier islands. Assessments of instrument calibration and signal drift suggest σ_a measurements are stable, but vary with height and location across the beach (Figure 3-3). Repeatability tests confirm σ_a values using different boom orientations collected during the same day are reproducible (Figure 3-4). Measurements over a 12-hour tidal cycle suggest there is a tide dependent step response in σ_a, complicating data processing and interpretation (Figures 3-6 and 3-7). Shore-normal surveys across the barrier/wind-tidal flats show that σ_a is roughly negatively correlated with topography, and that these

relationships can be used for characterizing different coastal habitats (Figure 3-8). For all surveys, σ_a increases with decreasing frequency. Alongshore surveys performed during different seasons and beach states reveal a high degree of variability in σ_a (Figure 3-10). Therefore, it is necessary to combine the recommended instrument calibrations used in the present study with detailed tidal records to separate the effects of hydrology and geology on the σ_a signal.

Surveys collected during dry conditions characterize the underlying geologic framework, whereas these features are somewhat masked during wet conditions. Differences in EMI signals should be viewed in a relative sense rather than as absolute magnitudes. Small-scale heterogeneities are related to changing hydrology, whereas low-frequency signals at the broadest scales reveal variations in geologic framework. This strategy enables the geophysicist to separate the effects of hydrology and geology from the σ_a signal. Thus, **Hypothesis 1** is supported, which leads to the following conclusions:

1. The effect of groundwater dynamics on EMI signals is shown to be more important at smaller spatial scales (<< 10 km), but is not statistically significant when looking at large-scale (> 10 km) framework geology (Chapter IV).
2. Repeat alongshore surveys during different seasons show different σ_a values, but may also be masked by tidal effects and/or changing beach states. During wet conditions, subsurface σ is relatively uniform, limiting the DOI and the ability of the EMI sensor to detect subsurface variations in lithology. Conversely, during

dry conditions the profiler probes deeper and is better able to detect variations in the underlying geologic framework (Chapter III).

3. Multiple EMI surveys are required along the same transect to account for the confounding effects of changing hydrologic conditions on EMI responses. For geologic framework investigations, EMI surveys should be performed in the backbeach environment during dry conditions when the water table is lower (Chapter III).
4. Once the effects of changing hydrology are taken into account, EMI profiling is shown to be an efficient way of characterizing the large-scale geology of the entire barrier island and is considerably more cost-effective than other geologic and/or geophysical methods (Chapter IV).

Hypothesis 2: *Subsurface features are related to/mirrored in the surface morphology along the shoreline and foredune ridge*

Because EMI methods have been shown to be useful in large-scale geologic investigations, the next step is to investigate whether subsurface features are related to/mirrored in the surface morphology along the shoreline and foredune ridge (**Hypothesis 2**). In order to test this hypothesis, multivariate analysis and ARIMA modeling was used to statistically evaluate the short and long-range correlations (LRD) within the EMI signal and each DEM metric (Tables 5-2 and 5-3). A family of ARIMA models was used to determine which combination of parameters (p,d,q) most accurately model each spatial data series (Figure 5-5). These models are specifically designed to

analyze both short and long-range contributions within a data series that other techniques including ARMA, Markov process, fGn, and fBm cannot. The results from the ARIMA models, demonstrate that both the EMI and DEM metric data series are most accurately modeled by a single parameter, *d*, and are not dominated by short-range correlations. This implies that the framework geology and island geomorphology at the largest spatial scales are governed by long memory effects that suggest self-similarity (i.e, are fractal signals). Thus, this hypothesis is supported, which leads to the following conclusions:

1. EMI signals at two different spatial scales (100 and 10 km) using two different step-sizes (10 and 1 m) both exhibit a strong tendency towards LRD as evidenced in three independent statistical tests (autocorrelation function, R/S analysis, PSD) (Figures 4-3 thru 4-5. In addition, the Hurst coefficients ($H > 0.8$) for each DEM metric also show LRD (Figure 5-4).
2. Both EMI and DEM metrics are most appropriately modeled by an ARIMA (0,*d*,0) process (Table 5-1), suggesting that FARIMA is the best model to fit the data. This finding demonstrates that each spatial data series is most accurately modeled by a single parameter, *d*, which means that by comparing *d*-values of each data series, statistical comparisons can be made between framework geology (as detected by EMI) and surface morphology (DEM-extracted morphometrics) along the island (Table 5-2).

Hypothesis 3: *Framework geology controls the current shoreline and dune morphology to varying degrees along the island*

Comparisons of how well each ARIMA model fit the EMI and DEM spatial data series was determined by inspection of the residuals (RMSE) and differencing (*d*-values) for each model iteration. The agreement (low RMSE values), or mismatch (high RMSE values) between models and the actual data makes it possible to evaluate the geologic controls (or lack thereof) on beach-dune and island morphology within PAIS. Because each data series is most accurately modeled by an ARIMA (0,*d*,0) process, this suggests that each series exhibits similar statistical behavior alongshore. The similarity in *d*-values (~ 0.35) for beach width, dune height, and EMI demonstrate that these data series have similar statistical models. However, the difference in *d*-values between EMI and dune height is significantly small (0.0054), demonstrating framework geology is a more important control on dune height alongshore. Therefore, **Hypothesis 3** is supported, which leads to the following conclusions:

1. This study demonstrates the utility in statistically modeling multiple spatial data series by a FARIMA process to better understand geologic controls on large-scale barrier island transgression. There is a strong statistical connection between framework geology and dune height at the global scale, suggesting that the geology forces the development and evolution of the dunes, which in turn forces the island as it transgresses in response to storms and sea-level rise (Table 5-2).

2. The difference in *d*-values between EMI and beach width is significantly small (0.0292), also suggesting a geologic control, but may be modified by morhodynamic processes including; wind, wave action, tides, currents, and sediment transport (Table 5-2).
3. FARIMA models offer a compact way of capturing the entire hydrogeological complexity of a barrier island that is contained in a single parameter *d* that cannot be achieved by other signal processing techniques. It is argued that these statistical models provide a robust and novel way for understanding the geologic controls on large-scale island transgression (Chapters IV and V).
4. With respect to large-scale framework geology investigations, a densely-spaced EMI survey is preferred. This provides better representation of varying framework geology as well as ensuring a better model fit to the data (Figure 4-2 and 4-5).

Future steps

Following the findings in this study, there are several avenues of future research that are needed to further assess the use of EMI, DEM-extracted morphometrics and time-series analysis to better understand the large-scale geologic framework controls on barrier island geomorphology:

- More comprehensive studies are needed to better characterize changing hydrology effects on EMI signals at smaller spatial scales

- There is a need to validate EMI surveys with both well-logging (subsurface conductivity probes), and cores to determine the true depth of sand-to-clay layer
- A full 1-D/2-D inversion and MCMC modeling would be the next step to create a 2-3 layered-Earth model, which would provide actual depth information and potentially map the thickness of sand/clay along the island
- Extract several spatial data series at different depths from the inversion models and perform LRD/FARIMA analysis on these signals as they are related to the EMI and DEM metrics
- Use other statistical and modeling techniques, (e.g., cross-wavelet analysis) to analyze the coherence and phase-relationships between framework geology and surface morphology
- Perform more field tests for testing the performance of the EMI profiler when being towed by a vehicle, which may considerably reduce the amount of time needed to perform large-scale surveys
- Test the utility of integrating large-scale EMI profiling with DEM-extracted morphometrics and ARIMA statistical models across different coastal field sites and in different geomorphic environments

REFERENCES

Aagaard, T., Davidson-Arnott, R., Greenwood, B., Nielsen, J., 2004. Sediment supply from shoreface to dunes: linking sediment transport measurements and long-term morphological evolution. Geomorphology 60, 205-224.

Abdu, H., Robinson, D., Jones, S.B., 2007. Comparing bulk soil electrical conductivity determination using the DUALEM-1S and EM38-DD electromagnetic induction instruments. Soil Science Society of America Journal 71, 189-196.

Adelman, I., 1965. Long cycles: fact or artifact? The American Economic Review 60, 444-463.

Amdurer, M., Land, L.S., 1982. Geochemistry, hydrology, and mineralogy of the Sand Bulge area, Laguna Madre flats, south Texas. Journal of Sedimentary Research 52, 703-716.

Andrle, R., 1996. The west coast of Britain: statistical self-similarity vs. characteristic scales in the landscape. Earth Surface Processes and Landforms 21, 955-962.

Auken, E., Christiansen, A.V., Westergaard, J.H., Kirkegaard, C., Foged, N., Viezzoli, A., 2009. An integrated processing scheme for high-resolution airborne electromagnetic surveys, the SkyTEM system. Exploration Geophysics 40, 184-192.

Aziz, Z., Van Geen, A., Stute, M., Versteeg, R., Horneman, A., Zheng, Y., Goodbred, S., Steckler, M., Weinman, B., Gavrieli, I., 2008. Impact of local recharge on arsenic

concentrations in shallow aquifers inferred from the electromagnetic conductivity of soils in Araihazar, Bangladesh. Water Resources Research 44, W07416.

Baas, A.C., 2002. Chaos, fractals and self-organization in coastal geomorphology: simulating dune landscapes in vegetated environments. Geomorphology 48, 309-328.

Barker, N., Morten, J., Shantsev, D., 2012. Optimizing EM data acquisition for continental shelf exploration. The Leading Edge 31, 1276-1284.

Beamish, D., 2011. Low induction number, ground conductivity meters: A correction procedure in the absence of magnetic effects. Journal of Applied Geophysics 75, 244-253.

Belknap, D.F., Kraft, J.C., 1985. Influence of antecedent geology on stratigraphic preservation potential and evolution of Delaware's barrier systems. Marine Geology 63, 235-262.

Benavides, A., Everett, M.E., Pierce Jr, C., 2009. Unexploded ordnance discrimination using time-domain electromagnetic induction and self-organizing maps. Stochastic Environmental Research and Risk Assessment 23, 169-179.

Beran, J., 1992. Statistical methods for data with long-range dependence. Stastical Science 7, 404-427.

Beran, J., 1994. Statistics for long-memory processes. Chapman & Hall, New York.

Bristow, C.S., Chroston, P.N., Bailey, S.D., 2000. The structure and development of foredunes on a locally prograding coast: insights from ground-penetrating radar surveys, Norfolk, UK. Sedimentology 47, 923-944.

Browder, A.G., McNinch, J.E., 2006. Linking framework geology and nearshore morphology: correlation of paleo-channels with shore-oblique sandbars and gravel outcrops. Marine Geology 231, 141-162.

Brown, L.F., Macon, J., 1977. Environmental geologic atlas of the Texas coastal zone: Kingsville area. Bureau of Economic Geology, University of Texas at Austin.

Burrough, P., 1981. Fractal dimensions of landscapes and other environmental data. Nature 294, 240-242.

Buynevich, I.V., Fitzgerald, D.M., 2003. High-resolution subsurface (GPR) imaging and sedimentology of coastal ponds, Maine, USA: implications for Holocene back-barrier evolution. Journal of Sedimentary Research 73, 559-571.

Cheesman, S., Law, L., Louis, B.S., 1993. A porosity mapping survey in Hecate Strait using a seafloor electro-magnetic profiling system. Marine Geology 110, 245-256.

Christensen, N.B., Halkjær, M., 2014. Mapping pollution and coastal hydrogeology with helicopterborne transient electromagnetic measurements. Exploration Geophysics 45, 243-254.

Cimino, G., Del Duce, G., Kadonaga, L., Rotundo, G., Sisani, A., Stabile, G., Tirozzi, B., Whiticar, M., 1999. Time series analysis of geological data. Chemical Geology, 161, 253-270.

Coleman, J.M., Gagliano, S.M., 1964. Cyclic sedimentation in the Mississippi River deltaic plain. Transactions of the Gulf Coast Association of Geological Societies 14, 67-80.

Colman, S.M., Halka, J.P., Hobbs, C., Mixon, R.B., Foster, D.S., 1990. Ancient channels of the Susquehanna River beneath Chesapeake Bay and the Delmarva Peninsula. Geological Society of America Bulletin 102, 1268-1279.

Cooper, J., Jackson, D., Dawson, A., Dawson, S., Bates, C., Ritchie, W., 2012. Barrier islands on bedrock: A new landform type demonstrating the role of antecedent topography on barrier form and evolution. Geology 40, 923-926.

Cowell, P.J., Stive, M.J., Niedoroda, A.W., de Vriend, H.J., Swift, D.J., Kaminsky, G.M., Capobianco, M., 2003. The coastal-tract (Part 1): a conceptual approach to aggregated modeling of low-order coastal change. Journal of Coastal Research 19, 812-827.

Cromwell, J.E., 1971. Barrier coast distribution: a world-wide survey. Second National Coastal and Shallow Water Research Conference. U.S. Office of Naval Research Geography Program. University Press, University of Southern California, Los Angeles, CA, p. 50.

Davidson-Arnott, R., 2010. Introduction to coastal processes and geomorphology. Cambridge University Press, New York.

De Jong, P., Penzer, J., 1998. Diagnosing shocks in time series. Journal of the American Statistical Association 93, 796-806.

de Smet, T., Everett, M., Pierce, C., Pertermann, D., Dickson, D., 2012. Electromagnetic induction in subsurface metal targets: Cluster analysis using local point-pattern spatial statistics. Geophysics 77, WB161-WB169.

Delefortrie, S., De Smedt, P., Saey, T., Van De Vijver, E., Van Meirvenne, M., 2014a. An efficient calibration procedure for correction of drift in EMI survey data. Journal of Applied Geophysics 110, 115-125.

Delefortrie, S., Saey, T., Van De Vijver, E., De Smedt, P., Missiaen, T., Demerre, I., Van Meirvenne, M., 2014b. Frequency domain electromagnetic induction survey in the intertidal zone: Limitations of low-induction-number and depth of exploration. Journal of Applied Geophysics 100, 14-22.

Demarest, J.M., Leatherman, S.P., 1985. Mainland influence on coastal transgression: Delmarva Peninsula. Marine Geology 63, 19-33.

Deszcz-Pan, M., Fitterman, D.V., Labson, V.F., 1998. Reduction of inversion errors in helicopter EM data using auxiliary information. Exploration Geophysics 29, 142-146.

Dillenburg, S.R., Roy, P.S., Cowell, P.J., Tomazelli, L.J., 2000. Influence of antecedent topography on coastal evolution as tested by the shoreface translation-barrier model (STM). Journal of Coastal Research 16, 71-81.

Dolan, R., Hayden, B., 1981. Storms and shoreline configuration. Journal of Sedimentary Petrology 51, 737-744.

Donnelly, C., Kraus, N., Larson, M., 2006. State of knowledge on measurement and modeling of coastal overwash. Journal of Coastal Research 22, 965-991.

Doukhan, P., Oppenheim, G., Taqqu, M.S., 2003. Theory and aplications of long-range dependence. Birkhäuser, Switzerland.

Duque, C., Calvache, M.L., Pedrera, A., Martin-Rosales, W., López-Chicano, M., 2008. Combined time domain electromagnetic soundings and gravimetry to determine marine intrusion in a detrital coastal aquifer (southern Spain). Journal of Hydrology 349, 536-547.

Eke, A., Herman, P., Bassingthwaighte, J., Raymond, G., Percival, D., Cannon, M., Balla, I., Ikrényi, C., 2000. Physiological time series: distinguishing fractal noises from motions. Pflügers Archive 439, 403-415.

Emery, K.O., 1969. A coastal pond: studied by oceanographic methods. American Elsevier Publishing, New York.

Evans, M.W., Hine, A.C., Belknap, D.F., Davis Jr, R.A., 1985. Bedrock controls on barrier island development: west-central Florida coast. Marine Geology 63, 263-283.

Evans, R., Law, L., St Louis, B., Cheesman, S., Sananikone, K., 1999. The shallow porosity structure of the Eel shelf, northern California: results of a towed electromagnetic survey. Marine Geology 154, 211-226.

Evans, R.L., Law, L., St Louis, B., Cheesman, S., 2000. Buried paleo-channels on the New Jersey continental margin: channel porosity structures from electromagnetic surveying. Marine Geology 170, 381-394.

Everett, M., Farquharson, C., 2012. Near-surface electromagnetic induction—Introduction. Geophysics 77, WB1-WB2.

Everett, M.E., 2013. Near-surface applied geophysics. Cambridge University Press, New York.

Everett, M.E., Weiss, C.J., 2002. Geological noise in near-surface electromagnetic induction data. Geophysical Research Letters 29, 10-1-10-4.

Field, M.E., Duane, D.B., 1976. Post-Pleistocene history of the United States inner continental shelf: Significance to origin of barrier islands. Geological Society of America Bulletin 87, 691-702.

Fisk, H.N., 1959. Padre Island and Laguna Madre Flats, coastal south Texas. Proceedings 2nd Coastal Geography Conference, Louisiana State University, Baton Rouge, LA, 103-151.

Fitterman, D.V., Deszcz-Pan, M., 1998. Helicopter EM mapping of saltwater intrusion in Everglades National Park, Florida. Exploration Geophysics 29, 240-243.

Fitterman, D.V., Stewart, M.T., 1986. Transient electromagnetic sounding for groundwater. Geophysics 51, 995-1005.

FitzGerald, D., Buynevich, I., Hein, C., 2012. Morphodynamics and facies architecture of tidal inlets and tidal deltas. In: Davis, R.A., Dalrymple, R.W., (Eds.), Principles of Tidal Sedimentology. Springer, New York, 301-333.

FitzGerald, D.M., Buynevich, I.V., Rosen, P.S., 2001. Geological evidence of former tidal inlets along a retrograding barrier: Duxbury Beach, Massachusetts, USA. Journal of Coastal Research SI 34, 437-448.

Fitzgerald, D.M., Van Heteren, S., 1999. Classification of paraglacial barrier systems: coastal New England, USA. Sedimentology 46, 1083-1108.

Foyle, A.M., Oertel, G.F., 1997. Transgressive systems tract development and incised-valley fills within a Quaternary estuary-shelf system: Virginia inner shelf, USA. Marine Geology 137, 227-249.

Frazier, D.E., 1967. Recent deltaic deposits of the Mississippi River: their development and chronology. Transactions of the Gulf Coast Association of Geological Societies 17, 287-315.

Frischknecht, F.C., 1967. Fields about an oscillating magnetic dipole over a two-layer earth, and application to ground and airborne electromagnetic surveys. Colorado School of Mines Q.62, 1-326.

Frischknecht, F.C., Labson, V.F., Spies, B.R., Anderson, W.L., 1991. Profiling methods using small sources. In: Nabighian, M.N. (Ed.), Electromagnetic Methods in Applied Geophysics 2: Applications. SEG Publishing, 105–270.

Garrison, J.R., Williams, J., Miller, S.P., Weber, E.T., McMechan, G., Zeng, X., 2010. Ground-penetrating radar study of North Padre Island: implications for barrier island internal architecture, model for growth of progradational microtidal barrier islands, and Gulf of Mexico sea-level cyclicity. Journal of Sedimentary Research, 80, 303-319.

Geophysical Survey Systems, I.G., 2007. Profiler EMP-400 user's manual, Geophysical Survey Systems, Incorporated, User's Manual.

George, R., Woodgate, P., 2002. Critical factors affecting the adoption of airborne geophysics for management of dryland salinity. Exploration Geophysics 33, 84-89.

Goldman, M., Gilad, D., Ronen, A., Melloul, A., 1991. Mapping of seawater intrusion into the coastal aquifer of Israel by the time domain electromagnetic method. Geoexploration 28, 153-174.

Gourlay, M.R., 1992. Wave set-up, wave run-up and beach water table: interaction between surf zone hydraulics and groundwater hydraulics. Coastal Engineering, 17, 93-144.

Gradstein, F.M., Ogg, J.G., van Kranendonk, M., 2008. On the geologic time scale 2008. Newsletters on Stratigraphy 43, 5-13.

Granger, C.W., Joyeux, R., 1980. An introduction to long-memory time series models and fractional differencing. Journal of Time Series Analysis 1, 15-29.

Gueguen, Y., Palciauskas, V., 1994. VII. Electrical conductivity. In: Introduction to the Physics of Rocks. Princton, NJ, Princton University Press, 182-211.

Guillemoteau, J., Sailhac, P., Boulanger, C., Trules, J., 2015. Inversion of ground constant offset loop-loop electromagnetic data for a large range of induction numbers. Geophysics 80, E11-E21.

Guillemoteau, J., Tronicke, J., 2015. Non-standard electromagnetic induction sensor configurations: evaluating sensitivities and applicability. Journal of Applied Geophysics 118, 15-23.

Hapke, C.J., Lentz, E.E., Gayes, P.T., McCoy, C.A., Hehre, R., Schwab, W.C., Williams, S.J., 2010. A review of sediment budget imbalances along Fire Island, New York: can nearshore geologic framework and patterns of shoreline change explain the deficit? Journal of Coastal Research 263, 510-522.

Harris, M.S., Gayes, P.T., Kindinger, J.L., Flocks, J.G., Krantz, D.E., Donovan, P., 2005. Quaternary geomorphology and modern coastal development in response to an inherent geologic framework: an example from Charleston, South Carolina. Journal of Coastal Research 211, 49-64.

Hayes, M.O., 1974. Hurricanes as geological agents: case studies of Hurricanes Carla, 1961, and Cindy, 1963. The University of Texas, Austin, Bureau of Economic Geology Report of Investigation 61.

Hayes, M.O., 1979. Barrier island morphology as a function of tidal and wave regime. In: Barrier islands from the Gulf of St. Lawrence to the Gulf of Mexico (Leatherman, S.P Ed.). Academic Press, New York, 1-27.

Hayes, O.M., 2005. Barrier island. In: Schwartz, M.L. (Ed.). Encyclopedia of Coastal Science. Springer, Dordrecht, Netherlands, 117-119.

Hegge, B.J., Masselink, G., 1991. Groundwater-table responses to wave run-up: an experimental study from Western Australia. Journal of Coastal Research 7, 623-634.

Hesp, P., 1988. Morphology, dynamics and internal stratification of some established foredunes in southeast Australia. Sedimentary Geology 55, 17-41.

Heteren, S.V., Fitzgerald, D.M., Mckinlay, P.A., Buynevich, I.V., 1998. Radar facies of paraglacial barrier systems: coastal New England, USA. Sedimentology 45, 181-200.

Honeycutt, M.G., Krantz, D.E., 2003. Influence of the geologic framework on spatial variability in long-term shoreline change, Cape Henlopen to Rehoboth Beach, Delaware. Journal of Coastal Research 38, 147-167.

Horn, D.P., 2002. Beach groundwater dynamics. Geomorphology 48, 121-146.

Hosking, J.R., 1981. Fractional differencing. Biometrika 68, 165-176.

Houser, C., 2012. Feedback between ridge and swale bathymetry and barrier island storm response and transgression. Geomorphology 173, 1-16.

Houser, C., 2013. Alongshore variation in the morphology of coastal dunes: implications for storm response. Geomorphology 199, 48-61.

Houser, C., Hamilton, S., 2009. Sensitivity of post-hurricane beach and dune recovery to event frequency. Earth Surface Processes and Landforms 34, 613-628.

Houser, C., Hapke, C., Hamilton, S., 2008. Controls on coastal dune morphology, shoreline erosion and barrier island response to extreme storms. Geomorphology 100, 223-240.

Houser, C., Mathew, S., 2011. Alongshore variation in foredune height in response to transport potential and sediment supply: South Padre Island, Texas. Geomorphology 125, 62-72.

Houser, C., Wernette, P., Rentschlar, E., Jones, H., Hammond, B., Trimble, S., 2015. Post-storm beach and dune recovery: implications for barrier island resilience. Geomorphology 234, 54-63.

Hoyt, J.H., 1967. Barrier island formation. Geological Society of America Bulletin 78, 1125-1136.

Huang, H., 2005. Depth of investigation for small broadband electromagnetic sensors. Geophysics 70, G135-G142.

Huang, H., Deszcz-Pan, M., Smith, B., 2008. Limitations of small EM sensors in resistive terrain. 21st EEGS Symposium on the Application of Geophysics to Engineering and Environmental Problems 21, 163-180.

Huang, H., Won, I., 2000. Conductivity and susceptibility mapping using broadband electromagnetic sensors. Journal of Environmental and Engineering Geophysics 5, 31-41.

Hurst, H.E., Black, R.P., Simaika, Y., 1965. Long-term storage: an experimental study. Constable, London.

Hyndman, R.J., 2015. Forecasting functions for time series and linear models. R package version 5.9., URL:http://github.com/robjhyndman/forecast.

Hyndman, R.J., Khandakar, Y., 2007. Automatic time series for forecasting: the forecast package for R, Monash University, Department of Econometrics and Business Statistics.

Jackson, D., Cooper, J., Del Rio, L., 2005. Geological control of beach morphodynamic state. Marine Geology 216, 297-314.

Jol, H.M., Smith, D.G., Meyers, R.A., 1996. Digital ground penetrating radar (GPR): a new geophysical tool for coastal barrier research (Examples from the Atlantic, Gulf and Pacific coasts, USA). Journal of Coastal Research 12, 960-968.

Kirkegaard, C., Sonnenborg, T.O., Auken, E., Jørgensen, F., 2011. Salinity distribution in heterogeneous coastal aquifers mapped by airborne electromagnetics. Vadose Zone Journal 10, 125-135.

Kittel, C., 2004. Introduction to Solid State Physics, 8th edn. John Wiley & Sons, New York.

Kocurek, G., Townsley, M., Yeh, E., Havholm, K., Sweet, M., 1992. Dune and dune-field development on Padre Island, Texas, with implications for interdune deposition and water-table-controlled accumulation. Journal of Sedimentary Petrology 62, 622-635.

Kraft, J., Belknap, D., McDonald, K., Maley, K., Marx, P., 1982. Models of a shoreface-nearshore marine transgression over estuarine and barrier systems and antecedent topography of the Atlantic Coast. Geological Society of America, Abstracts with Programs, pp. 32.

Kraft, J.C., 1971. Sedimentary facies patterns and geologic history of a Holocene marine transgression. Geological Society of America Bulletin 82, 2131-2158.

Kraft, J.C., John, C.J., 1979. Lateral and vertical facies relations of transgressive barrier. AAPG Bulletin 63, 2145-2163.

Kulp, M., Penland, S., Williams, S.J., Jenkins, C., Flocks, J., Kindinger, J., 2005. Geologic framework, evolution, and sediment resources for restoration of the Louisiana coastal zone. Journal of Coastal Research 44, 56-71.

Lanyon, J., Eliot, I., Clarke, D., 1982. Groundwater-level variation during semidiurnal spring tidal cycles on a sandy beach. Marine and Freshwater Research 33, 377-400.

Larsson, J., 2007. Electromagnetics from a quasistatic perspective. American Journal of Physics 75, 230-239.

Lazarus, E., Ashton, A., Murray, A.B., Tebbens, S., Burroughs, S., 2011. Cumulative versus transient shoreline change: Dependencies on temporal and spatial scale. Journal of Geophysical Research: Earth Surface 116, F02014.

Lazarus, E.D., Murray, A.B., 2011. An integrated hypothesis for regional patterns of shoreline change along the northern North Carolina Outer Banks, USA. Marine Geology 281, 85-90.

Leatherman, S.P., 1987. Coastal geomorphological applications of ground-penetrating radar. Journal of Coastal Research 3, 397-399.

Lentz, E.E., Hapke, C.J., 2011. Geologic framework influences on the geomorphology of an anthropogenically modified barrier island: Assessment of dune/beach changes at Fire Island, New York. Geomorphology 126, 82-96.

Lentz, E.E., Hapke, C.J., Stockdon, H.F., Hehre, R.E., 2013. Improving understanding of near-term barrier island evolution through multi-decadal assessment of morphologic change. Marine Geology 337, 125-139.

List, J.H., Sallenger, A.H., Hansen, M.E., Jaffe, B.E., 1997. Accelerated relative sea-level rise and rapid coastal erosion: testing a causal relationship for the Louisiana barrier islands. Marine geology 140, 347-365.

Mallinson, D.J., Smith, C.W., Culver, S.J., Riggs, S.R., Ames, D., 2010. Geological characteristics and spatial distribution of paleo-inlet channels beneath the outer banks barrier islands, North Carolina, USA. Estuarine, Coastal and Shelf Science 88, 175-189.

Mandelbrot, B.B., 1967. How long is the coast of Britain. Science 156, 636-638.

Masetti, R., Fagherazzi, S., Montanari, A., 2008. Application of a barrier island translation model to the millennial-scale evolution of Sand Key, Florida. Continental Shelf Research 28, 1116-1126.

Masselink, G., van Heteren, S., 2014. Response of wave-dominated and mixed-energy barriers to storms. Marine Geology 352, 321-347.

Matias, A., Ferreira, Ó., Vila-Concejo, A., Garcia, T., Dias, J.A., 2008. Classification of washover dynamics in barrier islands. Geomorphology 97, 655-674.

Matias, A., Vila-Concejo, A., Ferreira, Ó., Morris, B., Dias, J.A., 2009. Sediment dynamics of barriers with frequent overwash. Journal of Coastal Research 12, 768-780.

McBride, R.A., Byrnes, M.R., Hiland, M.W., 1995. Geomorphic response-type model for barrier coastlines: a regional perspective. Marine Geology 126, 143-159.

McBride, R.A., Penland, S., Hiland, M.W., Williams, S.J., Westphal, K.A., Jaffe, B.E., Sallenger, A.H., 1992. Analysis of barrier shoreline change in Louisiana from 1853 to 1989. In: Williams, S.J., Penland, S., and Sallenger, A.H. (Eds.), Atlas of Shoreline Changes in Louisiana from 1853 to 1989., U.S. Geological Survey Miscellaneous Investigation Series I-2150-A: 36-97.

McLeod, A.I., Yu, H., Mahdi, E., 2011. Time series analysis with R. Handbook of Statistics 30, 78-93.

McLeod, I., A., , Zhang, Y., 2008. Faster ARMA maximum likelihood estimation. Computational Statistics and Data Analysis 52, 2166-2176.

McNeill, J., 1980. Electromagnetic terrain conductivity measurement at low induction numbers. Geonics Limited Ontario, Canada.

McNeill, J., 1996. Why doesn't Geonics Limited build a multi-frequency EM31 or EM38? Geonics Limited Ontario, Canada.

McNinch, J.E., 2004. Geologic control in the nearshore: shore-oblique sandbars and shoreline erosional hotspots, Mid-Atlantic Bight, USA. Marine Geology 211, 121-141.

Miller, J.A., 1975. Facies characteristics of Laguna Madre wind-tidal flats. In: Ginsburg, R.N. (Ed.), Tidal Deposits. Springer, New York, 67–72.

Minsley, B.J., 2011. A trans-dimensional Bayesian Markov chain Monte Carlo algorithm for model assessment using frequency-domain electromagnetic data. Geophysical Journal International 187, 252-272.

Minsley, B.J., Smith, B.D., Hammack, R., Sams, J.I., Veloski, G., 2012. Calibration and filtering strategies for frequency domain electromagnetic data. Journal of Applied Geophysics 80, 56-66.

Miselis, J.L., Buster, N.A., Kindinger, J.L., 2014. Refining the link between the Holocene development of the Mississippi River Delta and the geologic evolution

of Cat Island, MS: implications for delta-associated barrier islands. Marine Geology 355, 274-290.

Miselis, J.L., McNinch, J.E., 2006. Calculating shoreline erosion potential using nearshore stratigraphy and sediment volume: Outer Banks, North Carolina. Journal of Geophysical Research: Earth Surface, 111(F2).

Morton, R.A., 2002. Factors controlling storm impacts on coastal barriers and beaches: a preliminary basis for near real-time forecasting. Journal of Coastal Research 18, 486-501.

Morton, R.A., Blum, M.D., White, W.A., 1996. Valley fills of incised coastal plain rivers, southeastern Texas. Transactions of the Gulf Coast Association of Geological Societies 46, 321-331

Morton, R.A., Holmes, C.W., 2009. Geological processes and sedimentation rates of wind-tidal flats, Laguna Madre, Texas. Transactions of the Gulf Coast Association of Geological Societies 59, 519-538.

Morton, R.A., McGowen, J., 1980. Modern depositional environments of the Texas coast. The University of Texas at Austin, Bureau of Economic Geology, Guidebook 20.

Morton, R.A., Paine, J.G., Blum, M.D., 2000. Responses of stable bay-margin and barrier-island systems to Holocene sea-level highstands, western Gulf of Mexico. Journal of Sedimentary Research 70, 478-490.

Morton, R.A., Sallenger, A.H., 2003. Morphological impacts of extreme storms on sandy beaches and barriers. Journal of Coastal Research 19, 560-573.

Murray, A.B., Thieler, E.R., 2004. A new hypothesis and exploratory model for the formation of large-scale inner-shelf sediment sorting and "rippled scour depressions". Continental Shelf Research 24, 295-315.

Nabighian, M.N., Macnae, J.C., 1991. Time domain electromagnetic prospecting methods. In: Nabighian, M.N. (Ed.), Electro-magnetic methods in applied geophysics, (Part 2A). Society of Exploration Geophysicists, 427–520.

Neal, A., Roberts, C.L., 2000. Applications of ground-penetrating radar (GPR) to sedimentological, geomorphological and geoarchaeological studies in coastal environments. Geological Society, London, Special Publications 175, 139-171.

Nenna, V., Herckenrath, D., Knight, R., Odlum, N., McPhee, D., 2013. Application and evaluation of electromagnetic methods for imaging saltwater intrusion in coastal aquifers: Seaside Groundwater Basin, California. Geophysics 78, B77-B88.

Nettleton, L.L., 1940. Geophysical prospecting for oil. McGraw-Hill, New York.

Nielsen, P., 1990. Tidal dynamics of the water table in beaches. Water Resources Research 26, 2127-2134.

Nielsen, P., 1997. Coastal groundwater dynamics. Proceedings Coastal dynamics' 97. ASCE, 546-555.

Nielsen, P., 1999. Groundwater dynamics and salinity in coastal barriers. Journal of Coastal Research 15, 732-740.

Nielsen, P., Kang, H.-Y., 1996. Groundwater dynamics in beaches and coastal barriers, International Conference on Coastal Research in Terms of Large Scale Experiments, 521-532.

NOAA, 2014. "Tropical Storm Arlene - June 18-23, 1993" accessed August 17, 2014 online at http://www.nhc.noaa.gov/data/.

NOAA, 2015. National Hurricane Center. Data set accessed 29 April 2015 online at http://www.nhc.noaa.gov/data/.

Oh, T.-M., Dean, R.G., 1994. Effects of controlled water table on beach profile dynamics. Proceedings of the 24th International Conference on Coastal Engineering, 2449–2460.

Orford, J.D., Carter, R., 1984. Mechanisms to account for the longshore spacing of overwash throats on a coarse clastic barrier in southeast Ireland. Marine Geology 56, 207-226.

Otvos, E.G., 1970. Development and migration of barrier islands, Northern Gulf of Mexico: Reply. Geological Society of America Bulletin 81, 3783-3788.

Otvos, E.G., Giardino, M.J., 2004. Interlinked barrier chain and delta lobe development, northern Gulf of Mexico. Sedimentary Geology 169, 47-73.

Paine J.G. and Minty R.S. 2005. Airborne hydrogeophysics. In: Hydrogeophysics (Eds Y. Rubin and S.S. Hubbard). Springer, Dordrecht, Netherlands, 333-357.

Paine, J.G., White, W.A., Smyth, R.C., Andrews, J.R., Gibeaut, J.C., 2004. Mapping coastal environments with lidar and EM on Mustang Island, Texas, US. The Leading Edge 23, 894-898.

Panageotou, W., Leatherman, S.P., 1986. Holocene-Pleistocene stratigraphy of the inner shelf off Fire Island, New York: Implications for barrier-island migration. Journal of Sedimentary Research 56, 528-537.

Penland, S., Suter, J.R., Boyd, R., 1985. Barrier island arcs along abandoned Mississippi River deltas. Marine Geology 63, 197-233.

Pérez-Flores, M.A., Antonio-Carpio, R.G., Gómez-Treviño, E., Ferguson, I., Méndez-Delgado, S., 2012. Imaging of 3D electromagnetic data at low-induction numbers. Geophysics 77, WB47-WB57.

Pincus, J.A., Smet, T.S., Tepper, Y., Adams, M.J., 2013. Ground-penetrating Radar and Electromagnetic Archaeogeophysical Investigations at the Roman Legionary Camp at Legio, Israel. Archaeological Prospection 20, 175-188.

Psuty, N.P., 1992. Spatial variation in coastal foredune development. Coastal dunes: geomorphology, ecology and management for conservation, Rotterdam, Balkema, 3-13.

Reide Corbett, D., Dillon, K., Burnett, W., 2000. Tracing groundwater flow on a barrier island in the north-east Gulf of Mexico. Estuarine, Coastal and Shelf Science 51, 227-242.

Reinson, G.E., 1992. Transgressive barrier island and estuarine systems, facies models: response to sea level change. Geological Association of Canada, 179-194.

Riggs, S., 1979. A geologic profile of the North Carolina coastal-inner continental shelf system. Ocean Outfall Wastewater Disposal Feasibility and Planning, 90-113.

Riggs, S., O'Connor, M., 1974. Relict sediment deposits in a major transgressive coastal system. Sea Grant Program, UNC-SG-74-04, University of North Carolina.

Riggs, S.R., Cleary, W.J., Snyder, S.W., 1995. Influence of inherited geologic framework on barrier shoreface morphology and dynamics. Marine Geology 126, 213-234.

Rodriguez, A.B., Fassell, M.L., Anderson, J.B., 2001. Variations in shoreface progradation and ravinement along the Texas coast, Gulf of Mexico. Sedimentology 48, 837-853.

Ruppel, C., Schultz, G., Kruse, S., 2000. Anomalous fresh water lens morphology on a strip barrier island. Groundwater 38, 872-881.

Sallenger, A.H., 2000. Storm impact scale for barrier islands. Journal of Coastal Research 16, 890-895.

Samorodnitsky, G., 2007. Long range dependence. Foundations and Trends in Stochastic Systems 1, 163-257.

Samorodnitsky, G., Taqqu, M.S., 1994. Stable non-Gaussian processes: stochastic models with infinite variance. Chapman and Hall, New York, London.

Santos, F., Triantafilis, J., Bruzgulis, K., Roe, J., 2010. Inversion of multiconfiguration electromagnetic (DUALEM-421) profiling data using a one-dimensional laterally constrained algorithm. Vadose Zone Journal 9, 117-125.

Sasaki, Y., Meju, M.A., 2006. A multidimensional horizontal-loop controlled-source electromagnetic inversion method and its use to characterize heterogeneity in aquiferous fractured crystalline rocks. Geophysical Journal International 166, 59-66.

Schneider, J.C., Kruse, S.E., 2003. A comparison of controls on freshwater lens morphology of small carbonate and siliciclastic islands: examples from barrier islands in Florida, USA. Journal of Hydrology 284, 253-269.

Schrott, L., Sass, O., 2008. Application of field geophysics in geomorphology: advances and limitations exemplified by case studies. Geomorphology 93, 55-73.

Schupp, C.A., McNinch, J.E., List, J.H., 2006. Nearshore shore-oblique bars, gravel outcrops, and their correlation to shoreline change. Marine Geology 233, 63-79.

Schwab, W.C., Baldwin, W.E., Hapke, C.J., Lentz, E.E., Gayes, P.T., Denny, J.F., List, J.H., Warner, J.C., 2013. Geologic evidence for onshore sediment transport from the inner continental shelf: Fire Island, New York. Journal of Coastal Research, 29, 526-544.

Schwab, W.C., Thieler, E.R., Allen, J.R., Foster, D.S., Swift, B.A., Denny, J.F., 2000. Influence of inner-continental shelf geologic framework on the evolution and behavior of the barrier-island system between Fire Island Inlet and Shinnecock Inlet, Long Island, New York. Journal of Coastal Research 16, 408-422.

Scott, J.H., 1983. Electrical and magnetic properties of rock and soil. US Geological Survey, 2331-1258.

Seijmonsbergen, A., Biewinga, D., Pruissers, A., 2004. a geophysical profile at the foot of the Dutch coastal dunes near the former outlet of the 'Old Rhine'. Geologie and Mijnbouw 83, 267-271.

Sherman, D.J., Bauer, B.O., 1993. Dynamics of beach-dune systems. Progress in Physical Geography 17, 413-447.

Sherman, D.J., Lyons, W., 1994. Beach-state controls on aeolian sand delivery to coastal dunes. Physical Geography 15, 381-395.

Short, A., Hesp, P., 1982. Wave, beach and dune interactions in southeastern Australia. Marine Geology 48, 259-284.

Short, A.D., 2010. Role of geological inheritance in Australian beach morphodynamics. Coastal Engineering 57, 92-97.

Simms, A.R., Anderson, J.B., Blum, M., 2006. Barrier-island aggradation via inlet migration: Mustang Island, Texas. Sedimentary Geology 187, 105-125.

Smith, R.C., Sjogren, D.B., 2006. An evaluation of electrical resistivity imaging (ERI) in Quaternary sediments, southern Alberta, Canada. Geosphere 2, 287-298.

Stevens, J.D., Sharp Jr, J.M., Simmons, C.T., Fenstemaker, T., 2009. Evidence of free convection in groundwater: field-based measurements beneath wind-tidal flats. Journal of Hydrology 375. 394-409.

Stewart, M.T., 1982. Evaluation of electromagnetic methods for rapid mapping of salt-water interfaces in coastal aquifers. Groundwater 20, 538-545.

Stive, M.J., Aarninkhof, S.G., Hamm, L., Hanson, H., Larson, M., Wijnberg, K.M., Nicholls, R.J., Capobianco, M., 2002. Variability of shore and shoreline evolution. Coastal Engineering 47, 211-235.

Stone, G.W., Liu, B., Pepper, D.A., Wang, P., 2004. The importance of extratropical and tropical cyclones on the short-term evolution of barrier islands along the northern Gulf of Mexico, USA. Marine Geology 210, 63-78.

Stutz, M.L., Pilkey, O.H., 2001. A review of global barrier island distribution. Journal of Coastal Research SI 34, 15-22.

Stutz, M.L., Pilkey, O.H., 2011. Open-ocean barrier islands: global influence of climatic, oceanographic, and depositional settings. Journal of Coastal Research 27, 207-222.

Sudduth, K., Drummond, S., Kitchen, N., 2001. Accuracy issues in electromagnetic induction sensing of soil electrical conductivity for precision agriculture. Computers and Electronics in Agriculture 31, 239-264.

Suter, J.R., Nummedal, D., Maynard, A.K., Kemp, P., 1982. A process-response model for hurricane washovers. 18th Coastal Engineering Conference, Capetown, South Africa, 1459-1789.

Swift, D.J., 1975. Barrier-island genesis: evidence from the central Atlantic shelf, eastern USA. Sedimentary Geology 14, 1-43.

Talley, D.M., North, E.W., Juhl, A.R., Timothy, D.A., Conde, D., Jody, F., Brown, C.A., Campbell, L.M., Garstecki, T., Hall, C.J., 2003. Research challenges at the land–sea interface. Estuarine, Coastal and Shelf Science 58, 699-702.

Taqqu, M.S., 2003. Fractional Brownian motion and long-range dependence. In: P. Doukhan, G. Oppenheim, and M.S. Taqqu (Eds.), Theory and applications of long-range dependence. Birkhäuser, Switzerland 5-38.

Taqqu, M.S., Teverovsky, V., Willinger, W., 1995. Estimators for long-range dependence: an empirical study. Fractals 3, 785-798.

Tebbens, S.F., Burroughs, S.M., Nelson, E.E., 2002. Wavelet analysis of shoreline change on the Outer Banks of North Carolina: An example of complexity in the marine sciences. Proceedings of the National Academy of Sciences 99 (Supplement 1), 2554-2560.

Thieler, E.R., Brill, A.L., Cleary, W.J., Hobbs III, C.H., Gammisch, R.A., 1995. Geology of the Wrightsville Beach, North Carolina shoreface: implications for the concept of shoreface profile of equilibrium. Marine Geology 126, 271-287.

Triantafilis, J., Roe, J., Monteiro Santos, F., 2011. Detecting a leachate plume in an aeolian sand landscape using a DUALEM-421 induction probe to measure electrical conductivity followed by inversion modelling. Soil Use and Management 27, 357-366.

Turner, I., 1993. The total water content of sandy beaches. Journal of Coastal Research SI 15, 11-26.

Twichell, D.C., Flocks, J.G., Pendleton, E.A., Baldwin, W.E., 2013. Geologic controls on regional and local erosion rates of three northern Gulf of Mexico barrier-island systems. Journal of Coastal Research 63, 32-45.

Van Heteren, S., 2014. Barrier systems. In: Masselink, G., and Gehrels, R. (Eds.), Coastal Environments and Global Change. John Wiley & Sons, New York, 194-226.

Van Heteren, S., FitzGerald, D., McKinlay, P., 1994. Application of ground penetrating radar in coastal stratigraphic studies. In: GPR ’94 – Procedings Fifth International Conferention on Ground Penetrating Radar (Eds. J.D. Redman, A.P

Annan, J.P. Greenhouse, T. Klym, and J.R., Rossiter). Waterloo Center for Groundwater Research, Kitchener, 869-881.

Veenstra, J., 2012. Persistence and anti-persistence: theory and sofware. Ph.D. Thesis, Western University.

Viezzoli, A., Christiansen, A.V., Auken, E., Sørensen, K., 2008. Quasi-3D modeling of airborne TEM data by spatially constrained inversion. Geophysics 73, F105-F113.

Vitousek, P.M., Mooney, H.A., Lubchenco, J., Melillo, J.M., 1997. Human domination of Earth's ecosystems. Science 277, 494-499.

Vrbancich, J., 2009. An investigation of seawater and sediment depth using a prototype airborne electromagnetic instrumentation system–a case study in Broken Bay, Australia. Geophysical Prospecting 57, 633-651.

Vrbancich, J., 2012. Airborne electromagnetic bathymetry and estimation of bedrock topography in Broken Bay, Australia. Geophysics 77, WB3-WB17.

Ward, S.H., 1967. Electromagnetic theory for geophysical application. In: Mining geophysics, Vol. II (Hansen D. A., Heinrichs W. E., Holmer R. C., MacDougall R. E., Rogers G. R., Summer J. S., Ward S. H., (Eds.) Chapter II (Part A). The Society of Exploration Geophysicists, Tulsa, Oklahoma.

Ward, S.H., Hohmann, G.W., 1988. Electromagnetic theory for geophysical applications. Electromagnetic Methods in Applied Geophysics 1, 131-311.

Weise, B.R., White, W.A., Ferguson, W.K., 1980. Padre Island National Seashore: A guide to the geology, natural environments, and history of a Texas barrier island, 17. Bureau of Economic Geology, University of Texas at Austin.

Wernette, P., Houser, C., Bishop, M.P., 2016. An automated approach for extracting Barrier Island morphology from digital elevation models. Geomorphology 262, 1-7.

West, G. F., and Macnae, J.C., 1991. Physics of the electromagnetic induction exploration method. In M. N. Nabighian (Ed.) Electromagnetic methods in applied geophysics, SEG, 5-45.

Weymer, B., Houser, C., Giardino, J.R., 2015a. Poststorm evolution of beach-dune morphology: Padre Island National Seashore, Texas. Journal of Coastal Research, 31, 634 – 644.

Weymer, B.A., Everett, M.E., de Smet, T.S., Houser, C., 2015b. Review of electromagnetic induction for mapping barrier island framework geology. Sedimentary Geology 321, 11-24.

Weymer, B.A., Everett, M.E., Houser, C., Wernette, P., Barrineau, P., *accepted*. Differentiating tidal and groundwater dynamics from barrier island framework geology: Testing the utility of portable multi-frequency EMI profilers. Geophysics.

Wiederhold, H., Siemon, B., Steuer, A., Schaumann, G., Meyer, U., Binot, F., Kühne, K., 2010. Coastal aquifers and saltwater intrusions in focus of airborne electromagnetic surveys in northern Germany, Proceedings 21st Salt Water Intrusion Meeting, Azores, 94-97.

Williams, S., Penland, S., Sallenger, A., McBride, R., Kindinger, J., 1991. Geologic controls on the formation and evolution of Quaternary coastal deposits of the northern Gulf of Mexico. Coastal Sediments. ASCE, 1082-1095.

Won, I., Keiswetter, D.A., Fields, G.R., Sutton, L.C., 1996. GEM-2: A new multifrequency electromagnetic sensor. Journal of Environmental and Engineering Geophysics 1, 129-137.

Woodroffe, C.D., 2002. Coasts: form, process and evolution. Cambridge University Press, New York.

Xu, T., Moore, I.D., Gallant, J.C., 1993. Fractals, fractal dimensions and landscapes—a review. Geomorphology 8, 245-262.

Zhang, K., Leatherman, S., 2011. Barrier island population along the US Atlantic and Gulf Coasts. Journal of Coastal Research 27, 356-363.